



NTNU – Trondheim
Norwegian University of
Science and Technology

Kinetics of the reaction between quartz and silicon carbide in different gas atmospheres

Feng Ni

Light Metals, Silicon and Ferroalloy Production

Submission date: June 2015

Supervisor: Merete Tangstad, IMTE

Norwegian University of Science and Technology
Department of Materials Science and Engineering

Preface

This thesis describes the kinetics of SiO_2+SiC reaction under different gas atmosphere. The laboratory work was carried out at the Institute of Materials Science and Technology, Norwegian University of Science and Technology (NTNU), Trondheim. The work presented here is the master thesis of the author and evaluation basis for the course TMT 4905 at Norwegian University of Science and Technology (NTNU) and is part of GASFERROSIL project funded by Norwegian Research Council.

Acknowledgements

First and foremost I would like to express my sincere gratitude to my supervisor Professor Merete Tangstad, for the excellent guidance and helpful advice during the thesis work, for reading and correcting the draft of this thesis, for many weekly inspiring discussions on various aspects of the work, for encouraging me to overcome difficulties. She has been supportive since the days I started my master study in NTNU. I could not have imagined having a better advisor and mentor for my master study.

I would like to thank Sarina Bao, Delphine Leroy, Jonas Einan Gjøvik, Dmitry Slizovskiy, Pål Tetlie and Fei Li who helped me with the operation of the high temperature furnace. I would also thank Yinda Yu, who taught me how to operate the scanning electron microscopy (SEM) and energy dispersive spectrometers (EDS). Thanks Mrten Raanes for doing EPMA and Kristin Høydalsvik for XRD analysis. My gratitude also goes to Edith Thomassen for synthesis of pellets, Irene Bragstad for particle size test, Ole Kjos for calibration of the gas analyzer.

My thanks also go to SiManTi Research Group for the knowledge worth spreading and sharing the constructive feedback of my presentations. Special thanks to my international classmates Pyeonghwa Kim, Adrea Estrogon Broggi, Bilal Nadir. Our time together has been greatly appreciated and will not be forgotten.

Finally, I would like to thank my parents for their unconditional love and support. Their support always inspires me to go through difficult time during all these years.

Feng Ni

June, 2015 Trondheim

Abstract

This thesis examined the influence of different gas species in the kinetics of SiO_2+SiC reaction. The quartz and silicon carbide were crushed to $< 38\mu\text{m}$, uniformly mixed together with weight ratio of 3:1 and pelletized into pellets. The reaction was studied in isothermal experiments at $1700\text{ }^\circ\text{C}$ in a high temperature furnace in argon, hydrogen, Ar-CO gas mixtures and Ar- H_2 gas mixtures. The concentration of CO in the off gas was measured by a gas analyzer. The samples before and after experiments were characterized by X-ray diffraction, scanning electron microscope, energy dispersive spectroscopy and electron microprobe micro-analyzer. The activation energy was determined to be 15.9 to 195kJ/mole by isoconversional method. The SiO_2+SiC reaction was accelerated by the increasing concentration of H_2 in Ar- H_2 gas mixtures, which was attributed to the faster diffusion of SiO gas or CO gas in H_2 . CO gas, as one of the products, suppressed this reaction. It is found that the unimolecular decay model described the reaction between SiO_2+SiC best and the mathematical expressions of the reaction rate in different gas species were proposed. The SEM results indicated that the quartz became softened at $1700\text{ }^\circ\text{C}$.

Key words: SiO_2+SiC reaction, isothermal experiment, CO gas, H_2 gas, Si production

Content

Chapter 1. Introduction	1
1.1 Background	1
1.2 Objective of the thesis	2
Chapter 2. Theory and literature.....	3
2.1 Silicon production process	3
2.2 Reactions in the furnace	4
2.3 Thermodynamic considerations	5
2.4 Kinetics considerations.....	7
2.4.1. Reaction rate	7
2.4.2. Arrhenius equation.....	8
2.4.3. Physio-geometric kinetics model.....	10
2.4.4. Influence of mass transfer.....	11
2.5 Previous work.....	13
Chapter 3. Experiments	28
3.1 Raw material.....	28
3.2 Apparatus.....	30
3.3 Procedures	32
3.3.1. High temperature experiments.....	32
3.3.2. SEM, EDS and EPMA methods.....	34
3.3.3. XRD methods.....	35
3.3.4. Mathematical calculations of reaction rate	36
Chapter 4. Results	38
4.1 Mass change	38
4.2 Actual and recalculated CO evolution rate.....	39
4.3 Morphology of unreacted and reacted pellets	48
4.4 XRD results	56
Chapter 5. Discussion.....	57
5.1 Influence of H ₂ in the reaction rate.....	57
5.2 Influence of CO in the reaction rate	60
5.3 Influence of the flow rate of Ar-CO gas mixture in the reaction rate.....	63
5.4 Influence of the flow rate of pure argon in the reaction rate	65

5.5	Activation energy	67
5.6	Kinetics modelling	68
5.7	Evaluation of experimental setup	77
5.7.1.	Condensation chamber	77
5.7.2.	Flow rate of CO gas	77
5.7.3.	Source of error	78
Chapter 6.	Conclusion.....	80
6.1	Influence of H ₂ in the reaction rate	80
6.2	Influence of CO in the reaction rate	80
6.3	Influence of the flow rate of CO-Ar gas mixture in the reaction rate	80
6.4	Influence of the flow rate of pure argon in the reaction rate	81
Chapter 7.	Future work	82
References.....		83
Appendix.....		86

List of Figure

Figure 2-1 A typical plant for silicon metal production[1]	3
Figure 2-2 Equilibrium diagram for the dominating reactions in silicon production process. Total pressure between SiO and CO has been assumed to be one bar [1].....	5
Figure 2-3 Equilibrium diagram for reaction 2.1 plotted against temperature and partial pressure of SiO, calculated with data from HSC 4.1. The total pressure of CO and SiO is assumed to be 1atm, 0.8atm and 0.5atm respectively.	6
Figure 2-4 Illustration of how to determine E from three different temperature at constant α by the Friedman methods.	9
Figure 2-5 SiO loss as a function of time, T=1400deg.[19]	13
Figure 2-6 SiO ₂ /SiC reacted as a function of the %SiO ₂ lost under various conditions.....	14
Figure 2-7 Arrhenius plot of SiO ₂ + SiC reaction taking place under constant evacuation[19].....	15
Figure 2-8. Effect of CO pressure on rate of SiO ₂ /SiC reaction relative to rate in vacuum (0-311mm). R/R ₀ against pressure of added CO at 1435 °C. • , time of run = 2 h, R ₀ = 0716 g; , time of run =4 h, R ₀ = 0.359 g. Dashed line constructed from eqn. (3.5) using k = 12.[20]	16
Figure 2-9 The conversion fraction of SiO ₂ /SiC mixture versus temperature with different heating rates[25].....	18
Figure 2-10 Non-parametric kinetic results for the SiO ₂ + SiC mixture. The f and k vectors are given in (a) and (b) respectively. (c), (d) and (e) illustrate the accuracy of the result by comparing measured conversion rate with the estimated conversion rate for each SiO ₂ +SiC experiment.[25]	19
Figure 2-11 The conversion of SiO ₂ +SiC reactions versus holding time at 1700°C for different quartz type in different atmosphere.[22]	20
Figure 2-12 The conversion rate for SiC+SiO ₂ [27]	21
Figure 2-13 The reaction rate for SiC+SiO ₂ [27].....	21
Figure 2-14 Conversion of SiO ₂ +SiC reaction under pure CO and pure Ar gas atmosphere	22
Figure 2-15 Conversion rate of SiO ₂ +SiC reaction under different gases versus	

temperature	23
Figure 2-16 Effect of hydrogen content in the Ar-H ₂ gas mixtures on the reduction of quartz. The furnace temperature was ramped from 573 K to 1873 K (300 °C to 1600 °C) at 3 K/min	23
Figure 2-17 Rate of SiO formation in H ₂ as a function of mass transfer coefficient at 1923K.....	25
Figure 2-18 The rate of silica reduction in CO as a function of mass transfer coefficient at 1923K.....	25
Figure 3-1 Volume distribution of raw materials (batch 2). Cumulative volume is shown in (a) and frequency is shown in (b).....	29
Figure 3-2 The appearance of Resina furnace	30
Figure 3-3 a sketch and a schematic drawing of the graphite crucible set-up	31
Figure 3-4 Temperature profile of an isothermal reaction experiment at 1700 °C	32
Figure 4-1 (a) CO evolution rate in the isothermal reaction between quartz and silicon carbide in pure Ar; (b) recalculated CO evolution rate based on total mass loss	40
Figure 4-2 (a) CO evolution rate in the isothermal reaction between quartz and silicon carbide in 0.1CO+0.3Ar; (b) recalculated CO evolution rate based on total mass loss	41
Figure 4-3 (a) CO evolution rate in the isothermal reaction between quartz and silicon carbide in 0.1CO+0.2Ar; (b) recalculated CO evolution rate based on total mass loss	42
Figure 4-4 (a) CO evolution rate in the isothermal reaction between quartz and silicon carbide in pure H ₂ ; (b) recalculated CO evolution rate based on total mass loss	43
Figure 4-5 (a) CO evolution rate in the isothermal reaction between quartz and silicon carbide in 0.2H ₂ +0.2Ar; (b) recalculated CO evolution rate based on total mass loss	44
Figure 4-6 (a) CO evolution rate in the isothermal reaction between quartz and silicon carbide in 0.1CO+0.3Ar(batch 1); (b) recalculated CO evolution rate based on total mass loss	45
Figure 4-7 (a) CO evolution rate in the isothermal reaction between quartz and	

silicon carbide in 0.8Ar; (b) recalculated CO evolution rate based on total mass loss	46
Figure 4-8 (a) CO evolution rate in the isothermal reaction between quartz and silicon carbide in pure 0.2CO+0.6Ar; (b) recalculated CO evolution rate based on total mass loss	47
Figure 4-9 SEM images, (a) the surface of initial pellets (b) the surface of reacted pellets, (c) the polished section of initial pellets, (d) the polished section of reacted pellets.....	50
Figure 4-10 Backscattering image, (a) the polished section of initial pellets, (b) the polished section of initial pellets in higher magnification, (c) the polished section of reacted pellets at 1700 °C. (d) the polished section of reacted pellets in higher magnification	52
Figure 4-11 EPMA of initial pellets.....	54
Figure 4-12 EPMA of reacted pellets at 1700 °C with the presence of Ar-CO	55
Figure 4-13 XRD patterns of initial pellets before and after sintering process, final pellets in the presence of H ₂ and Ar.....	56
Figure 5-1 (a) Conversion rate of SiO ₂ +SiC reaction versus time in the presence of H ₂ -Ar.....	58
Figure 5-2 (a) Conversion rate of SiO ₂ +SiC reaction versus temperature in the presence of H ₂ -Ar	59
Figure 5-3 (a) Conversion rate of SiO ₂ +SiC reaction versus time in the presence of CO-Ar	61
Figure 5-4(a) Conversion rate of SiO ₂ +SiC reaction versus temperature in the presence of CO-Ar	62
Figure 5-5 (a) conversion rate of SiO ₂ +SiC reaction with different rate of Ar-CO mixture(25%CO), (b) conversion of SiO ₂ +SiC reaction in different rate of Ar-CO mixture (25%CO).....	64
Figure 5-6 (a) conversion rate of SiO ₂ +SiC reaction with different rate of Ar, (b) conversion of SiO ₂ +SiC reaction in different rate of Ar.....	66
Figure 5-8 Logarithm of the reaction rate potted against 1/T for the SiO ₂ +SiC reaction. T=1650 °C and 1700 °C respectively.....	67
Figure 5-9 Reaction model: f(α) versus α.	70
Figure 5-10 (a) and (b) shows graphical representation the possible reaction	

models given in Table 2-1. (c) shows the similarity between the auxiliary function for the SiO_2+SiC reaction and the unimolecular decay model.....	72
Figure 5-11 d as a function of H_2 concentration, CO concentration and flow rate of gas flow.	74
Figure 5-12 Comparison of the measured reaction rate with the estimated values (0.4Ar).....	74
Figure 5-13 Comparison of the measured reaction rate with the estimated values (0.1CO+0.3Ar).....	75
Figure 5-14 Comparison of the measured reaction rate with the estimated values (0.2 H_2 +0.2Ar)	75
Figure 5-15 Comparison of the measured reaction rate with the estimated values (0.4 H_2).....	76
Figure 5-16 Comparison of the measured reaction rate with the estimated values (0.8Ar).....	76
Figure 5-17 CO concentration of off-gas with the process gas 0.4 l/min CO and 0.4 l/min Ar.	78

List of Table

Table 2-1 Reaction models [15].....	10
Table 2-2 Values of the kinetic parameters obtained by Filsinger et al. Here k refers to the equilibrium constant and A, B and E refers to equation 2.12.[23] ...	17
Table 2-3 Binary diffusivities and kinematic viscosities of gases at 1923K	26
Table 2-4 Summary of previous published articles relating kinetics of SiO ₂ +SiC reaction.....	27
Table 3-1 Chemical analysis of Tana quartz-15 (SINTEF).....	28
Table 3-2 Experiments overview	33
Table 4-1 Mass change in experiments performed in the Resina a furnace.....	38
Table 4-2 Elements analysis by EDS (at %)	53
Table 5-1 conversion and relative conversion of small peaks	60
Table 5-2 Kinetics data under different gas species.....	73
Table 5-3 Kinetics data under different gas species (recalculated).....	73

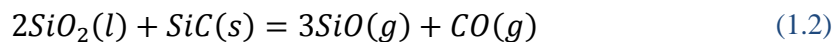
Chapter 1. Introduction

1.1 Background

As the second-most abundant element in the earth's crust, silicon has a large impact on modern world economy. Silicon has been used as raw material for the semiconductor industry since silicon with impurities in the ppb (part per billion) range was produced in 1950[1]. In recent years, a new and interesting application of silicon with impurities in the ppm (part per million) range is the photovoltaic industry. The main raw material for the photovoltaic industry is solar grade silicon (SoG-Si). SoG-silicon is mainly produced from metallurgical grade silicon (MG-Si). Industrially, MG-Si is produced by carbothermic reduction of quartz with carbon in the electric arc furnaces. The overall reaction is



The SiO gas is one of the main variables determining reactions in the furnace. As a major step in the silicon production process, the SiO-forming reaction between quartz and silicon carbide (reaction 1.2) is the main focus of this work. Having a good understanding of the reaction kinetics is vital for the improvement of the production efficiency.



However, using coke as the fuel source and the reducing agent in silicon production causes high CO₂ emission. An alternative solution is to use natural gas to replace coke. The benefits of using natural gas in silicon production is not only limited in the environmental aspect, it will also help the silicon producers to get rid of the reliance of coke. When natural gas is introduced into the silicon production process, cracking of methane will occur according to reaction 1.3[2]. As natural gas is heated above 500 °C, it is expected that formation of hydrogen will occur, accompanied with the deposition of carbon.



Therefore, H₂ and CO becomes the main gas species inside the furnace.

1.2 Objective of the thesis

The main objective of this work is to investigate the effect of different gas species on the rate of SiO_2+SiC reaction at 1700 °C.

The detailed objectives are listed below:

1. Find the effect of different CO gas concentration in CO-Ar mixture on the rate of the SiO_2+SiC reaction.
2. Find the effect of different H_2 gas concentration in Ar- H_2 mixture on the rate of the SiO_2+SiC reaction.
3. Find the effect of the gas flow rate on the rate of the SiO_2+SiC reaction.
4. Find the mathematical expression of the rate of the SiO_2+SiC reaction.
5. Evaluate the experimental setup and improve the stability of the furnace operation.

The methods used to achieve this goal include the off-gas and thermogravimetric analysis at 1700 °C and characterization methods of initial and final pellets including: particle size distribution test, XRD, SEM, BSD, EDS, EPMA analysis. Details of the experimental methods will be covered in experimental section.

Chapter 2. Theory and literature

2.1 Silicon production process

Metallurgical silicon is produced by the reduction of silica in an electric arc furnace by carbonaceous materials. Fig 2-1[1] shows a typical plant for the production of silicon metal. Quartz or quartzite and carbon material, such as charcoal, coal and woodchips, are charged on the top of furnace. As the raw materials descend down into the furnace, several reactions start occurring. The current supplied by electrodes heats part of the charge to about 2000°C in the hottest part. At this high temperature the silicon dioxide is reduced to molten silicon. As shown in fig 2-1, the silicon metal with impurities is tapped through a tap hole at the bottom of the furnace. Through the refining process, impurities will be removed and the silicon metal with high purity will be produced. The submerged arc furnace is the core part in silicon production process.

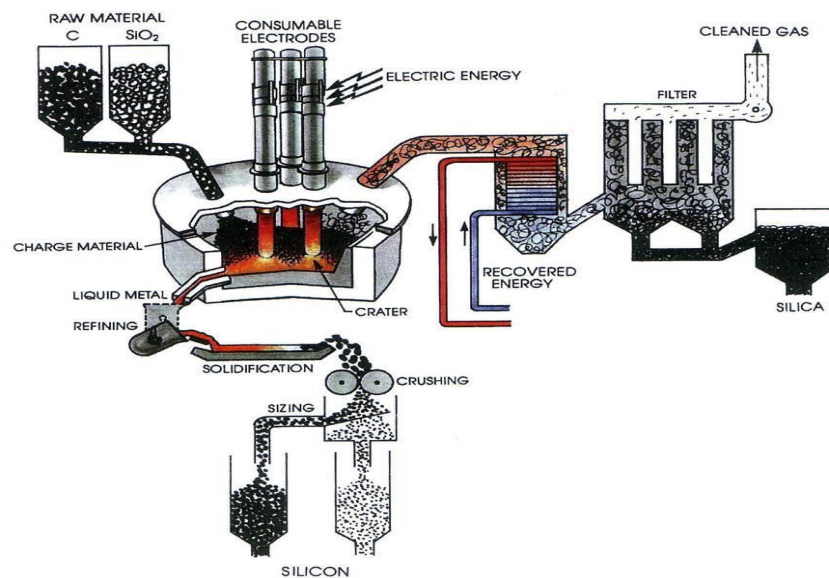
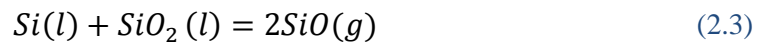
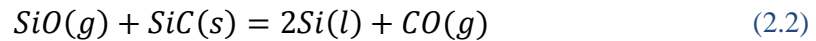
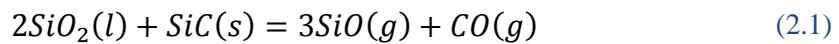


Figure 2-1 A typical plant for silicon metal production[1]

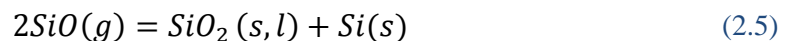
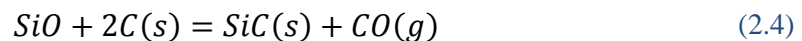
2.2 Reactions in the furnace

In the submerged arc furnace, the reaction between silica and carbon materials happens under atmospheric pressure in the range of temperature from 1573K to 2273K (1300 °C to 2000 °C). Based on the temperature difference, the furnace can be divided into two zones: the low temperature zone (outer zone) and the high temperature zone (inner zone).

In the inner zone, molten silica and silicon carbide react with each other and form SiO gas and CO gas according to reaction 2.1, which is the concern of this study. Poch and Dietzel [3] found that the reaction is rather slow in mixed powders [SiO₂+xSiC] at 1bar in a stream of CO and Ar below 1550°C. In vacuum, the reaction rate is significant at lower temperature. Silicon metal is finally produced as shown in reaction 2.2. Main reactions in the high temperature area are summarized as follow:



In the outer zone, the SiO gas will be captured by carbon when reaction 2.4 takes place. This is an important reaction regarding the total Si-yield in the industrial furnace. SiO gas may also condensate to SiO₂ and Si or SiC and CO gas. Poch and Dietzel [3] sent a mixture of Ar, SiO and CO through a chamber with corundum pieces at 1300°C-1500°C. They found a deposit that contained SiO₂ and Si, according to reaction 2.5. It has been confirmed by later studies.



2.3 Thermodynamic considerations

In the reduction furnace, there may be several solid phases, liquid phases and one gas phase in the reduction zone. The zone can be considered as a chemical system consisting of a number of phases. The thermodynamic variables of this system are temperature, pressure and composition of the phases. Figure 2-2 shows the equilibrium between two condensed phases and a gas phase in the $\text{SiO}_2\text{-SiC-C-SiO-Si}$ system in the temperature range of 1400-2200 °C. It is assumed that the gas phase consists only of SiO and CO gas, and the total pressure is equal to 1 bar. Activities of all condensed species are equal to unity. Thermodynamically, reaction 2.1 requires a temperature over 1400 °C and a low SiO-pressure to drive reaction 2.1 to the right. The distance from equilibrium determines the reaction rate, therefore, a low SiO pressure will give a high reaction rate.

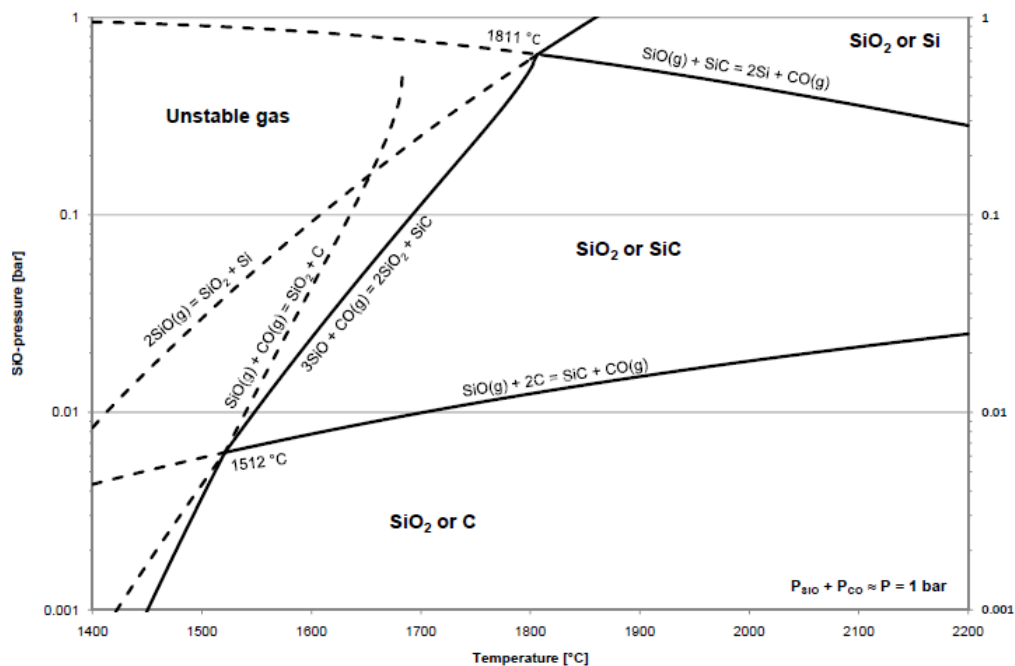


Figure 2-2 Equilibrium diagram for the dominating reactions in silicon production process.

Total pressure between SiO and CO has been assumed to be one bar [1]

The equilibrium diagram for reaction 2.1 plotted against the temperature and the partial pressure of SiO is presented in Figure 2-3, the data used in the diagram is calculated by HSC 4.1. The total pressure of CO and SiO is assumed to be 1 atm if no extra gas is added into the system. If Ar or H₂ is added into the system, the total pressure of CO and SiO is less than 1. Two lines with the total pressure of CO and SiO assumed to be 0.5 atm and 0.8 atm are shown in Figure 2-3.

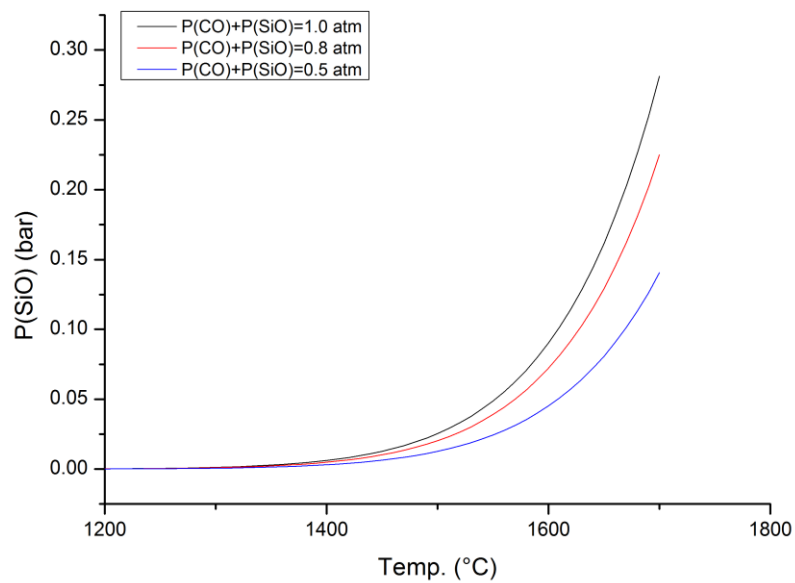


Figure 2-3 Equilibrium diagram for reaction 2.1 plotted against temperature and partial pressure of SiO, calculated with data from HSC 4.1. The total pressure of CO and SiO is assumed to be 1atm, 0.8atm and 0.5atm respectively.

2.4 Kinetics considerations

2.4.1. Reaction rate

Acquiring knowledge of the reaction kinetics is valuable not only for the ability to predict reaction rates under other environments than tested, but also for the prediction of the reaction mechanism. The reaction rate describes how fast a reaction approaches equilibrium. The general definition of reaction rate, r , for a general reaction (2.6), is given by Eq.2.7.



$$r = -\frac{1}{a} \frac{d[A]}{dt} = -\frac{1}{b} \frac{d[B]}{dt} = \frac{1}{c} \frac{d[C]}{dt} = \frac{1}{d} \frac{d[D]}{dt} \quad (2.7)$$

where $[X]$ denotes the concentration of the substance X.

$$r = \frac{dW}{dt} \quad (2.8)$$

If a gas product is formed, the mass change can be modified to express the reaction rate. Usually, this is done by defining a parameter, α , which expresses the extent of the reaction.2.10

$$\alpha = \frac{W - W_o}{W_f - W_o} \quad (2.9)$$

Here, W indicates the mass of the sample, W_o is the starting mass of the sample while W_f is the mass of the sample after completion of the reaction. If the reaction only has gaseous products the reaction rate is then expressed by Eq2.10.

$$r = \frac{d\alpha}{dt} = -\frac{1}{W_o} \cdot \frac{dW}{dt} \quad (2.10)$$

The reaction kinetics depends on a variety of parameters such as reactivity of materials, temperature, the surface area, the gas atmosphere, etc. A rate expression consisting of a temperature-dependent factor, a factor representing the change of solid particles as well as the influence of gas atmosphere were specified to model the reaction system. The reaction rate can be expressed by Eq.2.11.

$$\frac{d\alpha}{dt} = f(\alpha)k(T)g(X_{\text{gas}}) \quad (2.11)$$

Where $f(\alpha)$ indicates the reaction kinetics model, $k(T)$ represents the temperature-dependent factor and $g(X_{\text{gas}})$ is the gas-dependent factor.

2.4.2. Arrhenius equation

The temperature-dependent factor originates from the Arrhenius equation given in Eq.2.12. For homogenous reaction kinetics E is viewed as the energy barrier required for the molecules to react, R is the gas constant, T is temperature in Kelvin and A is a pre-exponential factor.

$$k(T) = A \exp\left(\frac{-E}{RT}\right) \quad (2.12)$$

The term $\exp\left(\frac{-E}{RT}\right)$ could then be regarded as the probability of two colliding molecules reacting, while A is the number of colliding reacting molecules per second. When it comes to heterogeneous reactions, the activation energy would be the sum of reactions running at the same time, making the physical interpretation rather obscure.

$f(\alpha)$, A and E are often called kinetic triplets. Isothermal and non-isothermal methods are often adapted to derive the kinetic triplets. Since the parameters of in the kinetics triplets are interlinked, it is important to start with one parameter with highest accuracy. Normally, the activation energy is the first parameter that can be derived through a ‘model-free’ approach. The most popular model-free approaches have been summarized by Ortega[4], Vyazovkin et al. [5] and Sewry et al. [6].

Iso-conversional methods are one of the most popular approaches. This method have been reviewed by several researchers such as Malek et al. [7], Elder et al. Budrugaec et al. [8-10], Simon[11] and Zsako[12].

Fridman [13] proposed the first model-free approaches in 1964. Disregarding $g(X_{\text{gas}})$ factor, combing Eq. 2.11 and Eq. 2.12 and taking the logarithm Eq.2.11 will be

$$\ln\left(\frac{d\alpha}{dt}\right) = \ln[Af(\alpha)] - \frac{E}{R}\left(\frac{1}{T}\right) \quad (2.13)$$

The plot between $\ln\left(\frac{d\alpha}{dt}\right)$ and $1/T$ gives the activation energy at the constant α . The

slope of the plot is the fraction $-E/R$. The Friedman methods require several runs with different temperature and are called a differential methods.

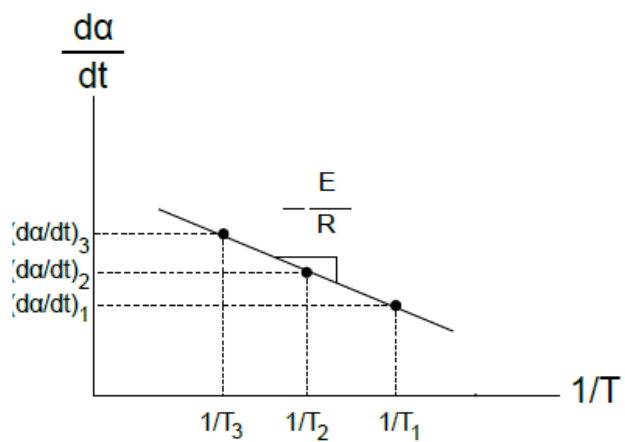


Figure 2-4 Illustration of how to determine E from three different temperature at constant α by the Friedman methods.

2.4.3. Physio-geometric kinetics model

The plot of $f(\alpha)$ versus α gives the characteristic of the reaction mechanism. Many mathematical models have been proposed to examine the reaction mechanism, as is summarized in Table 2-1. Each of the equations is derived from a physical phenomenon limiting the reaction. The diffusion equations are derived from Fick's diffusion law through a product layer. 1D-model (one dimensional) describes the diffusion through a plate layer, 2D-model represents a cylindrical layer and 3D-model shows diffusion through a spherical product layer. The diffusion-based models are well explained by Dickinson et al. [14].

Table 2-1 Reaction models [15]

Mechanism	Symbol	$f(\alpha)$
Unimolecular decay	F1	$(1 - \alpha)$
Nucleation and growth ($n = 0.5, 1, 1.5, 2, 2.5, 3, 4$)	JMA	$n(1 - \alpha)[- \ln(1 - \alpha)]^{1-1/n}$
Phase-boundary controlled reaction ($n = 0, 1/3, 2/3$)	R_n	$(1 - \alpha)^n$
1D-diffusion	D1	$1/2\alpha$
2D-diffusion	D2	$-1/\ln(1 - \alpha)$
3D-diffusion (Jander equation)	D3	$[3(1 - \alpha)^{2/3}]/[2[1 - (1 - \alpha)^{1/3}]]$
3D-diffusion (Ginstling-Brounshtein equation)	D4	$3/2[(1 - \alpha)^{-1/3} - 1]$
Solid-liquid (Contracting interface)	S1	$(1 - \alpha)^{4/3}$
Solid-liquid (Interface and product layer)	S2	$\frac{1}{1/(3(1 - \alpha)^{4/3}) - 1/(3(1 - \alpha))}$
Solid-liquid (Activity controlled diffusion of reactants)	S3	$\frac{1}{1/(3(1 - \alpha)^{8/3}) - 1/(3(1 - \alpha)^{7/3})}$

Previous work on the $\text{SiO}_2 + \text{SiC}$ reaction has shown that this reaction is controlled by unimolecular decay, 1D-diffusion, desorption and removal of the gaseous product.

2.4.4. Influence of mass transfer

When the gaseous product is involved in the reaction, the effect of mass transport of the product gas on reaction kinetics should also be taken into consideration. Altorfer [16] discussed the effect of mass transfer and suggested that a correction could be made through a correction term γ , yielding eq2.15. The correction term has been critically analyzed by Ortega [17] and Criado et. al [18].

$$\gamma = \frac{P_p}{P_{eq}} \quad (2.14)$$

$$\frac{d\alpha}{dt} = f(\alpha)k(T)(1 - \gamma) = f(\alpha)k(T)\left[\frac{P_{eq}-P_p}{P_{eq}}\right] \quad (2.15)$$

$$Q_r = \frac{P_{CO,P} \cdot P_{SiO,P}^3}{\alpha_{SiO_2}^2 \cdot \alpha_{SiC}} \quad (2.16)$$

$$K_{eq} = \frac{P_{CO,eq} \cdot P_{SiO,eq}^3}{\alpha_{SiO_2,eq}^2 \cdot \alpha_{SiC,eq}} \quad (2.17)$$

The correction term γ is given as the ratio between the partial pressure of the evolved product gas at the reaction site, P_p , and the equilibrium partial pressure for the given temperature, P_{eq} . $1-\gamma$ is basically an expression of the distance from equilibrium and can be expressed as the reaction state, Q_r , divided by the equilibrium constant, K_{eq} .

In order to investigate the effect of different gas atmosphere on the reaction rate, a gas-dependent factor, $g(X_{gas})$, is introduced. The reaction rate can be expressed by Eq. 2.18.

$$\frac{d\alpha}{dt} = A f(\alpha) \cdot \exp\left(-\frac{E}{RT}\right) \cdot g(X_{gas}) \quad (2.18)$$

Where X_{gas} = the concentration of added gas, E = activation energy, A = pre-exponential factor, α = the extent of the reaction and $f(\alpha)$ = physio-geometric kinetic model. A , E and $f(\alpha)$ are sometimes called kinetic triplet.[15]

To quantitative the effect of reaction conversion on the geometry of reactants in its simplest form (see Table 2-1), a linear relation between $f(\alpha)$ and α is expressed by Eq.2.18

$$f(\alpha) = a - b\alpha \quad (2.19)$$

Therefore, the reaction rate can be expressed by eq.2.19

$$\frac{d\alpha}{dt} = A (a - b\alpha) \cdot \exp\left(-\frac{E}{RT}\right) \cdot g(X_{gas}) \quad (2.20)$$

2.5 Previous work

Sufficient knowledge of the reactions kinetics in silicon process is crucial of a good understanding of the production process. Previous publications investigating the kinetics of SiO_2+SiC reaction are listed below.

Pultz and Hertl [19] investigated the mechanism and kinetics of the reaction between silica and silicon carbide by the non-isothermal method in 1966. The experiments were conducted isothermally by heating samples at a constant temperature. In Figure 2-5, one experiment is held at 1400 for 6 hours without added gas. The silica loss was used as a measure of reaction rate in the experiments. Figure 2-5 shows that the loss of silica is linear with time. This is because only the upper layers of the charge are contributing to the net forward reaction rate. The reacted stoichiometries are plotted in Figure 2-6 as the SiO_2/SiC reacted against %silica lost. Also included in the figure are data for the reaction taking place in the presence of various gases and at various temperatures. The two solid lines bracketing the points were constructed assuming that the extent of the reaction taking place with a stoichiometry of 0.5/1 is 2% and 6% separately. Almost all the experimental points fall within the two constructed lines. From this, it is concluded that the silicon produced initially via reaction 2.21 desorbs and is transported downstream.

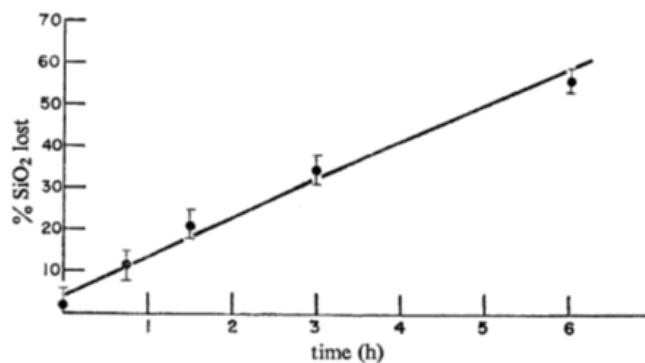


Figure 2-5 SiO loss as a function of time, $T=1400\text{deg}$. [19]

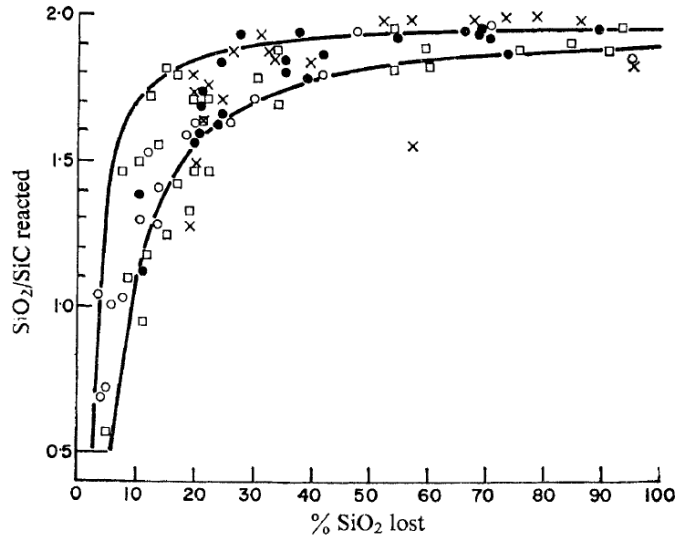
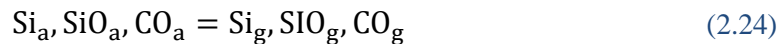
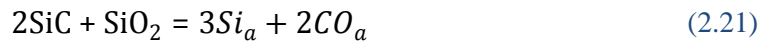


Figure 2-6 SiO_2/SiC reacted as a function of the % SiO_2 lost under various conditions.

●, constant evacuation and also added inert gas (1270-1610 °C) ; ○, added CO (1434 °C) ; ×, N_2 (1434 °C) ; □, with and without added inert gas (1400-1460 °C).

Pultz et al. proposed the following reaction scheme:



Here, the subscript $_a$ denotes gas in an adsorbed state.

Pultz et al. concluded that the desorption or the diffusion of product gas was the rate limiting step. It was also found that silica reacts with silicon carbide at temperature above about 1250°C and added CO gas suppressed the reaction rate. Pultz et al. believed that the CO gas blocked available reaction sites. In the absence of added CO gas, the desorption of carbon monoxide from SiC surface was considered as rate limiting step.

The Arrhenius plot is shown in Figure 2-7 and the apparent activation energy of the desorption of carbon monoxide from the active sites vary from 548 to 406 KJ/mole (131 to 97 kcal/mole) in the temperature between 1270°C and 1430°C.

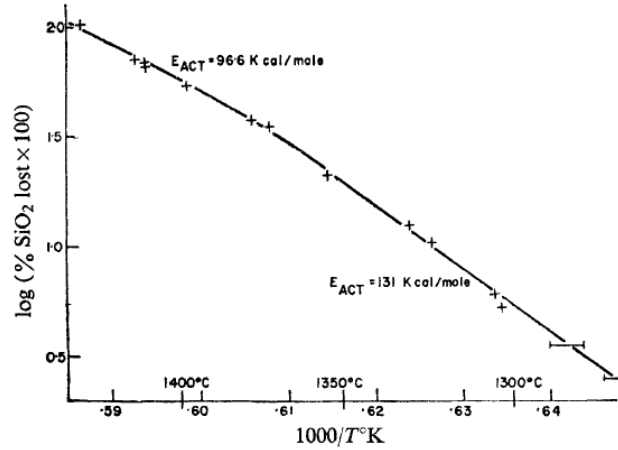


Figure 2-7 Arrhenius plot of SiO₂+ SiC reaction taking place under constant evacuation[19]

The effect of different gas species on the reaction between silica and silicon carbide was also investigated by Hertl et al [20]. In general, the rate of reaction between silica and silicon carbide is depressed by added gases. With inert gases this depression is a function of the molecular weight and pressure of the gas. Experiments were run by heating SiO₂/SiC samples in the temperature range 1425-1445 °C for a period of 4-8 hours under different gas atmosphere. The silica loss is used as a measure of the amount of net forward reaction and is given as R/ R₀ where R is the observed silica loss for a given experiment and R₀ is the same silica loss under the same conditions without added gas. The data for experiments with added carbon monoxide is shown in Figure 2-8. The rate using CO gas is decreased to less than 10% of the rate with no gas added. Since the rate-limiting step in the reaction is the desorption of carbon monoxide from the silicon carbide surface, an active site becomes available for further reaction. The observed rate should then be

$$R = R_0 f(1 - \theta) \quad (2.25)$$

$$(1 - \theta) = \left[1 - \frac{P_{CO}}{k + P_{CO}} \right] = \frac{R}{R_0} \quad (2.26)$$

Here, (1-θ) is the fraction of uncovered surface sites. Eqn. (2.26) is adsorption isotherm form. P_{CO} is the pressure of added carbon monoxide and k is a constant, the curve was fitting to the experimental point in Figure 2-8.

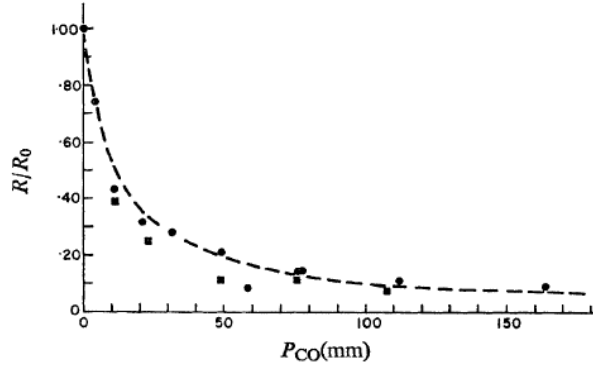
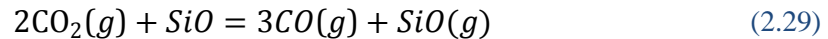
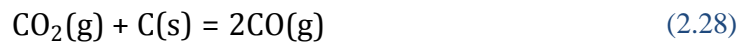


Figure 2-8. Effect of CO pressure on rate of SiO₂/SiC reaction relative to rate in vacuum (0-311mm). R/R₀ against pressure of added CO at 1435 °C. •, time of run = 2 h, R₀ = 0.716 g.; time of run = 4 h, R₀ = 0.359 g. Dashed line constructed from eqn. (3.5) using k = 12.[20]

Wiik [21] investigated the kinetics between silica and carbon in 1990 and he found the rate of weight loss of cristobalite + graphite was two times higher than the rate of quartz + graphite at 1558°C in 1.066 bar CO, which means cristobalite accelerates the reaction of SiO₂ and carbon. Adisty [22] found similar results in reaction between quartz and silicon carbide in 2013. This is because cristobalite has a higher surface area than quartz.

The mechanism of reaction between quartz and carbon was thought to be through the CO-CO₂ mechanism. The reaction series are shown below:



Wiik proposed the same reaction mechanism for reaction between SiO₂+SiC, which involves four stages, as follows:

- 1) Adsorption of CO (g) on the SiO₂ surface
- 2) Production of SiO (g)
- 3) Desorption of SiO (g) and CO₂ (g) from the quartz surface
- 4) Diffusion of SiO (g) and CO₂ (g) and away from the quartz surface by bulk gas flow

Adsorption of carbon monoxide on the silica surface was determined as the rate-determining step.

This reaction was also studied by Filsinger et al [23]. The reaction path and kinetics were determined through TGA analysis, CO measurements and XRD analysis of the products. All experiments were done under helium atmosphere. Both non-isothermal methods and isothermal methods were used to determine the kinetic parameters. Table 2-2 shows the value of the kinetic parameters for the reactions in this report.

Table 2-2 Values of the kinetic parameters obtained by Filsinger et al. Here k refers to the equilibrium constant and A, B and E refers to equation 2.12.[23]

Reaction	$\ln k = A(10^4/T) + B$			E [$\frac{kJ}{mol}$]
	T [K]	A	B	
$2SiO_2 + SiC = 3SiO + CO$	1833-2033	-4.18	17.55	348
$SiO_2 + Si = 2SiO$	1683-1883	-4.18	16.95	348

The reaction mechanism, $f(\alpha)$, was found to fit the unimolecular decay law (F1) well as given by Table 2-1, that is a linear correlation between $f(\alpha)$ and α

Khrushchev [24] investigated the reaction between silica and silicon carbide by treating samples isothermally at temperature of 1800°C, 1850°C, and 1900°C for different time. It worth noting that temperatures were above the melting point of silica (1730°C), which means the reaction taking place inside the furnace was a solid-liquid reaction. Several experiments showed that the deposit, brown or pale blue, was typically present between 1400°C and 1500°C. XRD analysis of the deposit showed that it consisted of cristobalite, silicon and silicon carbide. This indicates that part of SiO decomposes into SiO₂ + Si while the rest of SiO reacts with CO to form SiO₂+SiC.

The author believed that the reaction rate is limited by the carbon diffusion from the SiC bulk to the SiC/SiO₂ interface, where carbon reacts with the SiO and oxygen from SiO₂ decomposition. The conversion of this reaction can be expressed by the one-dimensional diffusion equation as follow:

$$\alpha = \left(6D \frac{M}{\rho} \frac{1}{4\pi r_0^5} \tau\right)^{1/2} \quad (2.30)$$

Where D=diffusion coefficient of carbon in SiC, M and ρ are the molecular weight and density of SiC, r_0 is the particle size of SiC.

The activation energy of this reaction, equal to that of the carbon diffusion from SiC to SiC/SiO₂, was 795 kJ/mol.

Vegar Andersen [25] investigated the kinetics of reaction between SiO₂ and SiC in a stream of argon. The molar ratio of SiO₂ (below 38µm) and SiC is 2:1. Several experiments were carried out by heating samples non-isothermally from 1450 to 2000 °C. Thermogravimetric analyses (TGA) and visual observations of the reactions are used throughout this work. The author found that the reaction rate went through the following stages, as shown in Figure 2-9.

- 1) Exponential increase of reaction rate from 1450 °C to about 1700 °C
- 2) Constant or reduced reaction rate between 1730 °C and 1770 °C
- 3) Rapid increase in reaction rate from 1770 °C.

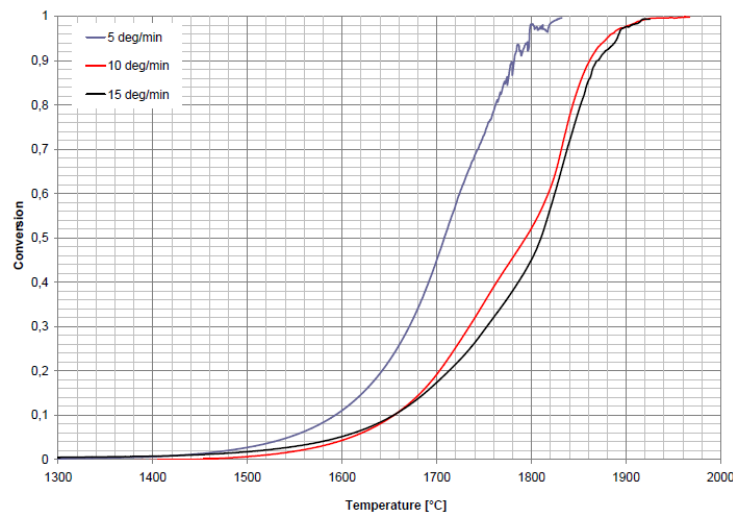


Figure 2-9 The conversion fraction of SiO₂/SiC mixture versus temperature with different heating rates[25]

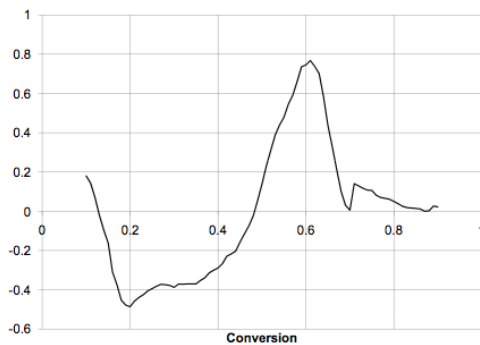
The first stage of reaction is a solid-solid reaction and can be described as a reaction independent of the conversion. The activation energy equals 402kJ/mole and the pre-exponential factor equals $1.301 \times 10^9 \text{ min}^{-1}$. This is given by Eq.2.31.

$$\frac{da}{dt} = 1.301 \times 10^9 \exp\left(-\frac{402000}{RT}\right) \quad (2.31)$$

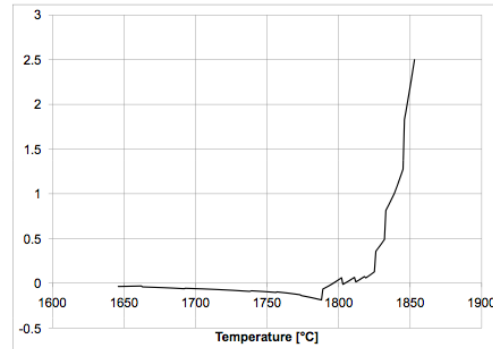
The activation energy is found to be 398 kJ/mole and 404 kJ/mole for the differential and integral method respectively. The solid-solid stage is defined as the range between $a=0.05$ and $a=0.20$.

In the second stage of reaction, the temperature is close to melting point of silica. Molten silica is very viscous at temperature close to melting point and will inhibit transfer of gas severely; therefore, the reaction rate is reduced.

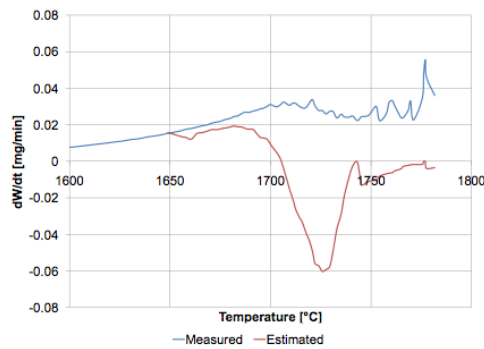
A significant increase of the reaction rate at 1770 °C could be caused by a sufficient reduction of the viscosity of silica, making gas transport through the bubbles easier.



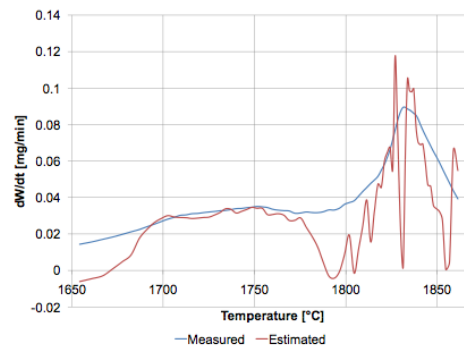
(a) $f(\alpha)$ -vector



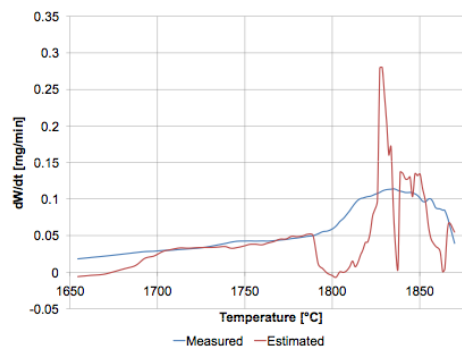
(b) $k(T)$ -vector



(c) 5 deg /min



(d) 10 deg /min



(e) 15 deg /min

Figure 2-10 Non-parametric kinetic results for the $\text{SiO}_2 + \text{SiC}$ mixture. The f and k vectors are given in (a) and (b) respectively. (c), (d) and (e) illustrate the accuracy of the result by comparing measured conversion rate with the estimated conversion rate for each $\text{SiO}_2 + \text{SiC}$ experiment.[25]

Dian Adisty [22] investigated the effects of different types of quartz (quartz and cristobalite) on the reaction between $\text{SiO}_2 + \text{SiC}$. The weight of the mixture of SiO_2 and SiC was measured before and after the experiment and the conversion value of the samples can be seen in Figure 2-11. The conversion versus holding time graph shows that the conversion/weight loss of sample was higher in argon atmosphere than in CO atmosphere. The conversion of β -cristobalite + SiC was higher than α -quartz + SiC in argon flow. The difference of conversion of β -cristobalite + SiC and α -quartz + SiC in CO gas was insignificant. It can be found that the conversion of α -quartz + SiC was slightly higher than β -cristobalite + SiC .

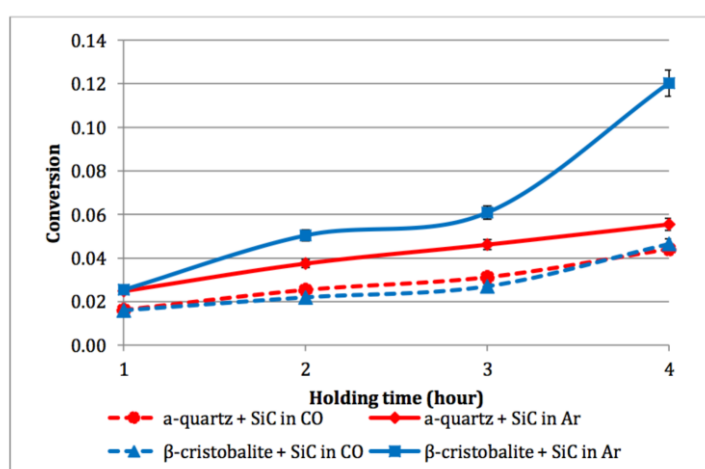
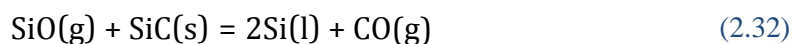


Figure 2-11 The conversion of $\text{SiO}_2 + \text{SiC}$ reactions versus holding time at 1700°C for different quartz type in different atmosphere.[22]

Dian Adisty [26] also investigated the effect of temperature, dwelling time and interfacial surface area on kinetics of $\text{SiO}_2 + \text{SiC}$ reaction. In her study, two different type of pellets, i.e. quartz + SiC and cristobalite + SiC , were heated up to certain temperature and then held to certain dwell time with argon gas at a rate of 1L/min. She found that the conversion of $\text{SiO}_2 + \text{SiC}$ reaction was 0.819 for charges with quartz and 0.914 for charges with cristobalite. The full conversion ($\alpha > 0.990$) was achieved at 1700°C in less than 2 hours for both type of pellets. The higher porosity of cristobalite was found to be the reason for higher conversion. In the temperature range of $1500\text{-}1750^\circ\text{C}$, the reaction of $\text{SiO}_2 + \text{SiC}$ first occurred and then followed by the reaction 3.12.



The presence of SiO_2 , Si and SiC was found by XRD analysis of blackish-brown condensate.

Bao [27] has carried out similar work with approximately 100mg hand pressed powder mixed with SiC and SiO₂, in the molar ratio of 2:1, in a Ta crucible with a graphite holder. Samples were heated to 1550, 1730 or 1820°C at a constant heating rate of 15°C/min and held at 1550, 1730 for 2 hours and at 1820°C for 1 hour respectively. She found that reaction rate was almost constant at 1500°C, and then increases exponentially to 1730 and 1820°C. Higher temperature accelerates the reaction substantially. Figure 2-12 shows that the conversion rate increased obviously with the increase of the temperature until it reached around 0.8. Figure 2-13 shows that the reaction rate of the SiC + SiO₂ agglomerate increased from about 0.1 to 1.3 and 4.1 mg/min with the temperature increasing from 1550 to 1730 and 1820°C, which would give an activation energy of 351 kJ/mole.

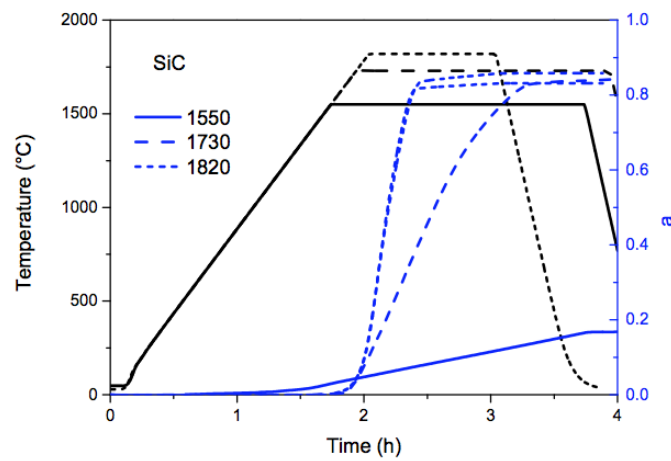


Figure 2-12 The conversion rate for SiC+SiO₂ [27]

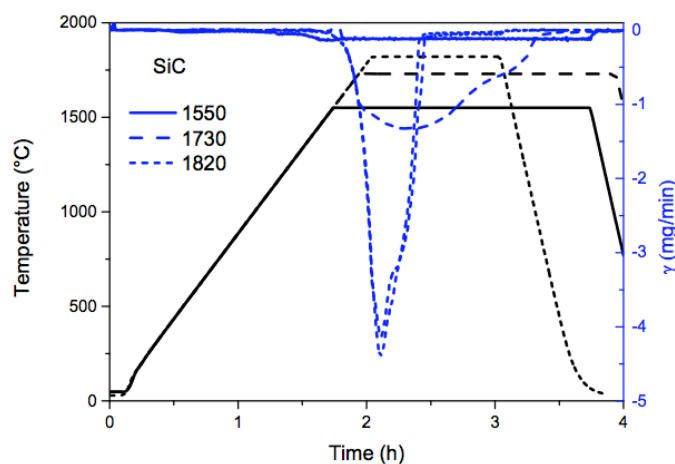


Figure 2-13 The reaction rate for SiC+SiO₂ [27]

The kinetics of SiO_2+SiC reaction in the presence of pure Ar and pure CO gas was investigated by Feng Ni [28]. Experiments were carried out in a TG furnace at $1700\text{ }^\circ\text{C}$ with Ar and CO gas blowing into the furnace. The conversion rate of SiO_2+SiC reaction under Ar and CO was 0.13 and 0.055 respectively, as is shown in Figure 2-15. The conclusion was made that added CO gas suppressed this reaction. The conversion of SiO_2+SiC reaction under Ar and CO atmosphere is shown in Figure 2-14 .

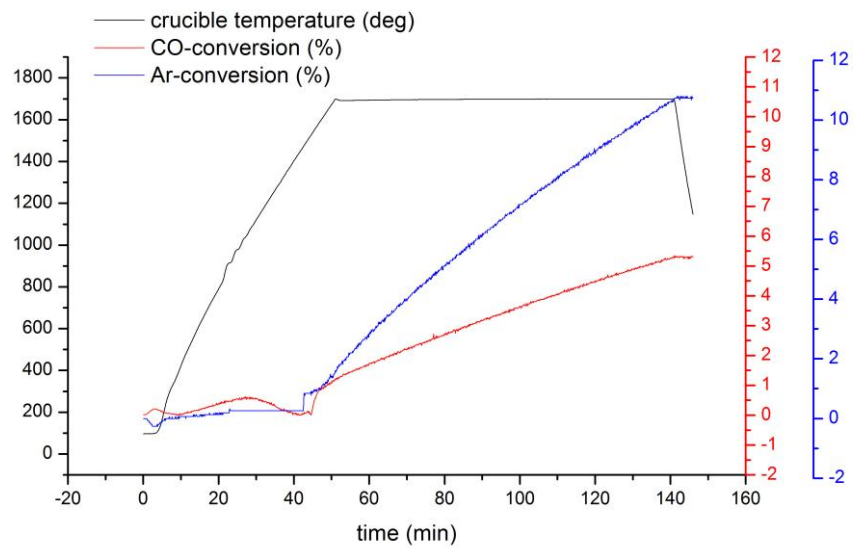
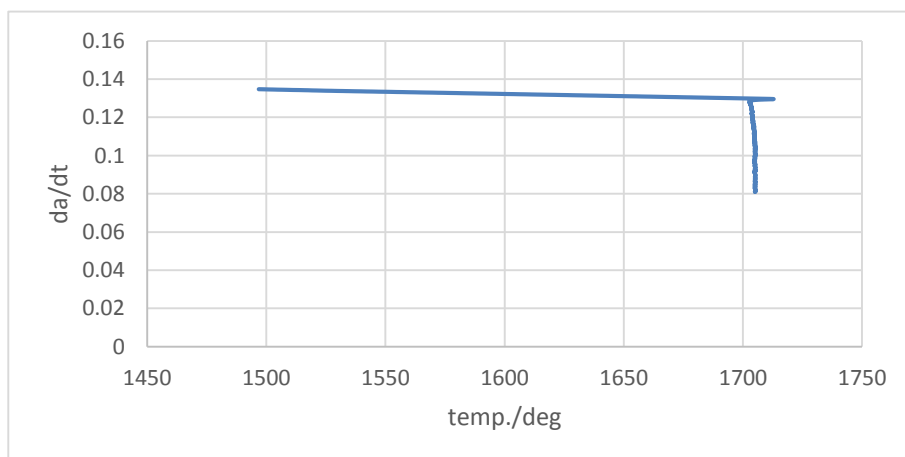
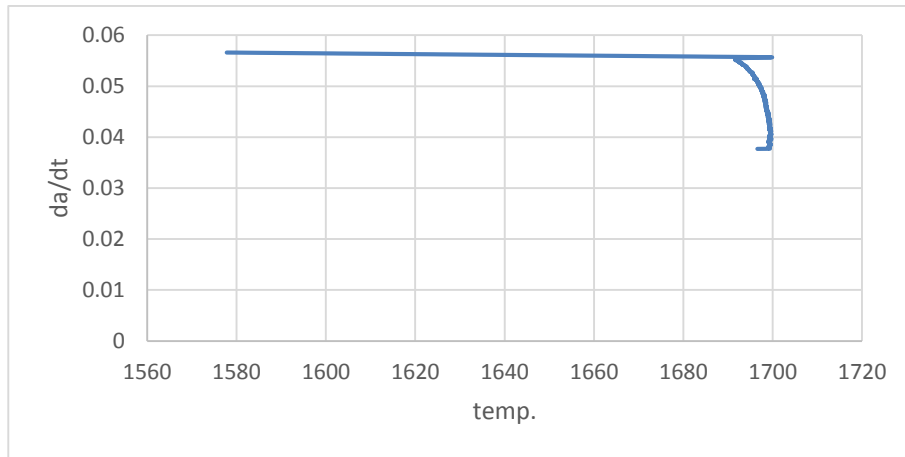


Figure 2-14 Conversion of SiO_2+SiC reaction under pure CO and pure Ar gas atmosphere



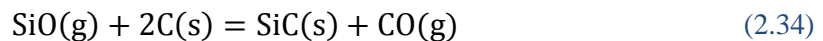
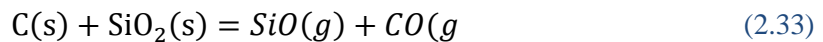
(a)



(b)

Figure 2-15 Conversion rate of SiO_2+SiC reaction under different gases versus temperature
(a) pure Ar, (b) pure CO

The carbothermal reduction of quartz in different gas atmospheres was investigated by Xiang Li [29]. Reduction was studied in isothermal and temperature-programmed reduction experiments in a tube reactor in argon, hydrogen and Ar- H_2 gas mixtures.



The concentrations of CO , CO_2 and CH_4 in the off gas were measured online using an infrared gas analyzer. The carbothermal reduction of quartz in hydrogen was faster than that in argon, as is shown in Figure 2-16. Formation of SiC started at 1573K (1300 °C) in argon, and 1473K (1200 °C) in hydrogen.

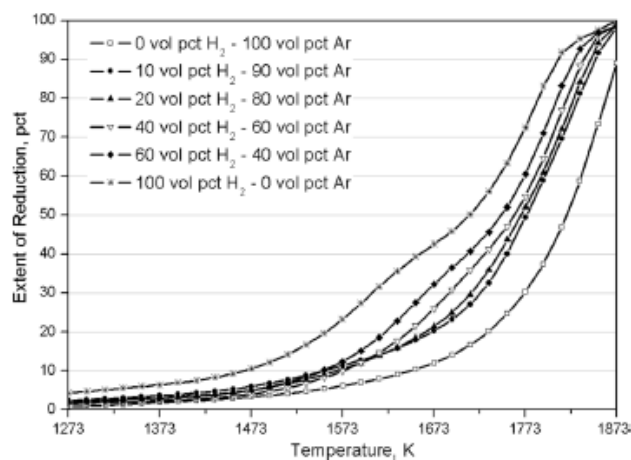


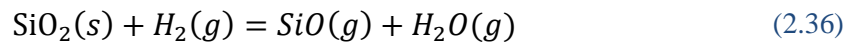
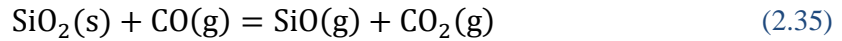
Figure 2-16 Effect of hydrogen content in the Ar- H_2 gas mixtures on the reduction of quartz.

The furnace temperature was ramped from 573 K to 1873 K (300 °C to 1600 °C) at 3 K/min

The author believed that faster carbothermal reduction rate in hydrogen was attributed to the involvement of hydrogen in the reduction reactions by directly reducing silica, or indirectly, by reacting with graphite to form methane as an intermediate reductant.

Recent work demonstrated that the gas atmosphere has a strong effect on the kinetics of the carbothermal reduction of stable metal oxides. Ostrovski et al. [30] investigated the carbothermal solid state reduction of manganese, titanium and aluminum oxides in argon, helium and hydrogen. Gases such as helium and argon were not involved in reduction. The author believed that the difference in reduction in helium and argon was reflected by different diffusion coefficients of gaseous reactants and products, which are much higher in helium than in argon. When hydrogen was introduced to reduction process, the reduction of oxide by hydrogen and methane formation should be involved.

B.Ozturk [31] studied the rate of formation of SiO by the reaction of CO or H₂ with silica. A carbon resistor furnace with a 4.40cm diameter recrystallized alumina reaction tube was used for the reduction of silica by CO and H₂. The rate of silicon monoxide formation was determined from measuring weight loss as a function of time. The weight loss was also checked by weighing the sample before and after the experiments. The reduction reaction of silica by CO and H₂ is listed below



The rate of reduction in terms of the flux of SiO is plotted vs the calculated mass transfer coefficient in Figure 2-17 for varying gas flow rates and sphere diameters. The average mass transfer coefficient is calculated by using Eq. 2.37 and data presented in Table 2-3.

$$m = \frac{D}{d} (2 + 0.6\text{Re}^{\frac{1}{2}} \text{Sc}^{\frac{1}{3}}) \quad (2.37)$$

Where D is the interdiffusivity, d is the diameter of the sphere, Re is Reynolds number, Sc is the Schmidt number. The dashed line in is calculated using Eq. 2.38.

$$J_{\text{SiO}} = \frac{m_i}{RT} (P_{\text{SiO}}^S - P_{\text{SiO}}^B) \quad (2.38)$$

Where J_{SiO} is the flux of SiO, m_i is the average mass transfer coefficient for SiO away from the surface, $P_{\text{SiO}}^{\text{S}}$ and $P_{\text{SiO}}^{\text{B}}$ are the pressure of SiO at the surface and bulk phase.

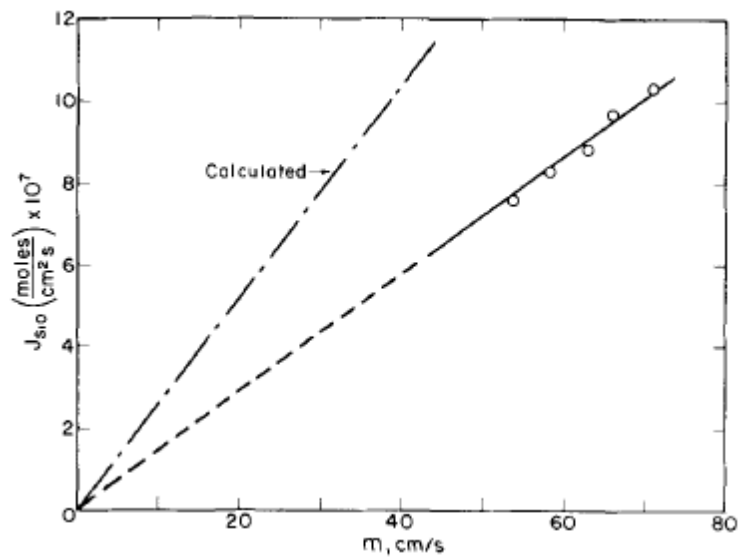


Figure 2-17 Rate of SiO formation in H_2 as a function of mass transfer coefficient at 1923K. As indicated, the rate changes with mass transfer coefficient as would be expected for the gas mass transfer control.

The rate of reduction of SiO_2 given as the flux of SiO is plotted vs mass transfer coefficient in Figure 2-18. The rate does not increase with the mass transfer coefficient as would be expected for mass transfer control. It is probably controlled by chemical kinetics at the gas-solid interphase.

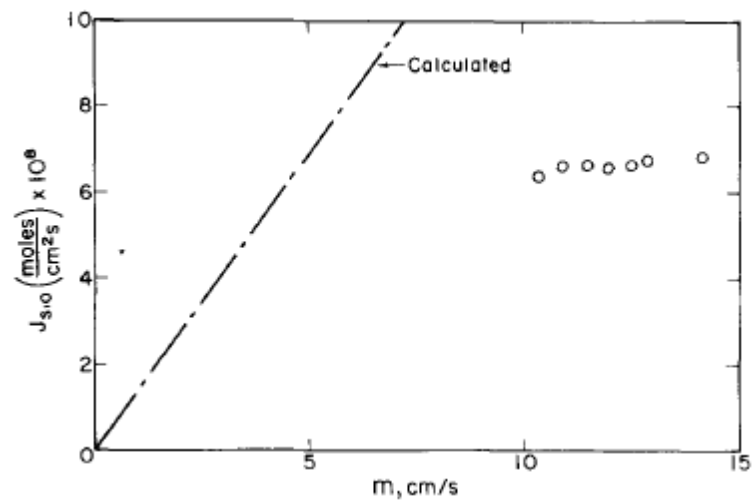


Figure 2-18 The rate of silica reduction in CO as a function of mass transfer coefficient at 1923K

Table 2-3 Binary diffusivities and kinematic viscosities of gases at 1923K

Gas	D, cm ² /sec	Gas	Kinematic Viscosity cm ² /sec
H ₂ O-H ₂	20.59	H ₂	23.59
H ₂ O-He	19.51	H ₂ O	5.62
H ₂ O-Ar	5.89	CO	3.47
H ₂ -He	34.93	CO ₂	2.17
H ₂ -Ar	17.53	He	26.63
CO ₂ -CO	3.72	Ar	3.15
CO ₂ -He	13.18	H ₂ -50 pct He	25.52
CO ₂ -Ar	3.49	H ₂ -50 pct Ar	5.59
CO-He	15.48	CO-50 pct He	6.57
CO-Ar	4.47	CO-50 pct Ar	3.23

The published articles relating to kinetics of SiO₂+SiC reaction are shown in table 2-4. In each article, activation energies are determined by different methods in different temperature ranges. Heating methods in the previous works can be divided into isothermal method and non-isothermal method. Non-isothermal heating method is suitable for the evaluation of SiO₂+SiC reaction in the whole temperature range of Si production process while isothermal method is used to study a certain reaction stage by heating samples at a certain temperature. In addition to the reaction rate, the kinetics data shows the proposed reaction mechanism.

Table 2-4 Summary of previous published articles relating kinetics of SiO₂+SiC reaction

Researchers	Method	Results
Pultz&Hertl (1996)	Non-isothermal 1270-1430°C Solid-solid stage	✓ E = 548 to 406 KJ/mole ✓ RDS: desorption of CO from SiC surface ✓ Si was an intermediate product
Wiik (1990)	Isothermal 1558°C Solid-solid stage	✓ Mechanism: CO-CO ₂ mechanism ✓ RDS: adsorption of CO on SiO ₂ surface
Filsinger (1990)	Non-isothermal 1833-2033°C Isothermal 1410-1800°C	✓ E = 348kJ/mole (non-isothermal)
Khruschev (1990)	Isothermal 1800,1850,1900°C Liquid-solid stage	✓ E = 795kJ/mole ✓ Mechanism, f(α): 1D-diffusion ✓ RDS: diffusion of C in SiC bulk to the SiC/SiO ₂ interface
Andersen (2010)	Non-isothermal 1300-2000°C Mix stages	<i>Solid-solid reaction 1450-T_{melt} (SiO₂):</i> ✓ α=0.05-0.20 ✓ E~400kJ/mole (Integral method) <i>Liquid-solid reaction T > 1760 °C</i> ✓ α > 0.65
Adistry (2013)	Isothermal 1500,1600,1700,1750°C Mixed stages	<i>T=1500 °C, t = 2hours</i> ✓ α=0.819 (quartz) ✓ α=0.914 (cristobalite) <i>T=1700 °C, t = 2hours,</i> ✓ Full conversion α > 0.990
Bao (2014)	Isothermal 1550,1730,1820°C Mix stages	✓ E = 351 kJ/mole

Chapter 3. Experiments

The reaction between quartz and silicon carbide in argon, Ar-CO gas mixtures, hydrogen and Ar-H₂ gas mixtures was studied in a graphite crucible heated in an electric vertical tube furnace. Both reacted and unreacted pellets were characterized by XRD, SEM, EDS and EPMA.

3.1 Raw material

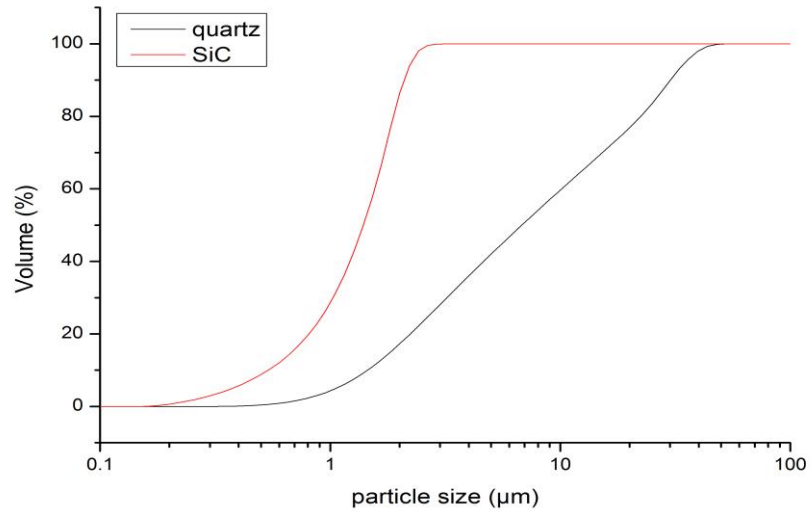
Quartz (Qz-15) and silicon carbide (Washington Mills) were crushed into fine powder and then mixed with the weight ratio of 3:1. A steel rotating mill was used to make powder into pellets, and water was used as binder in pelletizing process. Iron is introduced as pollutant when quartz is crushed into powder with steel. Pellets in the size range from 1 mm to 3.35 mm were first dried at 105 °C in a graphite crucible overnight and then sintered in a muffle furnace up to 1200 °C with the heating rate of 25 °C/min.

Two batches of quartz and silicon carbide pellets were made using the same type of quartz and silicon carbide through the same procedure. However, the particle size and porosity of the two batches of pellets might be different. The chemical analysis of quartz was determined by inductively coupled plasma (ICP-OES) as shown in Table 3-1.

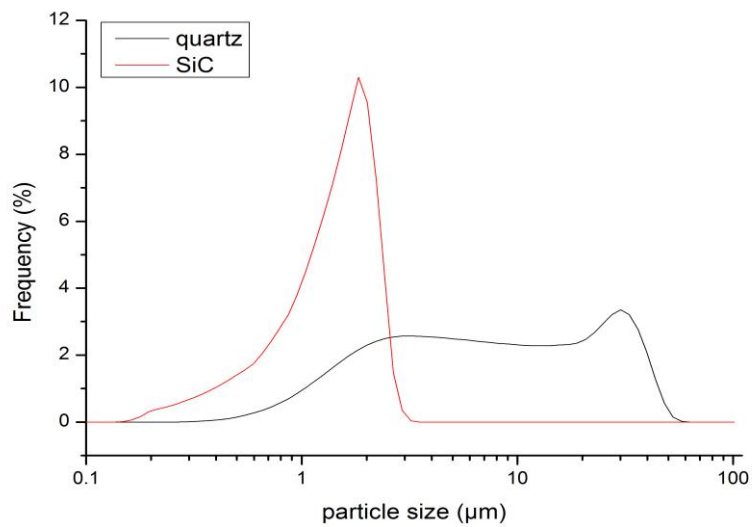
Table 3-1 Chemical analysis of Tana quartz-15 (SINTEF)

Composition	Amount
SiO ₂	99.44%
Al ₂ O ₃	0.437%
Fe ₂ O ₃	0.0327%
CaO	0.0016%
MgO	0.0876%
P	32 ppm
TiO ₂	291 ppm

The particle size distribution of quartz and silicon carbides powder (batch 2) was analyzed by the laser diffraction technique as shown in Figure 3-1.



(a)



(b)

Figure 3-1 Volume distribution of raw materials (batch 2). Cumulative volume is shown in (a) and frequency is shown in (b)

3.2 Apparatus

The electric tube vertical furnace used to heat the samples is called ReSiNa furnace, as shown in Figure 3-2. This furnace can be operated up to 2000 °C in vacuum or reducing atmosphere. The furnace is equipped with a B-type thermocouple. The gas analyzer ABB2020 is connected to the off-gas lance to detect the concentration of certain gas species.

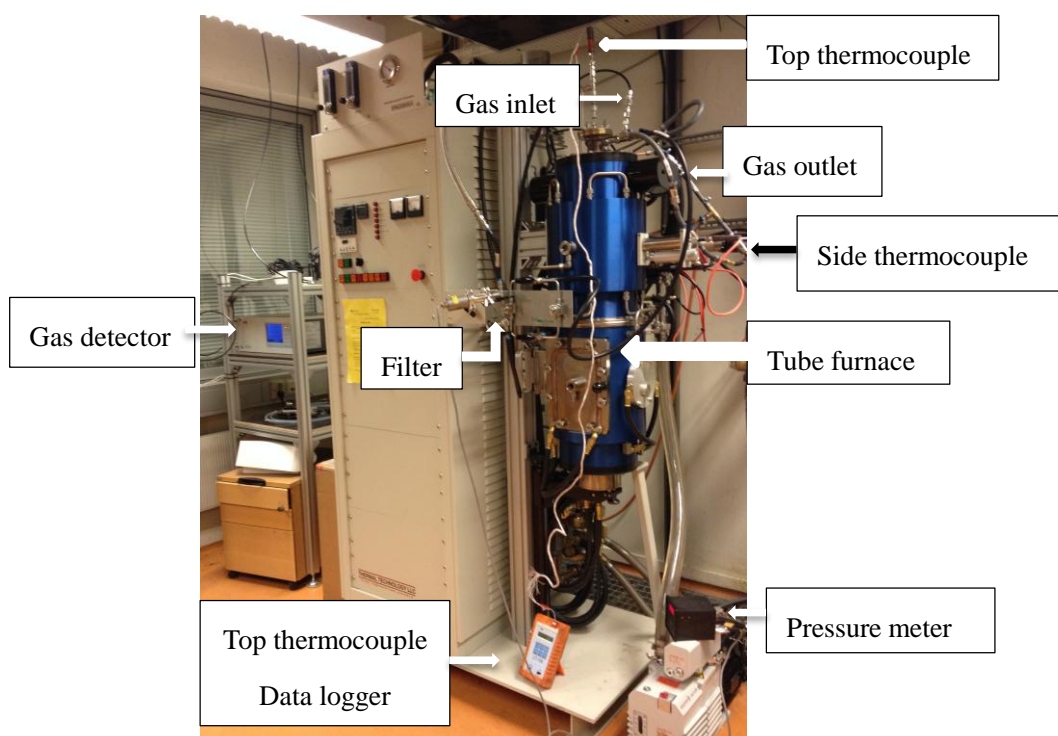


Figure 3-2 The appearance of Resina furnace

The graphite chamber, with the dimension of 95 mm in diameter and 250 mm in length, is consisting of a bottom chamber (reaction chamber) and a top chamber (condensation chamber) as shown in Figure 3-3. Pellets were placed in a small graphite crucible inside the bottom chamber. The bottom chamber can also be regarded as the reaction chamber where reaction quartz reacted with silicon carbide in this chamber under certain gas atmosphere. The added gas was controlled by the mass flow controllers and purged through the alumina gas tube to the small crucible. The silicon carbide particles with diameter of 4-5mm were placed in the condensation chamber to capture SiO gas generated by $\text{SiO}_2 + \text{SiC}$ reaction.

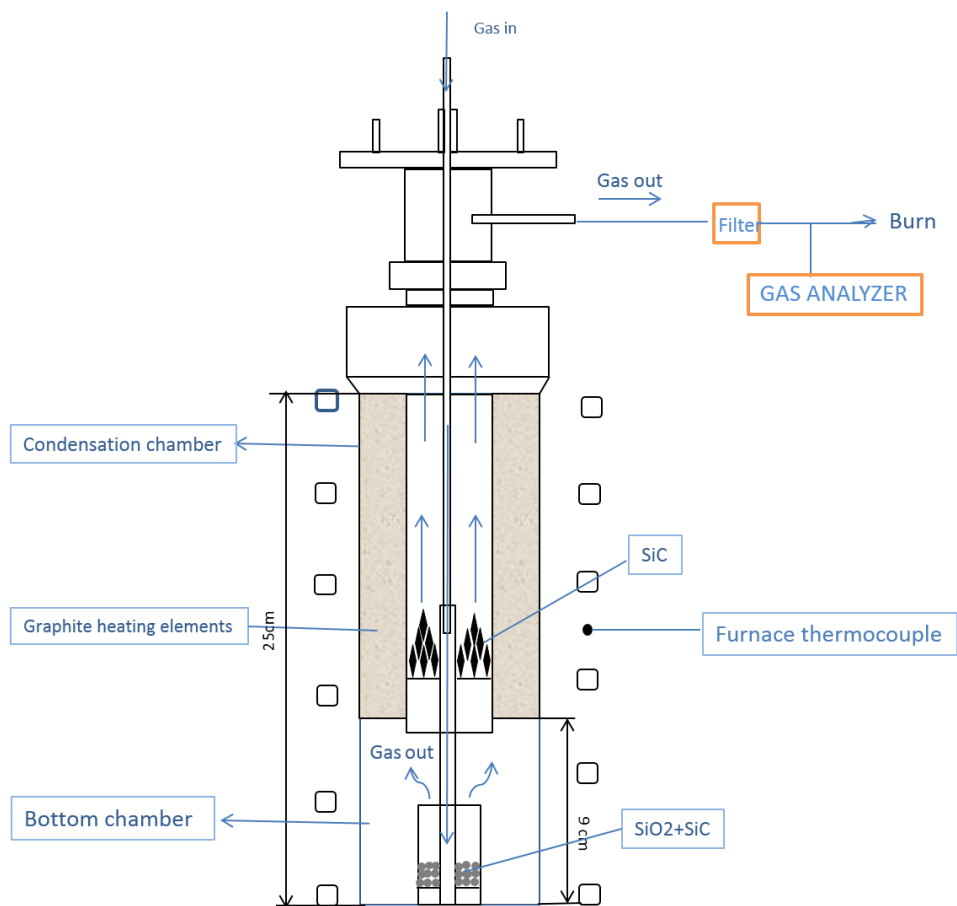
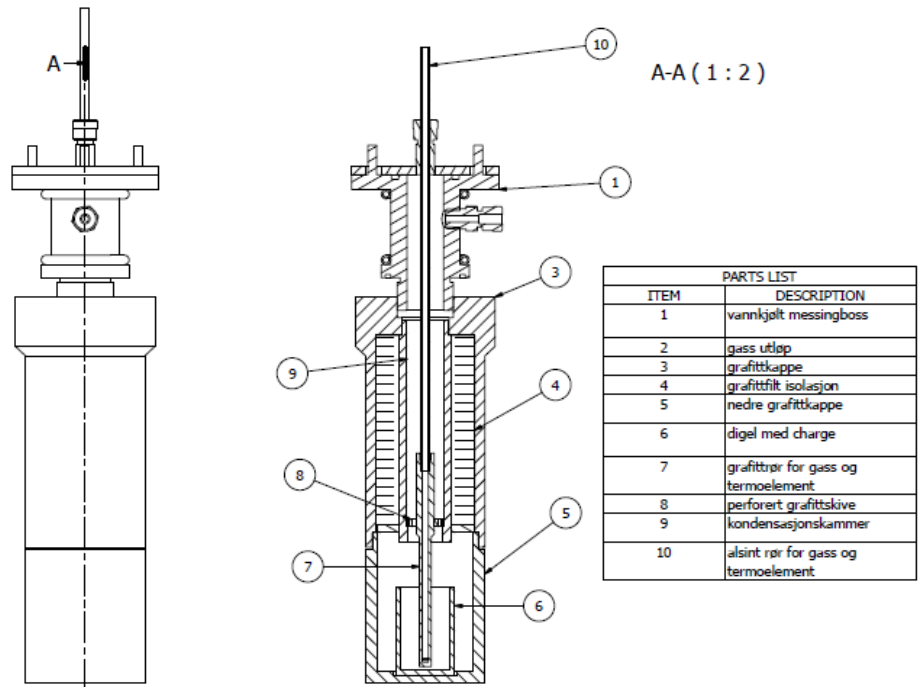


Figure 3-3 a sketch and a schematic drawing of the graphite crucible set-up

3.3 Procedures

3.3.1. High temperature experiments

The ReSiNa furnace was used to heat the samples up to 1700 °C at a constant heating rate of 15 °C/min. The holding time at 1700 °C is 60 min. The temperature profile is shown in

Figure 3-4.

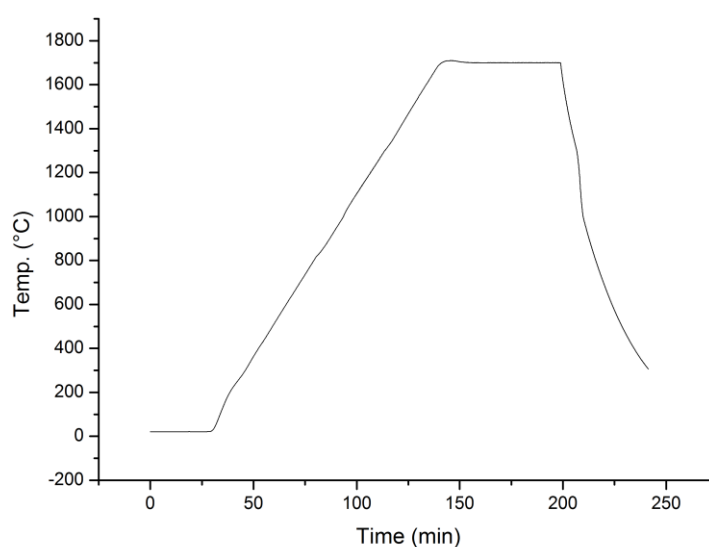
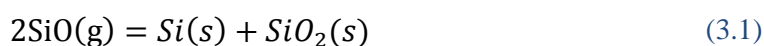


Figure 3-4 Temperature profile of an isothermal reaction experiment at 1700 °C

In case that SiO gas blocked the gas lances, a graphite condensation chamber with SiC particles (4-5mm) inside was used to condense the SiO gas from the reaction chamber. The reaction could be:



The off-gas, including the inert Ar gas, the process gas Ar-CO mixture and the CO gas produced by quartz reacting with silicon carbide, was sent to the gas analyzer ABB 2020. The CO concentration in the off-gas was registered in the computer logbook and used to calculate the reaction rate.

Nine runs were performed with different batches of pellets, temperatures and gas species. The first five runs were designed to study the effect of different gas species on kinetics of the SiO₂+SiC reaction. Composition of added gas was the only variable of the five-run design. One run at 1650 °C was designed to obtain the activation energy in the iso-conversional method.

A different batch of pellets was used as charges in the last three runs. In addition, another difference in the last three runs is the flow rate of inert gas and process gas, which was twice of that in the first six runs. The effect of flow rate of process gas on reaction kinetics can be found by comparison of Run 1 and Run 8. Comparing Run 2, 7, 9, the influence of different charge and flow rate of CO-Ar gas mixtures in reaction kinetics can be found. An overview of these nine runs is given in Table 3-2.

Table 3-2 Experiments overview

Design	Run	Batch	Temperature & Dwelling time	Process gas rate(l/min)	Inert gas rate (l/min)
Five-run design	1			0.4Ar	
	2			0.1CO+0.3Ar	
	3	Batch 2	SiO ₂ +SiC,1700 °C,1h	0.1CO+0.2Ar	0.6
	4			0.2H ₂ +0.2Ar	
	5			0.4H ₂	
E-design	6	Batch 2	SiO ₂ +SiC,1650 °C,2h	0.4Ar	0.6
Comparative trials	7			0.1CO+0.3Ar	0.6
	8	Batch 1	SiO ₂ +SiC,1700 °C,1h	0.8Ar	1.2
	9			0.2CO+0.6Ar	1.2

3.3.2. SEM, EDS and EPMA methods

The scanning electron microscopy (SEM) is one of the most versatile instruments available for the examination and analysis of the microstructure morphology and chemical composition characterizations. SEM uses a focused electron probe to extract structural and chemical information point-by-point from a region of interest in the sample. The high spatial resolution of the SEM makes it a powerful tool to characterize a wide range of specimens at the nanometer to micrometer length scales.

The LVFESEM, Zeiss Ultra, was used to characterize the unreacted and reacted pellets. Both secondary and backscattered electron detectors are available for imaging at different working distance. Secondary electrons are used principally for topographic contrast in the SEM, i.e., for the visualization of the surface texture and roughness. Backscattered electron images in SEM display the compositional contrast that results from different atomic number elements and their distribution. Another valuable analytical method is the energy dispersive spectroscopy (EDS), which allows one to identify what those particular elements are and their relative proportions (Atomic % for example).

Electron probe microanalysis (EPMA) is a nondestructive analytical technique widely used for determining the local composition of solid samples. EPMA capabilities include point analysis, line profiles and x-ray mappings, both qualitative and quantitative, as well as the determination of the composition of specimens. EPMA, JEOLJXA 8500F was used in this work.

There are extensive facilities for preparing specimens for SEM examination. These include abrasive wheel, mounting press and grinding/polishing wheels. In this work, samples were made by pouring epoxy into the pellets and then coated with conductive carbon using Cressington coating units. Both unreacted and reacted pellets were characterized by these methods.

3.3.3. XRD methods

The X-ray diffraction technique is used to characterize the crystalline materials and determine the structures. Samples are scanned by a fingerprint diffractometer in a certain range of 2θ values at a constant angular velocity. Intensity of each peak will be obtained either qualitatively or quantitatively. Each crystalline material has its own characteristic X-ray pattern. By searching and matching these patterns, the chemical composition of samples is identified.

The pellets were crushed to fine powder with 50- μm upper size by means of a steel vibratory disk mill and analyzed by XRD. Settings were adjusted to 40 kV, 40 mA and Cu-K α radiation of wavelength K α_1 = 1.5406 Å and K α_2 = 1.54439 Å and a K α_1 /K α_2 ratio of 0.5. Diffractograms were recorded from 3-65 $^\circ 2\theta$, in 0.009 $^\circ 2\theta$ increments with 0.6 s counting time per increment and the total analysis time was 71 minutes per sample.[32]

3.3.4. Mathematical calculations of reaction rate

The conversion rate can be expressed by the rate of weight loss as shown in Eq.3.2. The final weight of sample is zero as the products are gaseous. W_0 is the initial sample weight. The weight loss rate is expressed by the CO gas flow rate, according to Eq.3.3. V_{CO} is the volume of CO gas and t is time. The flow rate of CO gas is defined as r_{CO} . The molar mass of SiO and CO is 44 g/mole and 28 g/mole respectively. Under standard condition, the volume of one mole gas species is 22.4 liter.

$$\frac{d\alpha}{dt} = -\frac{1}{W_0} \times \frac{dw}{dt} \quad (3.2)$$

$$\frac{dW}{dt} = -(3 \times 44 + 28) \times \frac{V_{CO}}{22.4} = -\frac{7.14V_{CO}}{t} = -7.14 \times r_{CO} \quad (3.3)$$

CO % is the CO concentration in the off-gas. The relation between CO concentration and the flow rate of generated CO gas is given by Eq.(3.4). The total rate of process gas is 0.4 l/min and the inert gas Ar is 0.6 l/min. As N_2 was used to be the inert gas, there is a converting parameter of 1.45 between Ar and N_2 . $CO_{generated}$ and $CO_{process}$ represent the CO gas produced from the reaction and CO gas purged by mass flow controller respectively.

$$CO\% = \frac{r_{CO_{generated}} + r_{CO_{process}}}{r_{CO_{process}} + r_{Ar_{process}} + r_{Ar_{inert}} \times 1.45} \quad (3.4)$$

Conversion of the reaction can be derived by integrating conversion rate with time as shown in Eq.3.5.

$$\alpha = \int \frac{d\alpha}{dt} dt \quad (3.5)$$

Plots of the conversion rate and conversion of SiO_2+SiC reaction vs the reaction time and temperature were obtained by normalizing the total amount of produced CO gas from gas analysis ($V'_{CO,tot}$) to the value determined by total weight loss ($V_{CO,tot}$). The relation between total volume of produced CO gas and conversion is

$$V'_{CO,tot} = \int r_{CO} dt \quad (3.6)$$

$$V_{CO,tot} = W_{initial} * \frac{\alpha}{7.14} = \beta * V'_{CO,tot} \quad (3.7)$$

$$\alpha = \frac{W_{\text{initial}} - W_{\text{final}}}{W_{\text{initial}}} \quad (3.8)$$

$$r_{\text{CO,actual}} = \beta * r_{\text{CO,recalculated}} \quad (3.9)$$

Where β is recalculated factor of actual CO flow rate and recalculated CO rate, r_{co} is CO flow rate (L/min).

Chapter 4. Results

4.1 Mass change

The mass change measured before and after experiments is shown in Table 4-1. The Δ Total category shows the difference between the entire chamber with crucible, gas tube, SiC, sieves and inside before and after experiments. Note that sample weight is not included in Δ Total category. The Δ Crucible + sieve category shows the difference between the mass of empty crucible and sieve before and after experiments. The increased weight of graphite crucible and sieve is attributed to two possible reasons: condensation of SiO gas on the graphite crucible and/or carbon reacting with Si to form SiC. Δ Crucible + sieve category is similar to what Anderson[25] found in his work. Ta crucible was used in his work and the author believed that the Ta crucible reacts with CO and SiO gas. The α category shows the extent of the reaction under different gas atmosphere. The extent of SiO₂+SiC reaction under different gas atmosphere can be summarized as: H₂ > Ar > CO.

Table 4-1 Mass change in experiments performed in the Resina a furnace

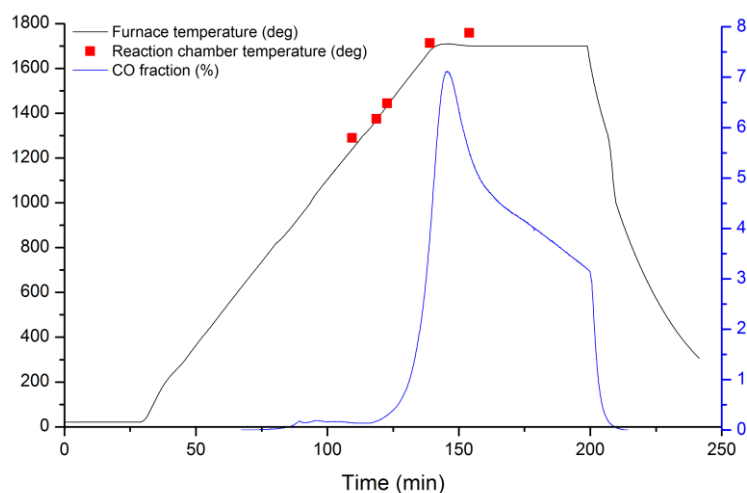
Design	Run	Batch	Gas flow	α [%]	Δ Total [g]	Δ Crucible [g]
Five-run design	Run 1		0.4Ar	32.1	3.45	0.61
	Run 2		0.1CO+0.3Ar	30%	2.86	0.31
	Run 3	Batch 2	0.1CO+0.2Ar	16.5%	2.42	0.26
	Run 4		0.4H ₂	53.71%	4.82	0.24
	Run 5		0.2H ₂ +0.2Ar	42%	4.43	0.48
E-design	Run 6	Batch 2	0.4Ar	50.5%	3.55	0.56
Comparative trials	Run 7		0.1CO+0.3Ar	33.3%	3.21	0.61
	Run 8	Batch1	0.8Ar	62.6%	4.33	0.23
	Run 9		0.2CO+0.6Ar	32.1%	3.28	0.47

4.2 Actual and recalculated CO evolution rate

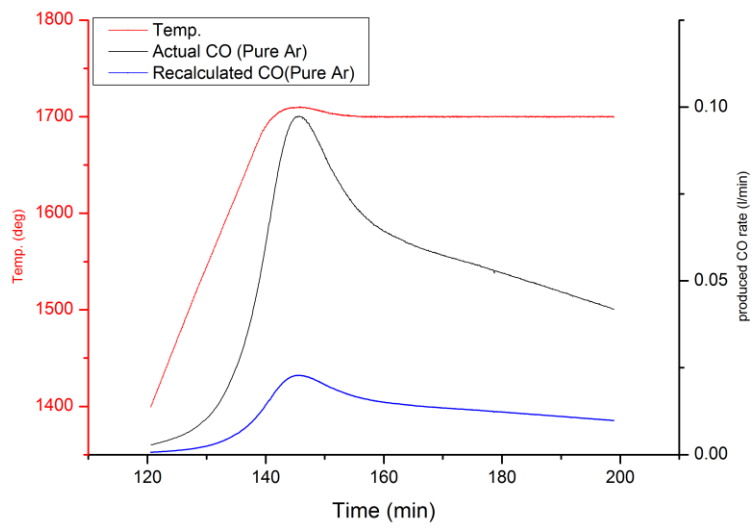
Plots of both actual and recalculated CO evolution rate (l/min) versus time in these nine runs are listed below.

Run 1 - 0.4Ar

In run (a), the furnace was heated up following the temperature profile, as is shown on furnace temperature curve. The temperature in the graphite crucible was registered by a C-type thermocouple. Above 1400 °C, the temperature recorded by thermocouple was quite closed to the furnace temperature. The CO gas started to increase dramatically to 7% when the temperature reached around 1400 °C and then decreased to 3% during the holding period at 1700 °C. Afterwards, the furnace started cooling down to room temperature.



(a)

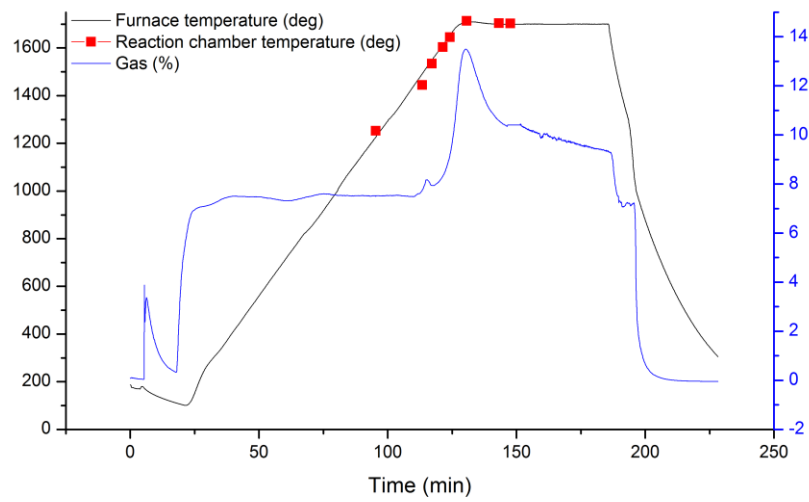


(b)

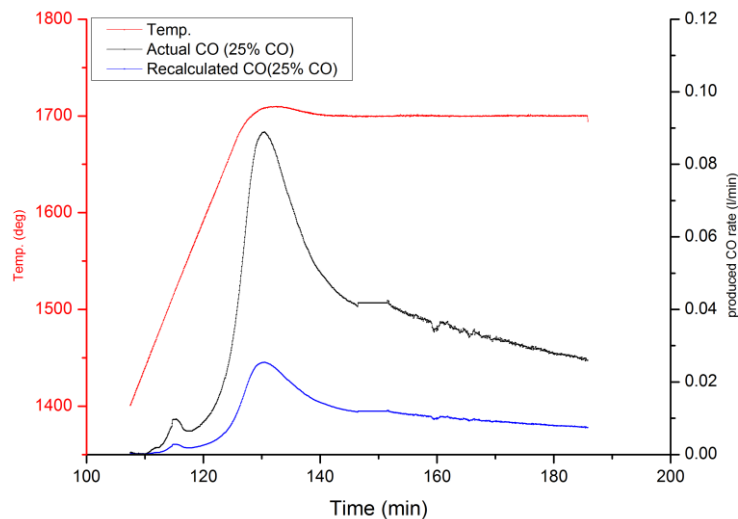
Figure 4-1 (a) CO evolution rate in the isothermal reaction between quartz and silicon carbide in pure Ar; (b) recalculated CO evolution rate based on total mass loss

Run2- 0.1CO+0.3Ar

The CO concentration in the off gas was quite stable before 1400 °C, indicating that the gas analyzer shows correct data. The CO concentration increased dramatically from around 8% to 13% and then decreased to 9% at 1700 °C. A small peak appeared at 1500 °C.



(a)

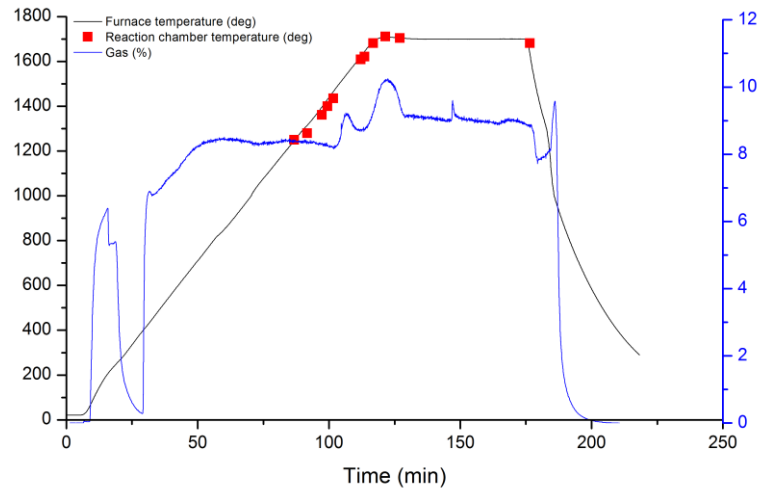


(b)

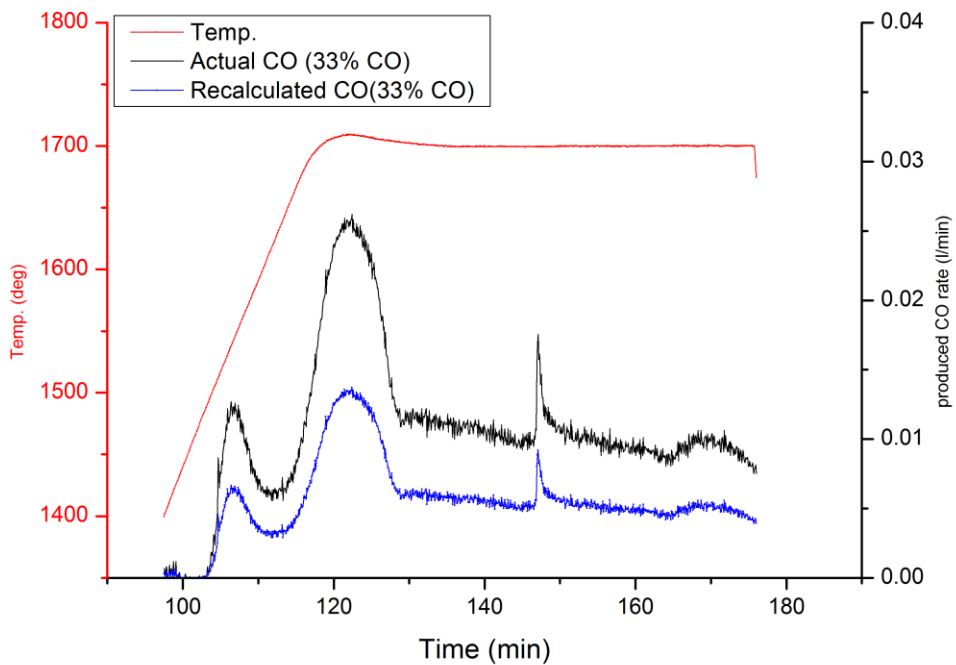
Figure 4-2 (a) CO evolution rate in the isothermal reaction between quartz and silicon carbide in 0.1CO+0.3Ar; (b) recalculated CO evolution rate based on total mass loss

Run 3- 0.1CO+0.2Ar

The CO concentration decreased in a small extent below 1400 °C due to the error in gas analyzer. A large of noise was shown when temperature was above 1400 °C.



(a)

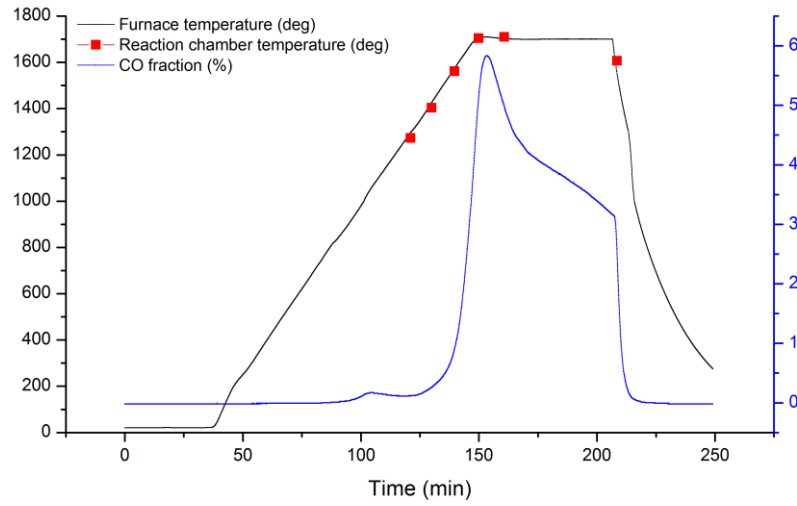


(b)

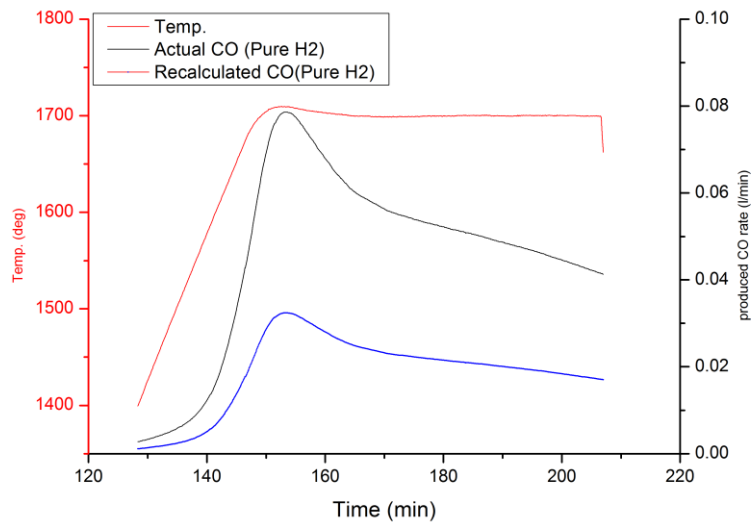
Figure 4-3 (a) CO evolution rate in the isothermal reaction between quartz and silicon carbide in 0.1CO+0.2Ar; (b) recalculated CO evolution rate based on total mass loss

Run 4- 0.4H₂

The CO concentration in pure hydrogen increased rapidly to approximately 6 % when the temperature reached around 1400 °C. During the holding period at 1700 °C, the CO concentration decreased to 3%/.



(a)

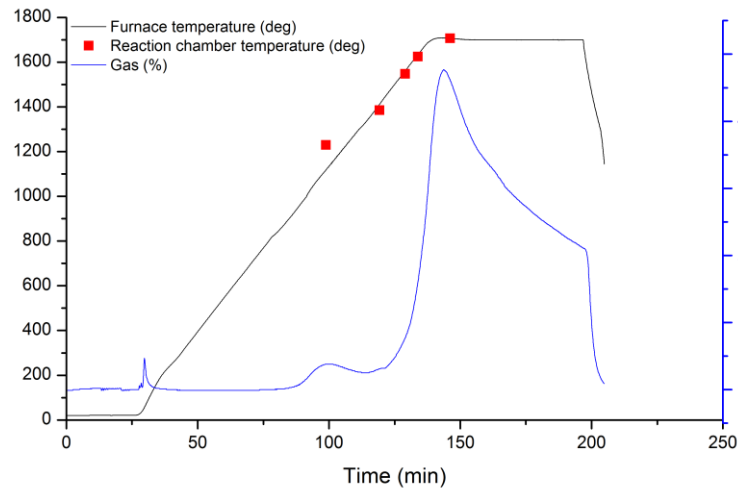


(b)

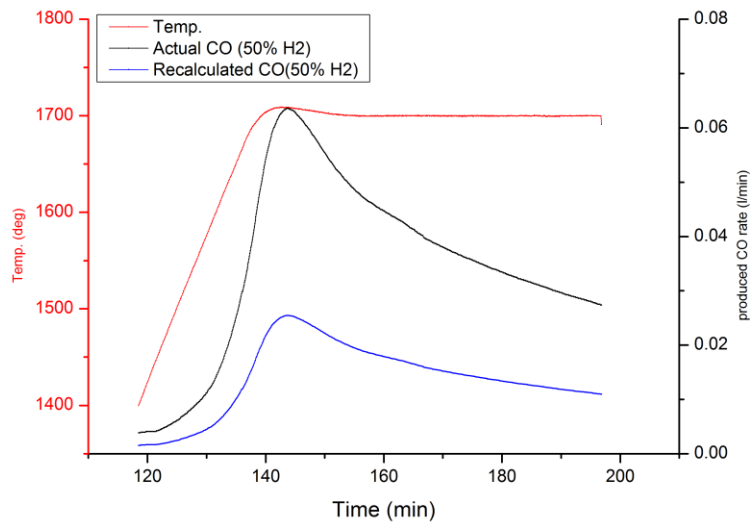
Figure 4-4 (a) CO evolution rate in the isothermal reaction between quartz and silicon carbide in pure H₂; (b) recalculated CO evolution rate based on total mass loss

Run 5- 0.2H₂+0.2Ar

When the process gas containing 50% H₂ was purged into the graphite crucible, the CO concentration in the off gas increased to 4.5% at 1700 °C and then decreased to 2% during the holding time.



(a)

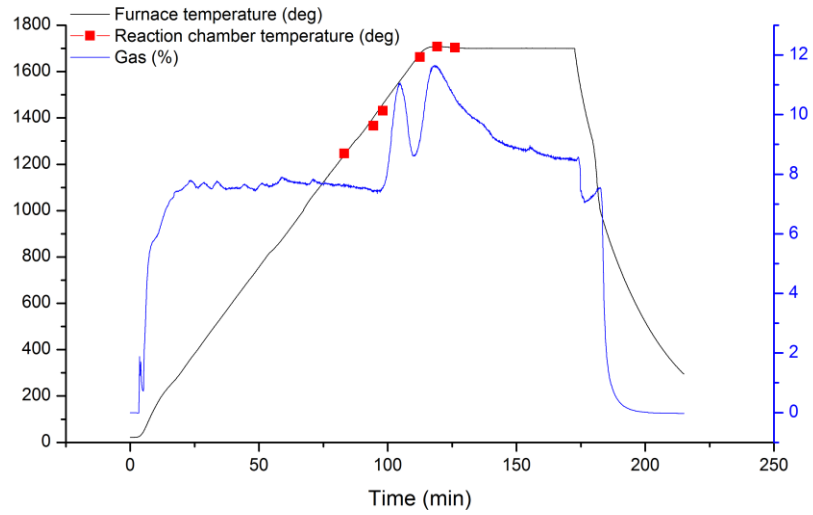


(b)

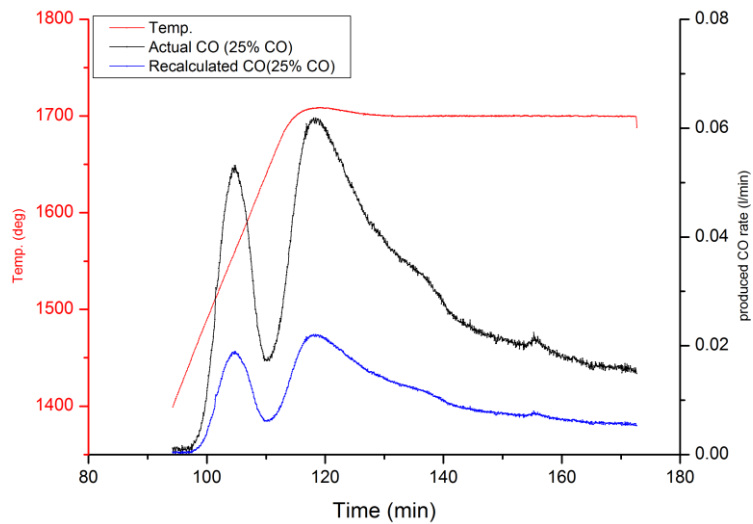
Figure 4-5 (a) CO evolution rate in the isothermal reaction between quartz and silicon carbide in 0.2H₂+0.2Ar; (b) recalculated CO evolution rate based on total mass loss

Run 7- 0.1CO+0.3Ar (batch 1)

The CO concentration started increasing from around 8% when the temperature reached 1400 °C. There are two peaks appearing on the graph: one was obtained at around 1600 °C and the other was obtained at 1700 °C.



(a)

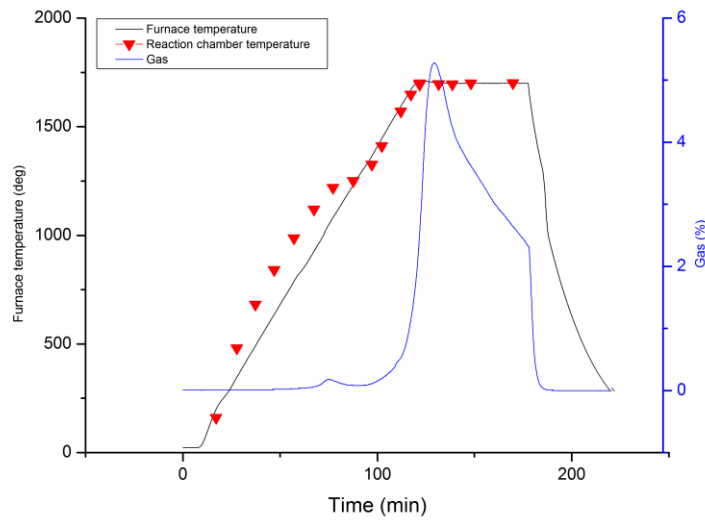


(b)

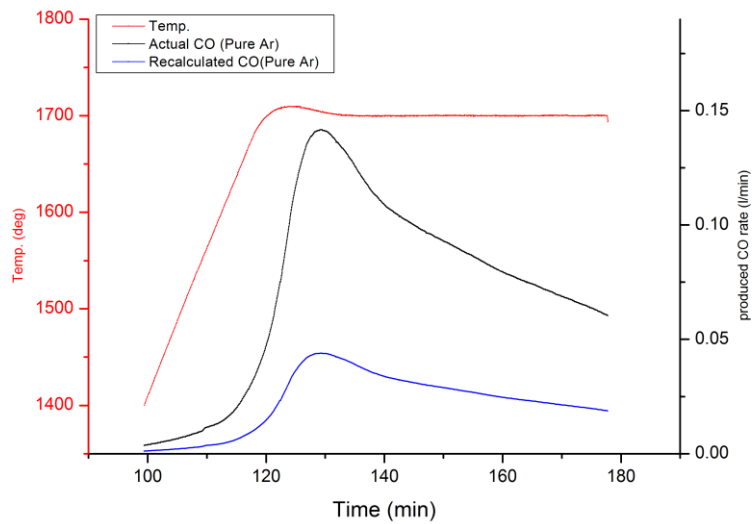
Figure 4-6 (a) CO evolution rate in the isothermal reaction between quartz and silicon carbide in 0.1CO+0.3Ar(batch 1); (b) recalculated CO evolution rate based on total mass loss

Run 8- 0.8Ar (batch 1)

The CO concentration in the off gas increased to about 5% at 1700 °C and decreased to 2% during the holding time.



(a)

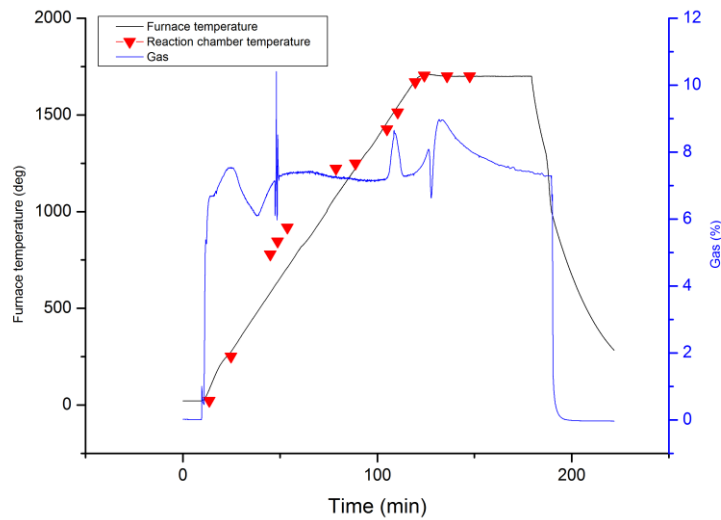


(b)

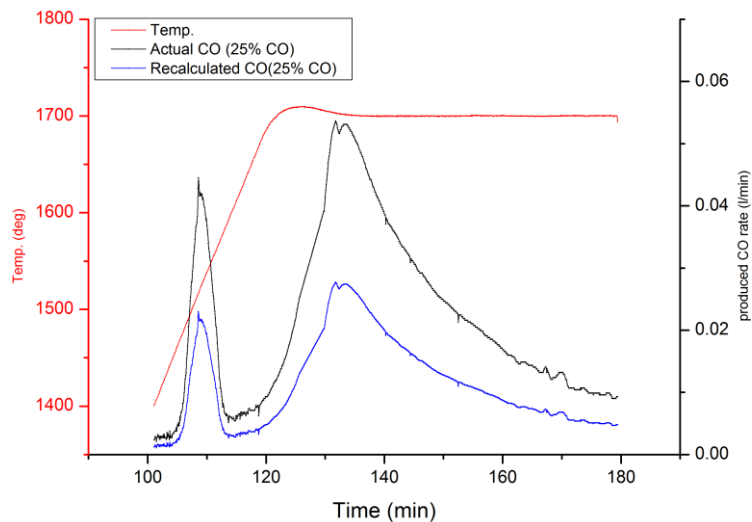
Figure 4-7 (a) CO evolution rate in the isothermal reaction between quartz and silicon carbide in 0.8Ar; (b) recalculated CO evolution rate based on total mass loss

Run 9- 0.2CO+0.6Ar

When 0.2CO+0.6Ar gas mixture was purged into the graphite crucible, the CO concentration curve showed a slight decreasing trend below 1400 °C, indicating the inaccuracy in the CO concentration measured by the gas analyzer. Several peaks were obtained during the holding time at 1700 °C, which is caused by the error in the measurement of CO concentration in the off gas.



(a)



(b)

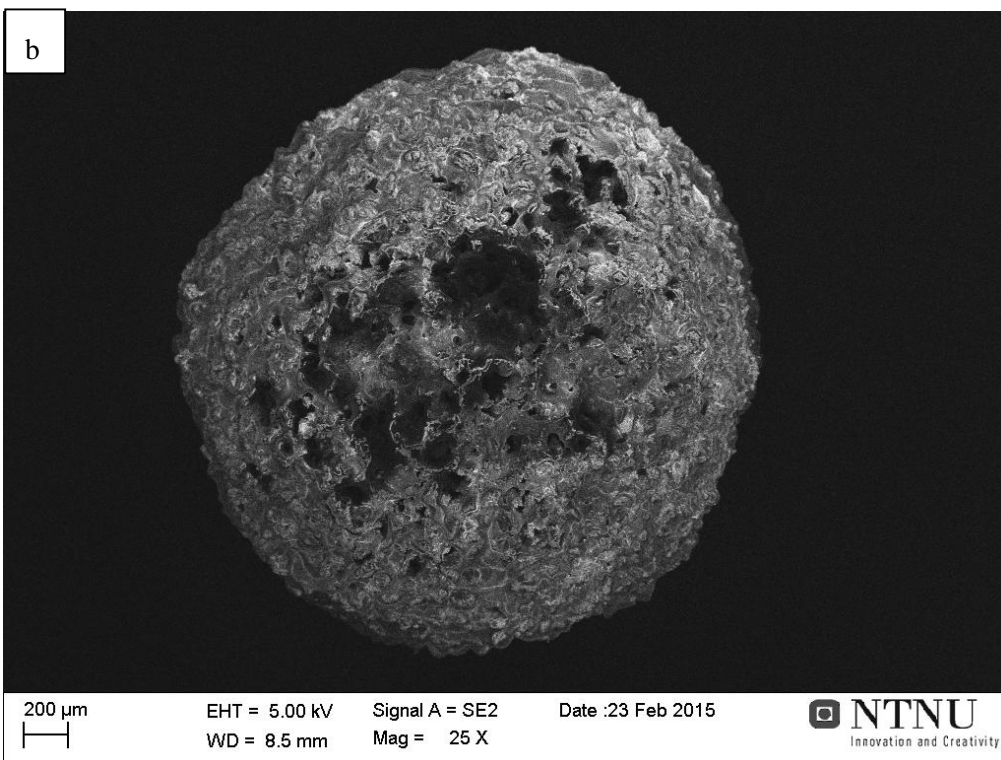
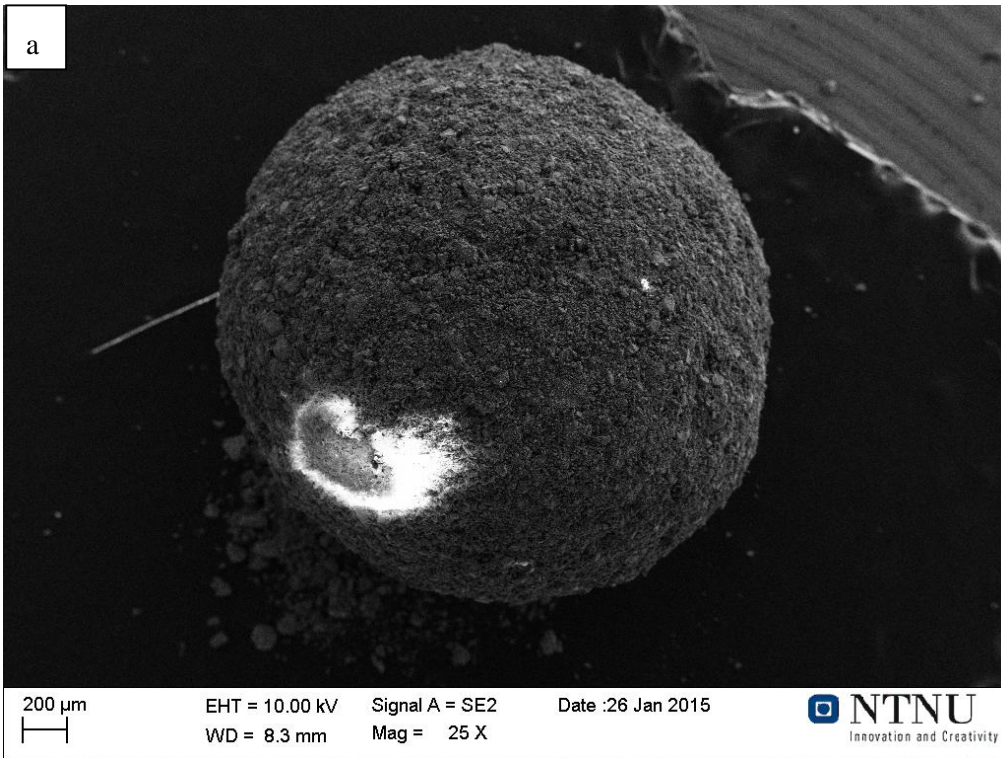
Figure 4-8 (a) CO evolution rate in the isothermal reaction between quartz and silicon carbide in pure 0.2CO+0.6Ar; (b) recalculated CO evolution rate based on total mass loss

4.3 Morphology of unreacted and reacted pellets

The morphologies of unreacted pellets and reacted pellets in Ar-CO gas mixtures were examined by SEM. Figure 4-9 and Figure 4-10 compares the morphologies of the unreacted and reacted pellets. EDS and EPMA were used to identify the chemical composition of different phases. The chemical composition of initial and reacted pellets examined by EDS is presented in Table 4-2. The results of EPMA were presented in Figure 4-11 and Figure 4-12 and fit the results of EDS.

It can be found that the surface of the pellets became more porous, quartz became soften and packed, FeSi metal nucleated on SiC particles, after heated at 1700 °C for one hour. Silicon metal was probably formed by the reaction between SiO gas and silicon carbides (Eq.4.1)





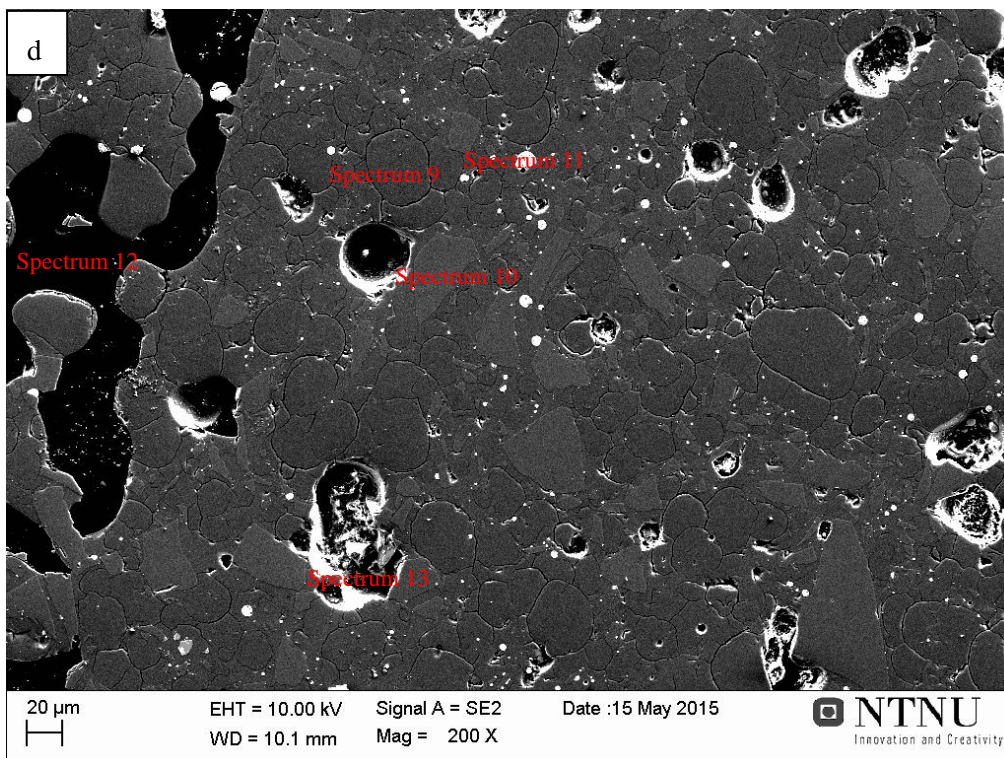
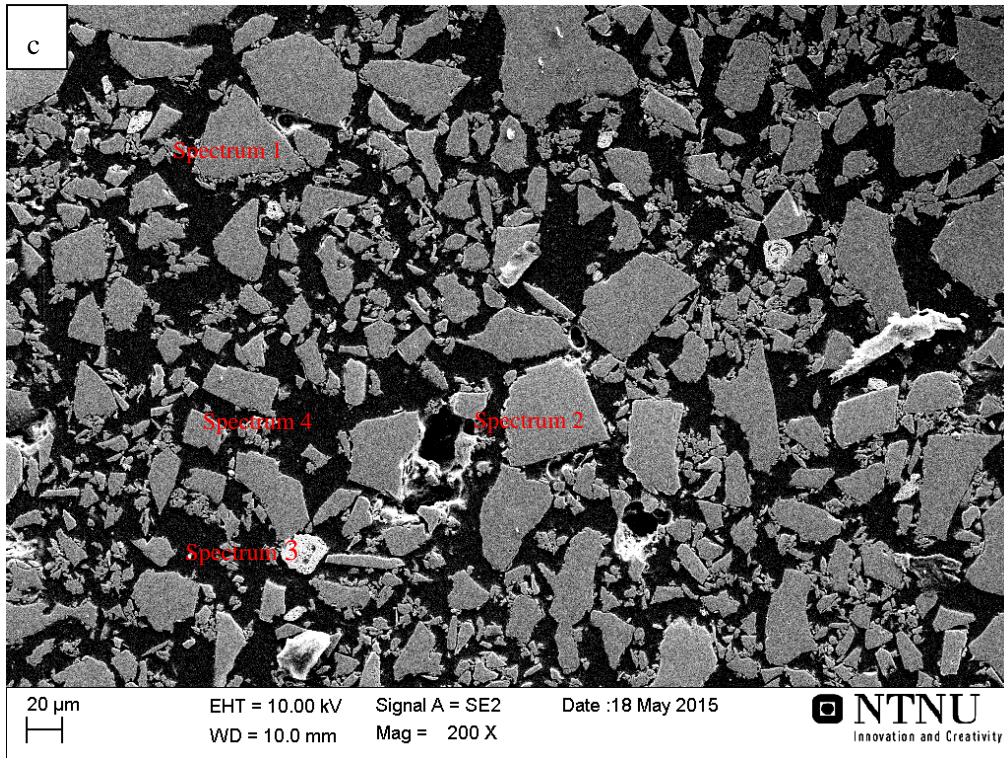
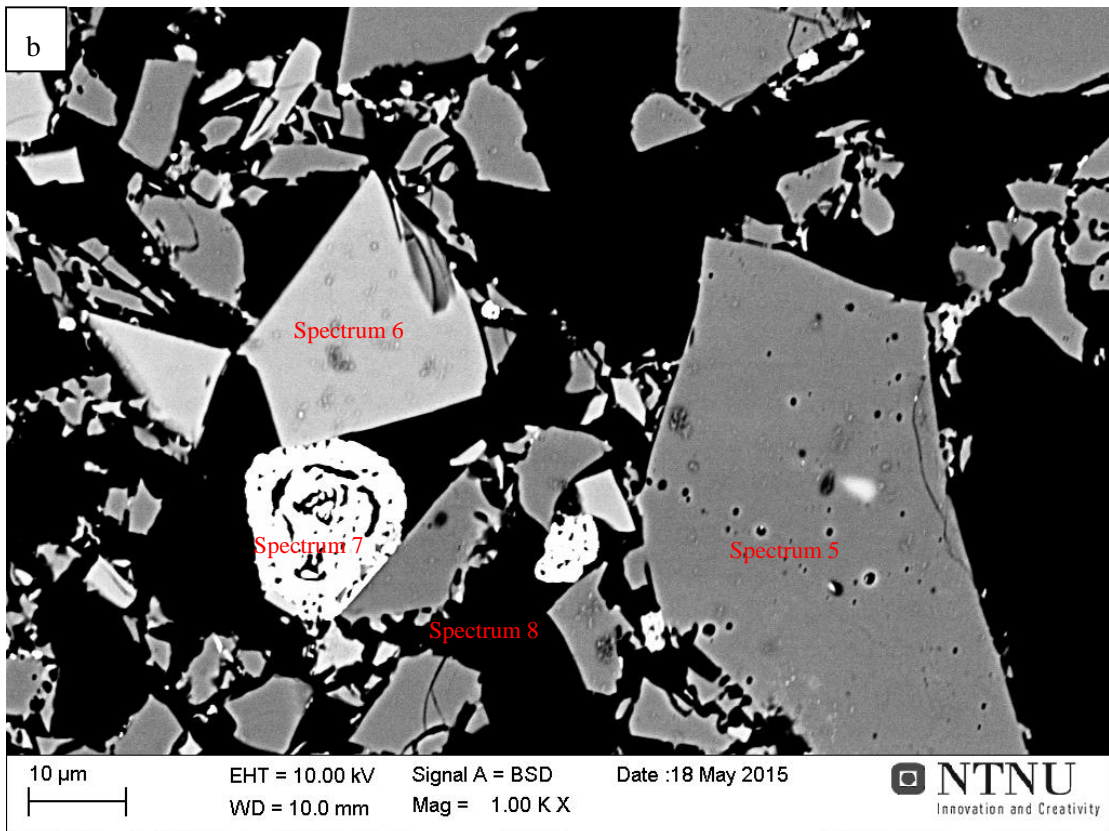
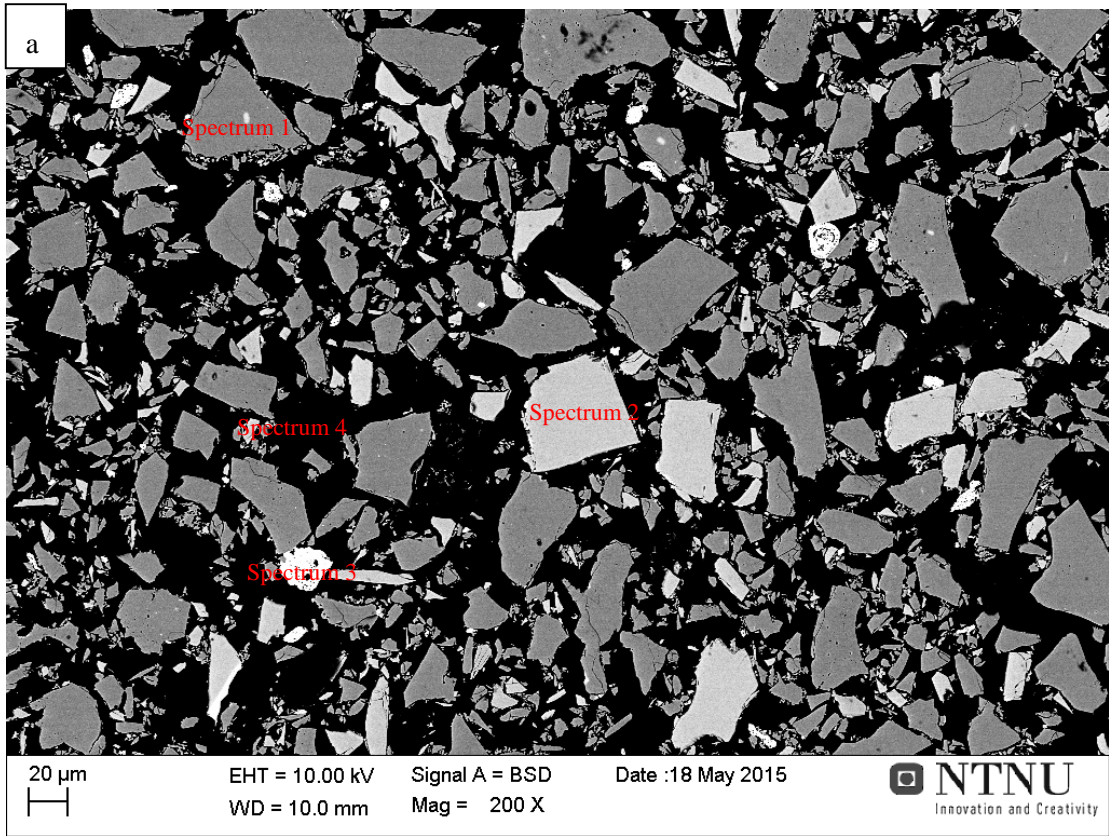


Figure 4-9 SEM images, (a) the surface of initial pellets (b) the surface of reacted pellets, (c) the polished section of initial pellets, (d) the polished section of reacted pellets



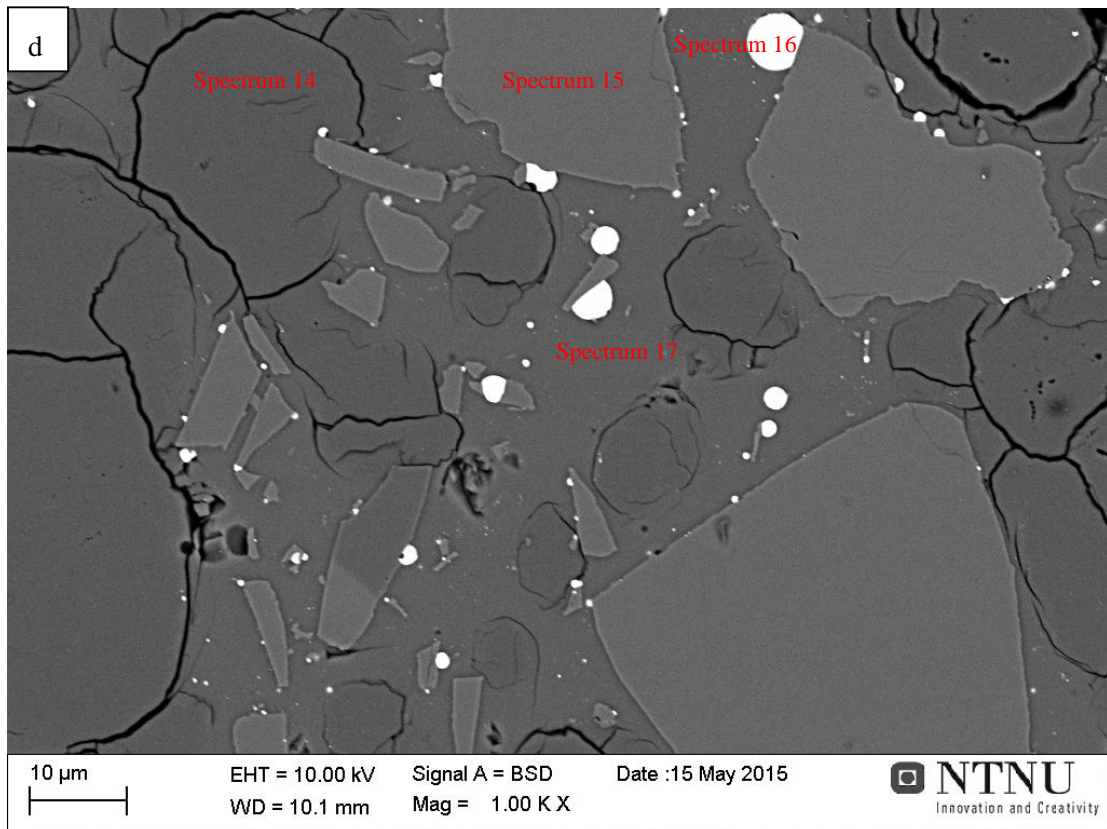
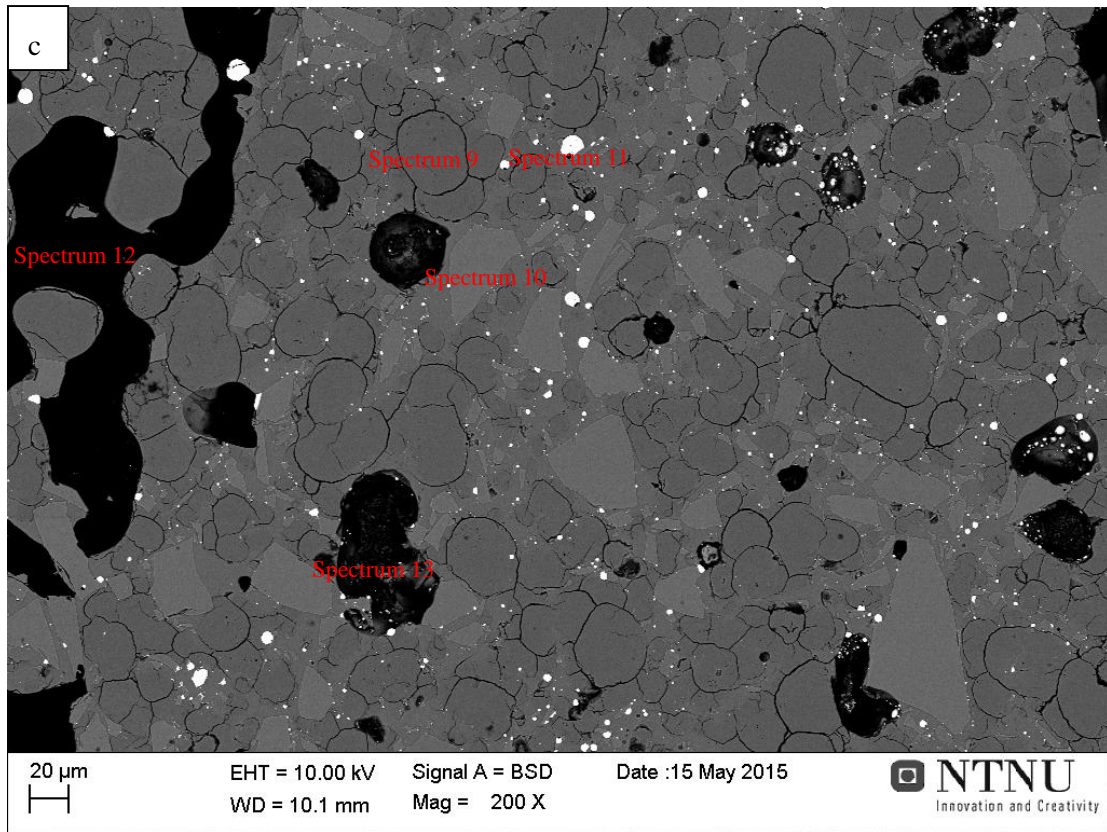
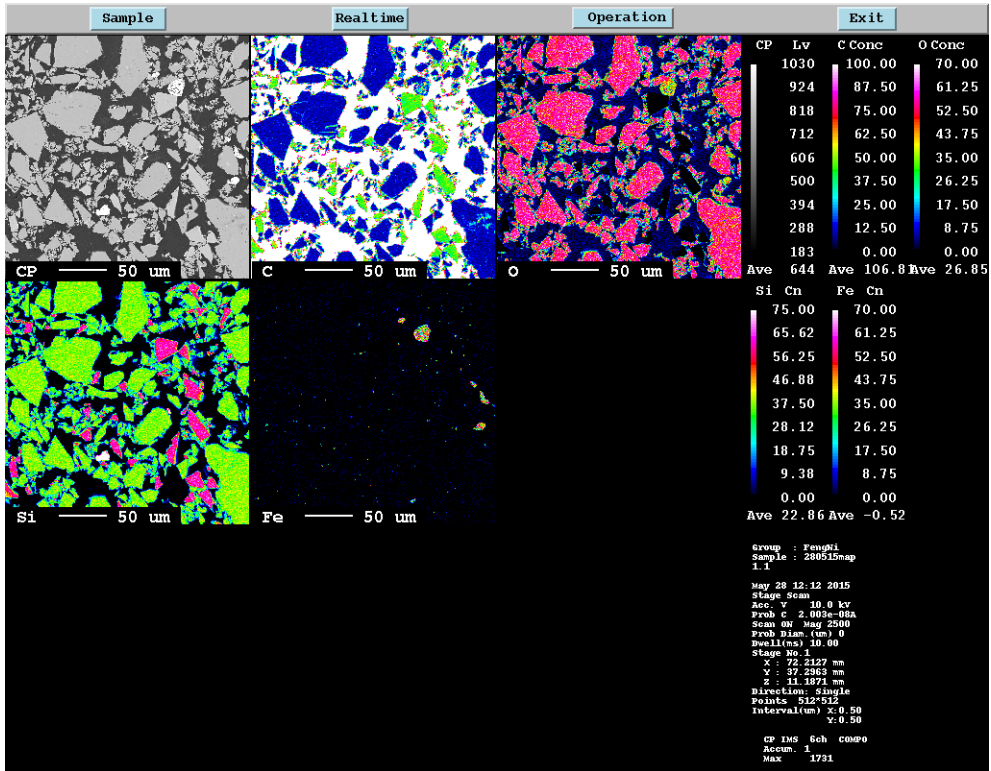


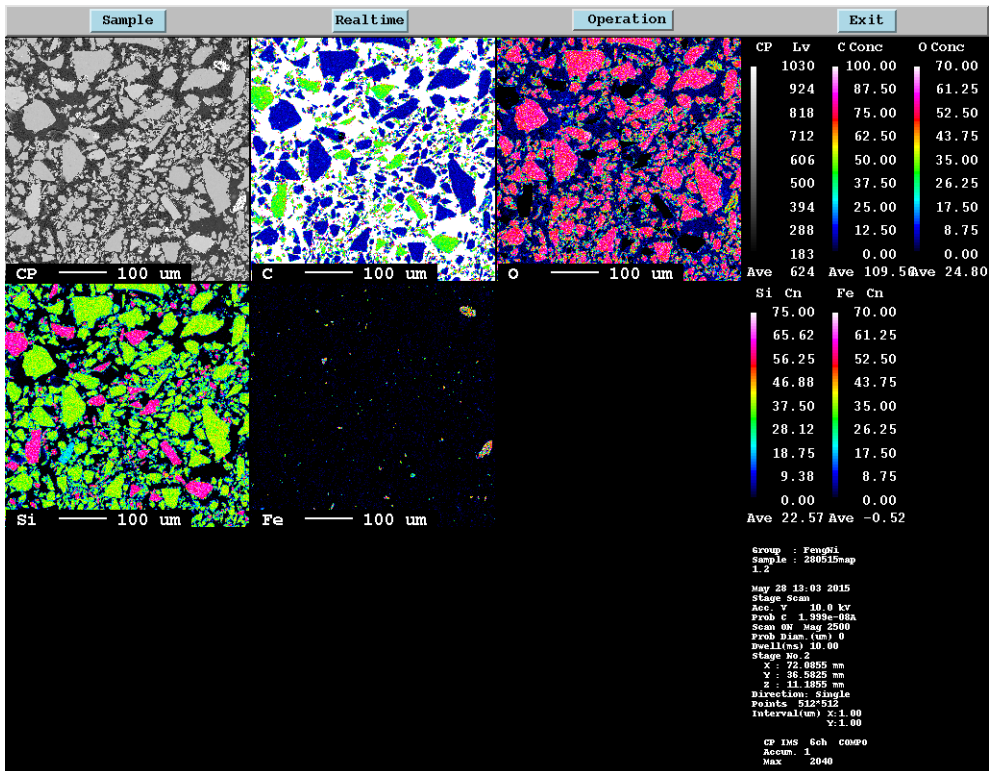
Figure 4-10 Backscattering image, (a) the polished section of initial pellets, (b) the polished section of initial pellets in higher magnification, (c) the polished section of reacted pellets at 1700 °C. (d) the polished section of reacted pellets in higher magnification

Table 4-2 Elements analysis by EDS (at %)

Figure	Spectrum	C	Si	O	Fe	Cl	Ca	Phase
Figure	1	21.22	27.01	51.77				SiO ₂
5-13(a)	2	57.41	41.76	0.48				SiC
Figure	3	21.80		41.86	33.34			Fe
5-12(c)	4	81.94		17.58		0.22		Epoxy
	5	22.44	26.08	51.48				SiO ₂
Figure	6	57.60	40.85	1.54				SiC
5-13(b)	7	24.47	5.21	46.84	23.48			Fe
	8	85.54		14.07		1.06		Epoxy
	9	19.24	28.38	52.38				SiO ₂
Figure	10	56.45	42.55	1.00				SiC
5-13(c)	11	34.82	34.16		31.02			FeSi
Figure	12	87.69		11.24		1.07		Epoxy
5-12(d)	13	86.38	1.92	11.35	0.15		0.20	Impurities
	14	19.23	28.23	52.54				SiO ₂
Figure	15	56.49	42.66	0.85				SiC
5-13(d)	16	35.39	36.27		28.34			FeSi
	17	19.91	29.09	51				SiO ₂

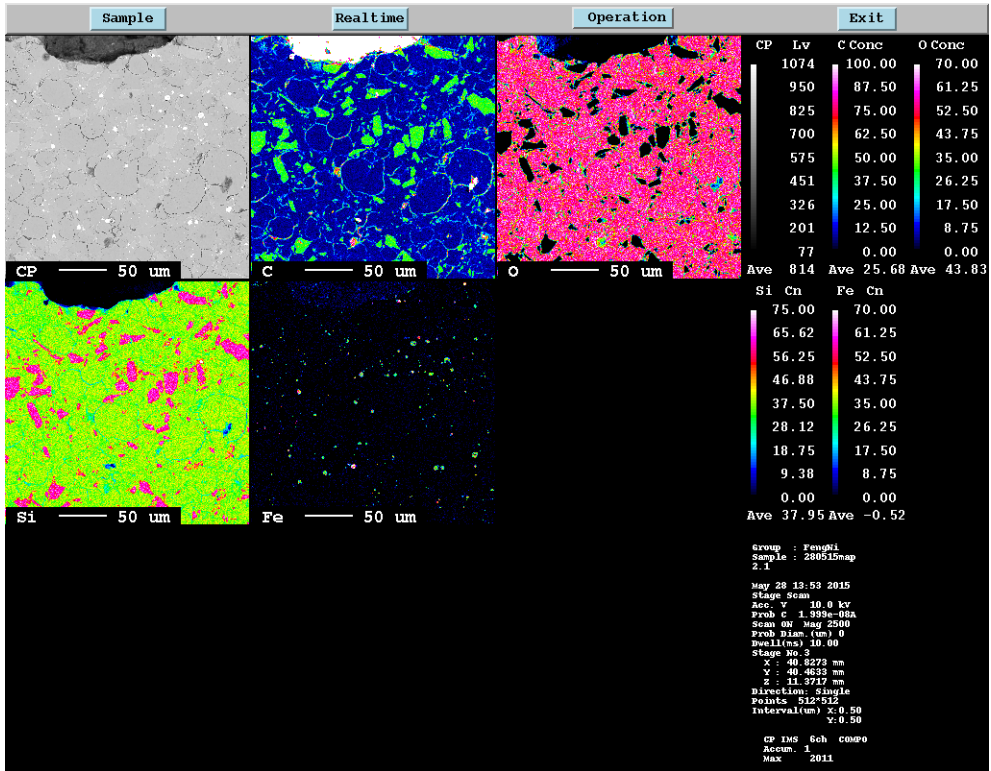


(a)

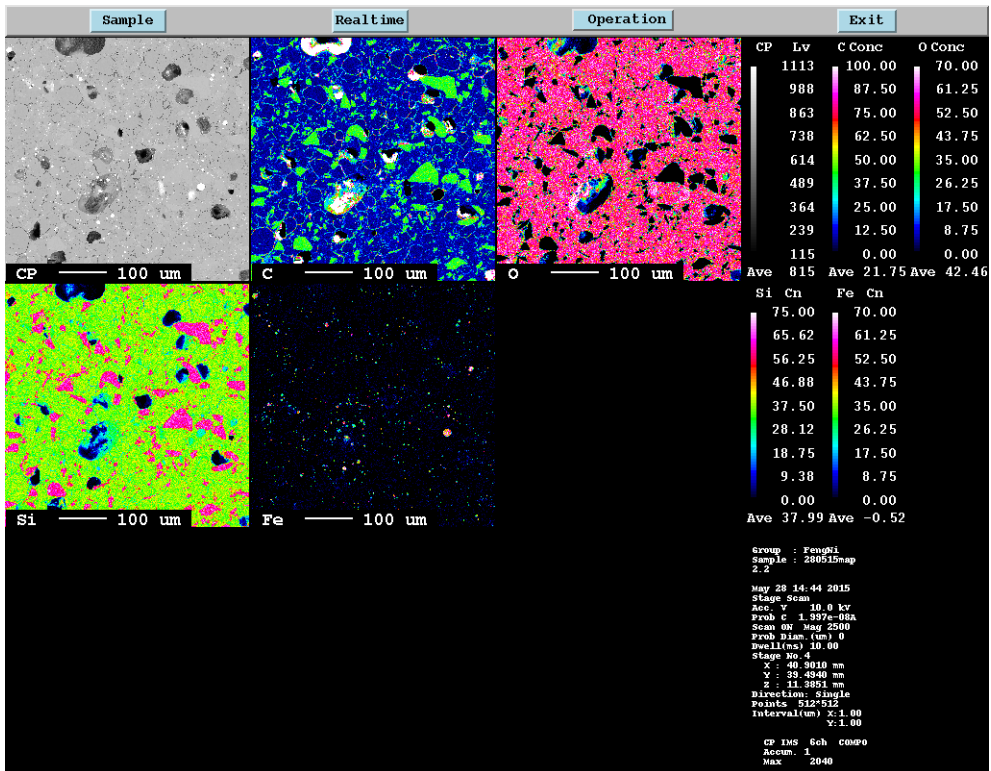


(b)

Figure 4-11 EPMA of initial pellets



(a)



(b)

Figure 4-12 EPMA of reacted pellets at 1700 °C with the presence of Ar-CO

4.4 XRD results

The XRD results are shown in Figure 4-13. Quartz, silicon carbide are identified as the major phases in initial pellets without sintering. Iron is introduced when quartz lumps are crushed into powders and is presented as the trace phase. After sintered at 1200 °C, cristobalite was presented with quartz. The cristobalite can theoretically be attained through heating up the quartz to the range temperature of 1479-1705 °C at 1 bar pressure. However the cristobalite transformation is a slow reconstructive process where the full conversion can only be obtained in a long firing time[33]. The XRD patterns of final pellets treated at 1700 °C in Ar and H₂ for 60 min indicate that quartz was fully transformed into cristobalite and a small amount of silicon was presented in the form of Fe₃Si.

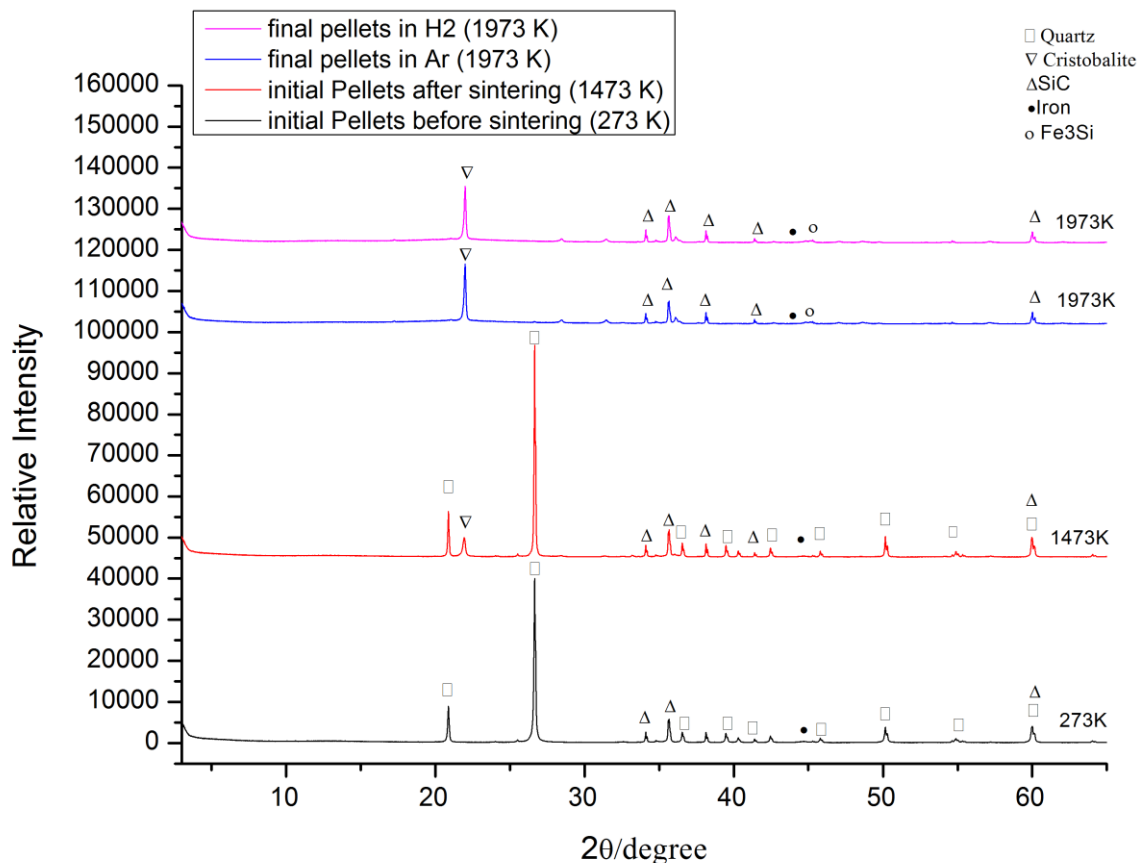


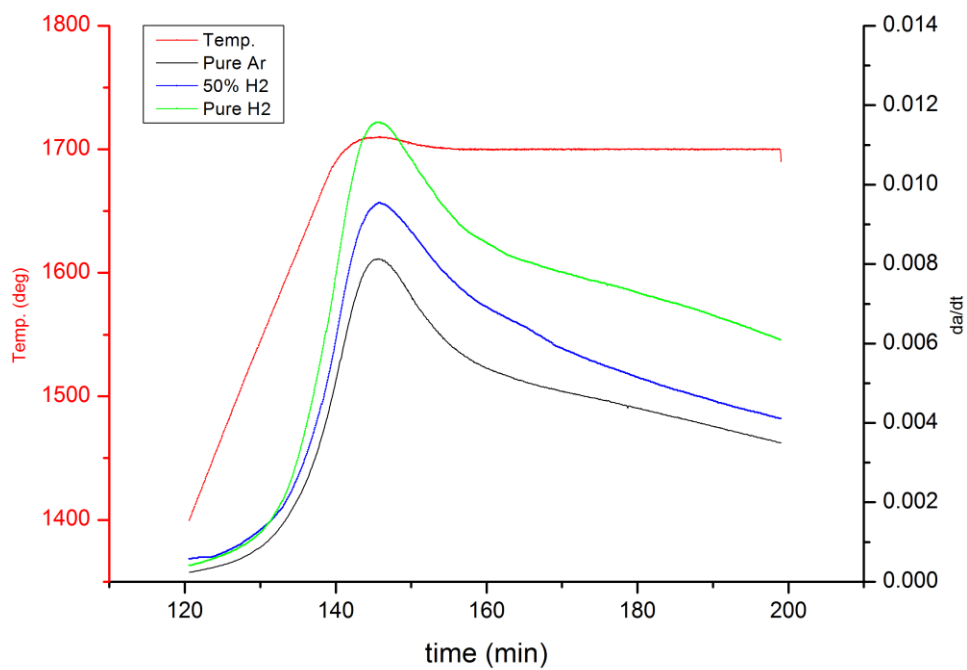
Figure 4-13 XRD patterns of initial pellets before and after sintering process, final pellets in the presence of H₂ and Ar

Chapter 5. Discussion

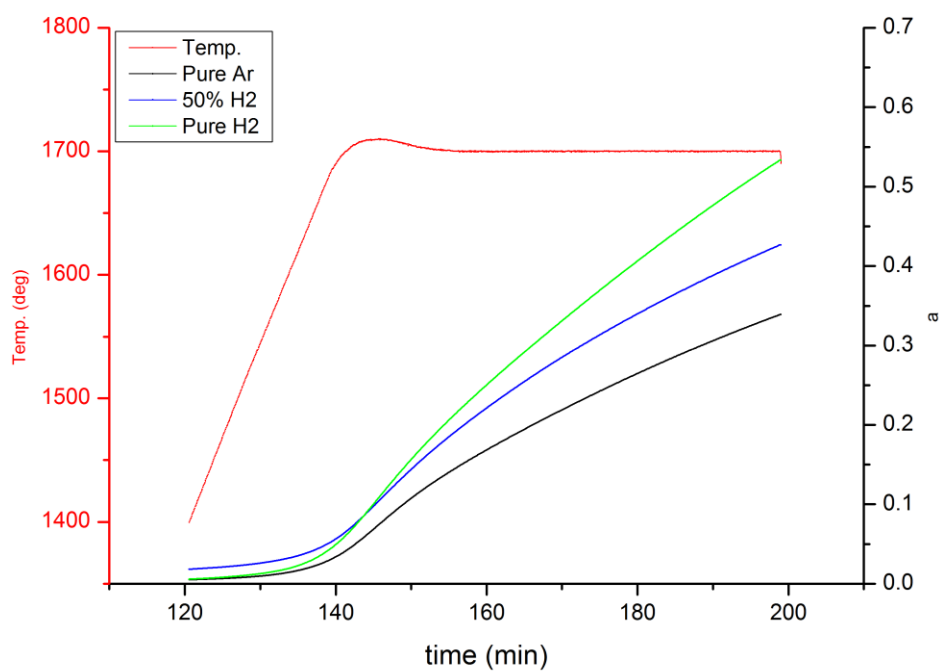
5.1 Influence of H₂ in the reaction rate

Run1, 4 and 5 were performed to investigate the effect of different H₂ concentration in Ar-H₂ gas mixtures on the reaction conversion and conversion rate. The conversion rate and conversion of SiO₂+SiC reaction versus time and temperature in Ar-H₂ mixtures is presented in Figure 5-1. The conversion rate of the reaction increased slowly from 1400 °C to 1600 °C and then increased dramatically from 1600 °C to 1700 °C. When the temperature was kept at 1700 °C, the conversion rate decreased again. The peaks of these curves were obtained at 1700 °C. The increase of reaction conversion was mostly obtained when the temperature reached 1700 °C. SEM images of reacted pellets shows that quartz became softened at 1700 °C. It is more difficult for gaseous product to evolve away from the reaction surface through softened quartz, which explains the decrease of conversion rate at 1700 °C.

The H₂ concentration in Ar-H₂ gas mixtures exerts a profound effect on the conversion and conversion rate. Increasing H₂ concentration in Ar-H₂ gas mixture gives higher conversion and conversion rate of SiO₂+SiC reaction. Xiang Li [29] reported that the higher rate of the carbothermal reduction of quartz in hydrogen was attributed to the involvement of hydrogen in the reduction reactions by directly reducing silica or indirectly, by reacting with graphite to form methane as an intermediate reductant. However, since CO is the main product from the reaction occurring at 1700 °C, it is believed that quartz reacted with silicon carbide instead of H₂, even if H₂ is presented. Therefore, the acceleration of the reaction was caused by the mass transport of gaseous product. The author believes that the diffusion of SiO or CO gas away from the particle surface is faster in H₂ than Ar.

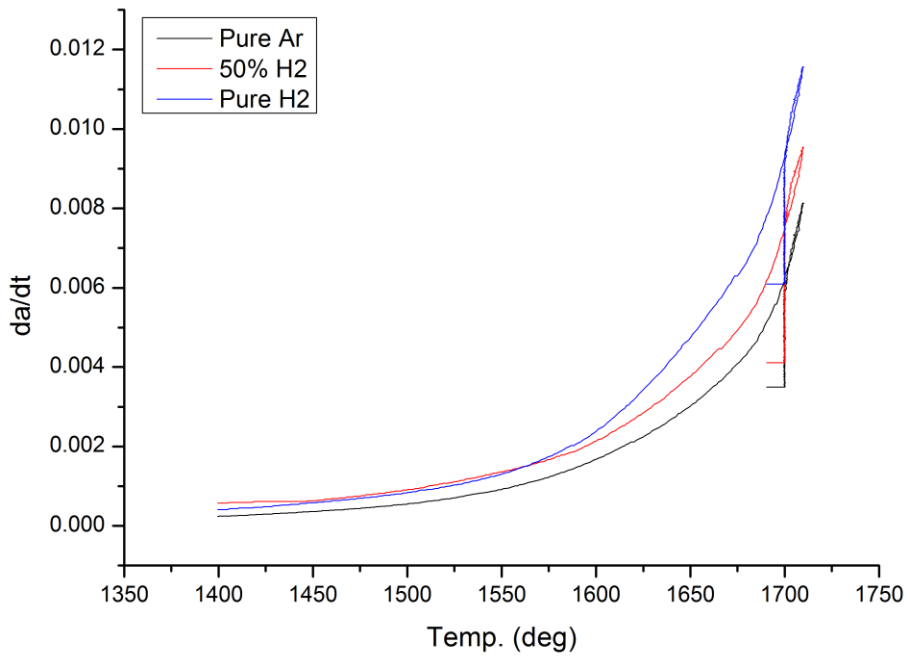


(a)

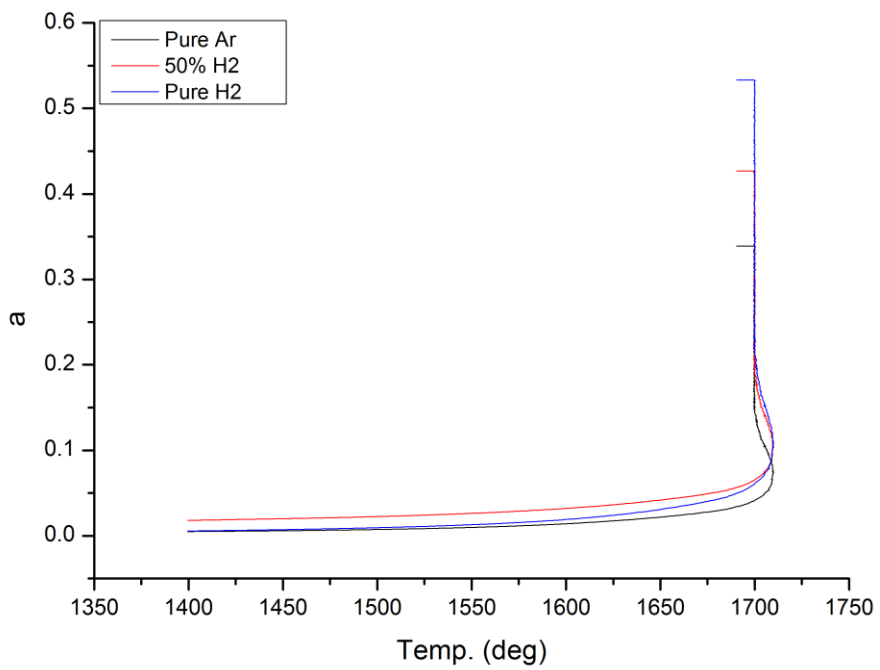


(b)

Figure 5-1 (a) Conversion rate of SiO_2+SiC reaction versus time in the presence of $\text{H}_2\text{-Ar}$
 (b) Conversion of SiO_2+SiC reaction versus time in the presence of $\text{H}_2\text{-Ar}$



(a)



(b)

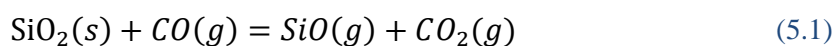
Figure 5-2 (a) Conversion rate of SiO₂+SiC reaction versus temperature in the presence of H₂-Ar

(b) Conversion of SiO₂+SiC reaction versus temperature in the presence of H₂-Ar

5.2 Influence of CO in the reaction rate

Run1, 2 and 3 were performed to investigate the effect of different CO concentration in Ar-CO gas mixtures on the reaction conversion and conversion rate. The conversion rate and conversion of SiO₂+SiC reaction versus time and temperature in the Ar-CO gas mixture is presented in Figure 5-3. The conversion rate is low at 1400 °C. With the temperature increasing from 1400 °C to 1700 °C, the conversion rate is increasing and the highest value is obtained at 1700 °C. Then it decreases during the holding time at 1700 °C. In contrary to H₂, increasing the CO concentration in Ar-CO gas mixtures gives lower reaction conversion and conversion rate. It is well recognized that the added CO gas suppress the reaction as one of the products.

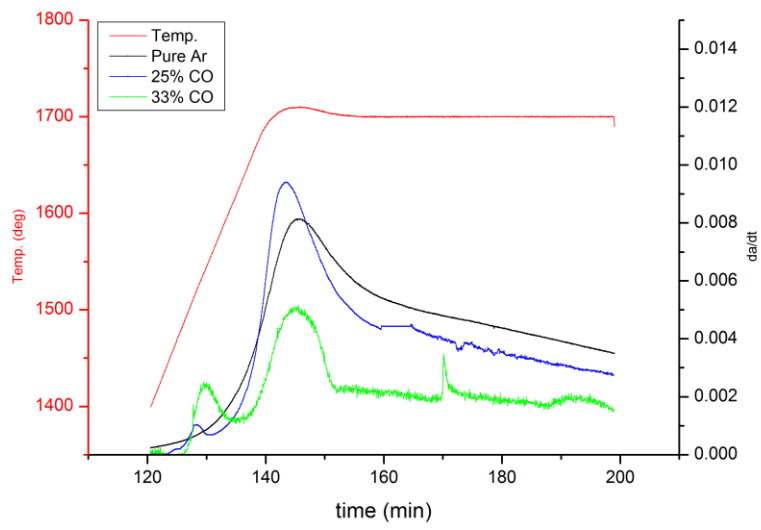
In general, the reaction curves in Ar-CO gas mixtures include two peaks. However, in the reaction curves in argon and Ar-H₂ mixture, only one peak was observed. The first peak always appeared at 1500 °C. A possible reason for the existence of the first peak is that carbon dioxide was formed by quartz reacting with carbon monoxide and CO₂ formed in reaction 5.1 is converted back to CO by Boudouard reaction which is highly favored thermodynamically within the temperature range of isothermal reduction experiments of this investigation.



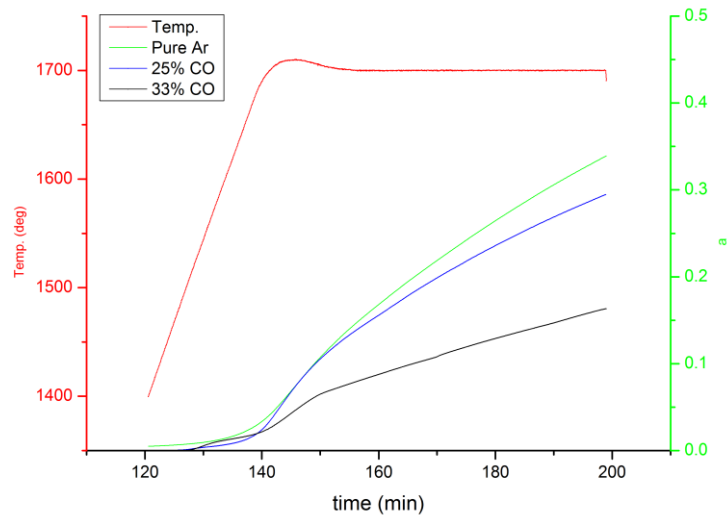
With the presence of CO gas, small peaks appeared before 1700 °C. The small peaks were probably caused by another reaction occurring inside the furnace or inaccuracy of gas analyzer. The conversion and relative conversion caused by the small peaks are shown in Table 5-1.

Table 5-1 conversion and relative conversion of small peaks

Run	α (small peak)	α (total)	α (relative)
2	0.025	0.3	8.3%
7	0.036	0.33	11%
9	0.039	0.32	12%

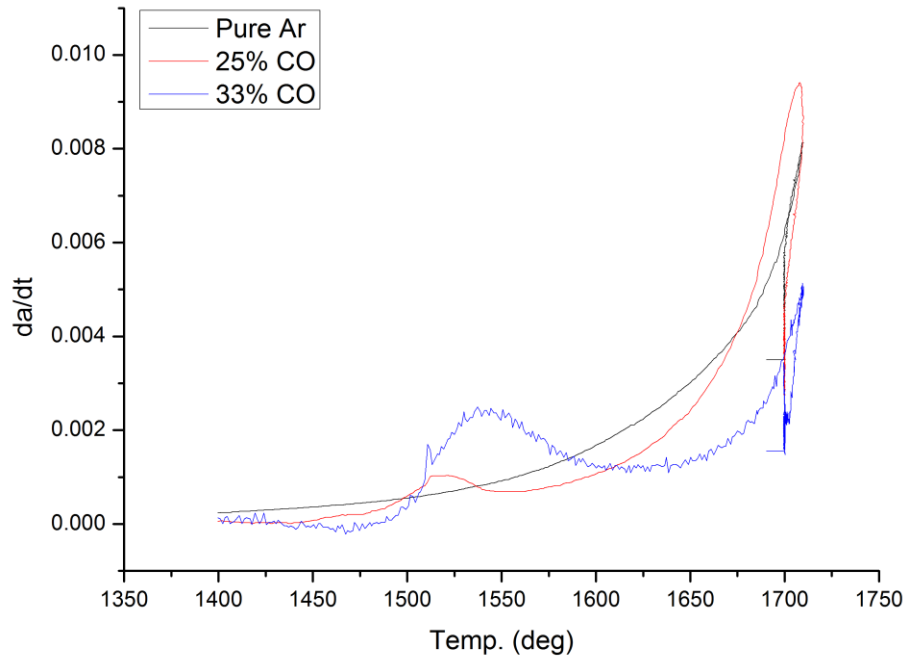


(a)

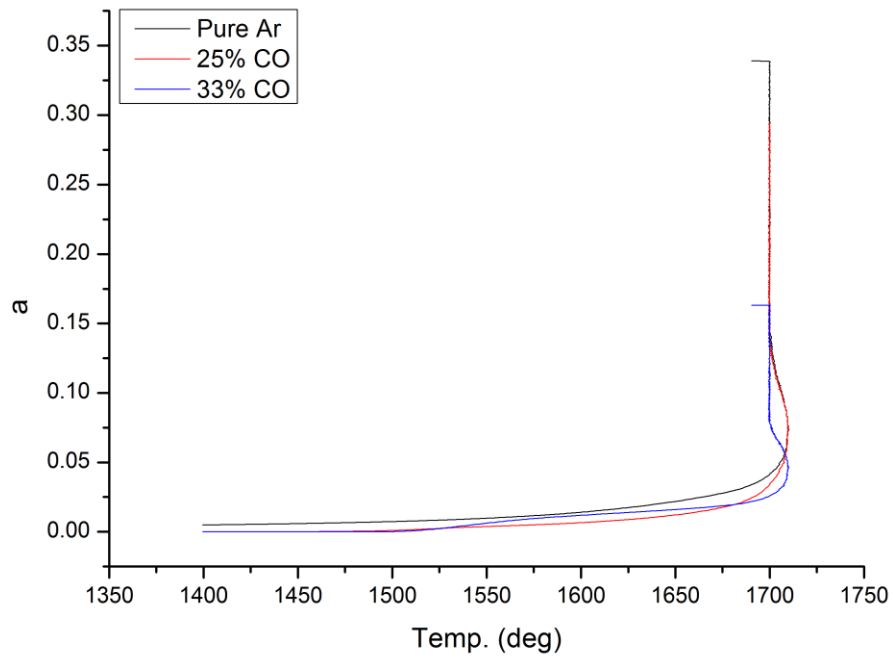


(b)

Figure 5-3 (a) Conversion rate of SiO_2+SiC reaction versus time in the presence of CO-Ar
 (b) Conversion of SiO_2+SiC reaction versus time in the presence of CO-Ar



(a)



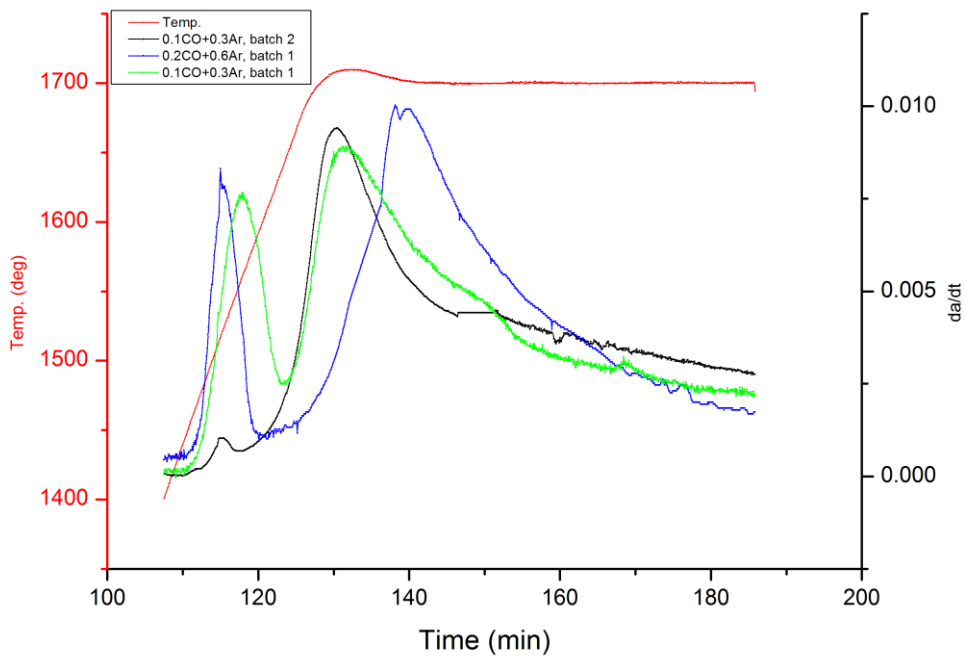
(b)

Figure 5-4(a) Conversion rate of SiO_2+SiC reaction versus temperature in the presence of CO-Ar

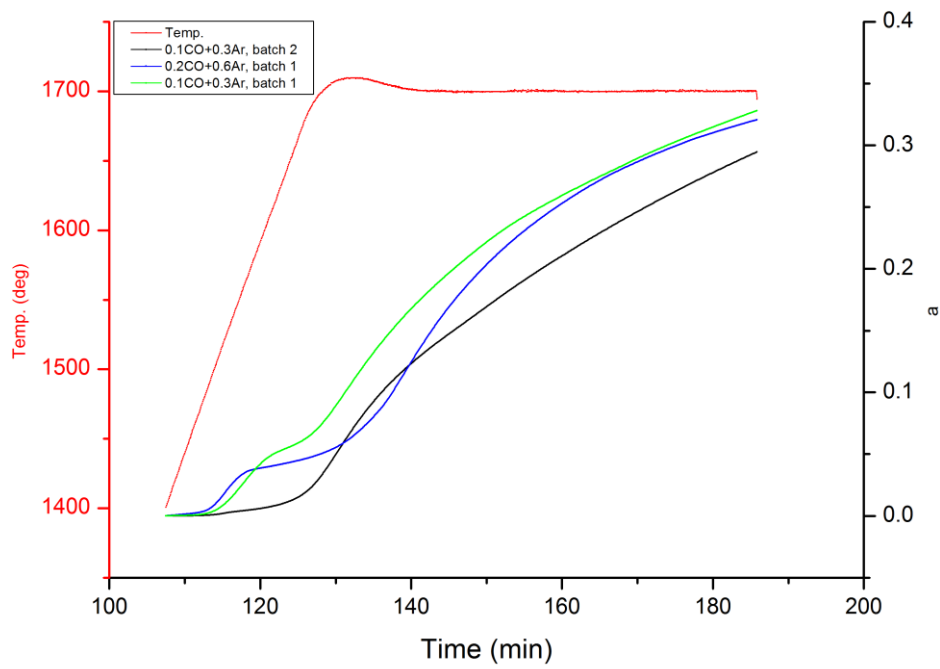
(b) Conversion of SiO_2+SiC reaction versus temperature in the presence of CO-Ar

5.3 Influence of the flow rate of Ar-CO gas mixture in the reaction rate

Figure 5-5 shows the conversion rate and conversion of SiO_2+SiC from run 2, 7 and 9. The composition of added gas is 25% CO in Ar-CO gas mixtures. The variables in these three comparative experiments are the batch of initial pellets and the gas flow rate. Comparing the results from run 2 and run 7, the different batch of pellets with same flow rate of gas mixture gives the similar conversion and conversion rate, which indicates that the effect of difference in raw material can be ignored. Comparing the results from run 7 and run 9, the variable in these two runs is the flow rate of Ar-CO gas mixtures. The gas flow rate in run 9 is twice of that in run 7, however, the conversion and conversion rate of the reaction in these two runs are similar. With the presence of CO gas in the added gas mixture, the reaction is limited by the CO concentration, instead of the flow rate of added gas.



(a)

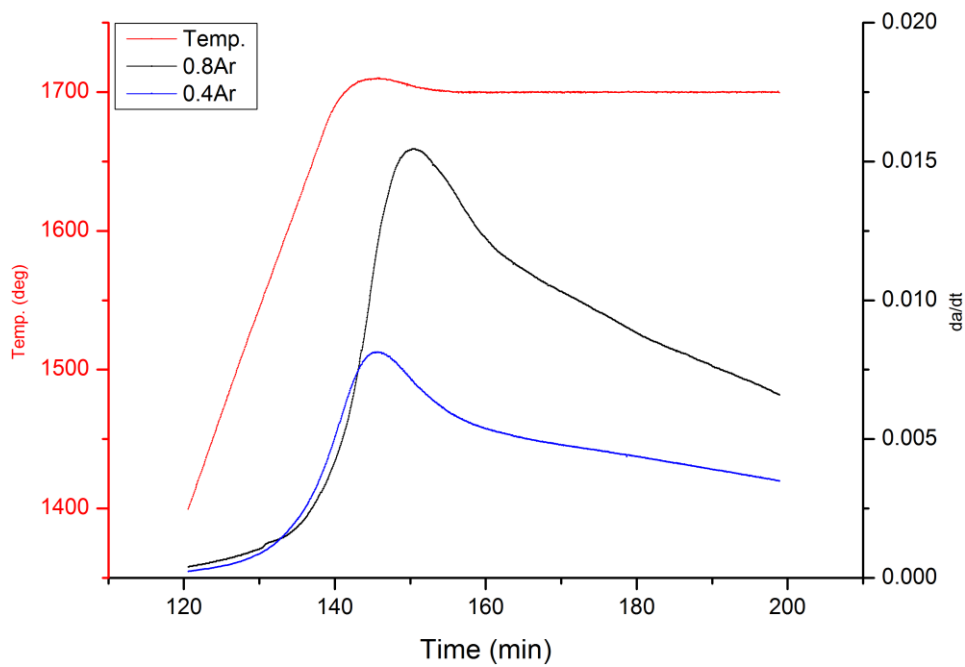


(b)

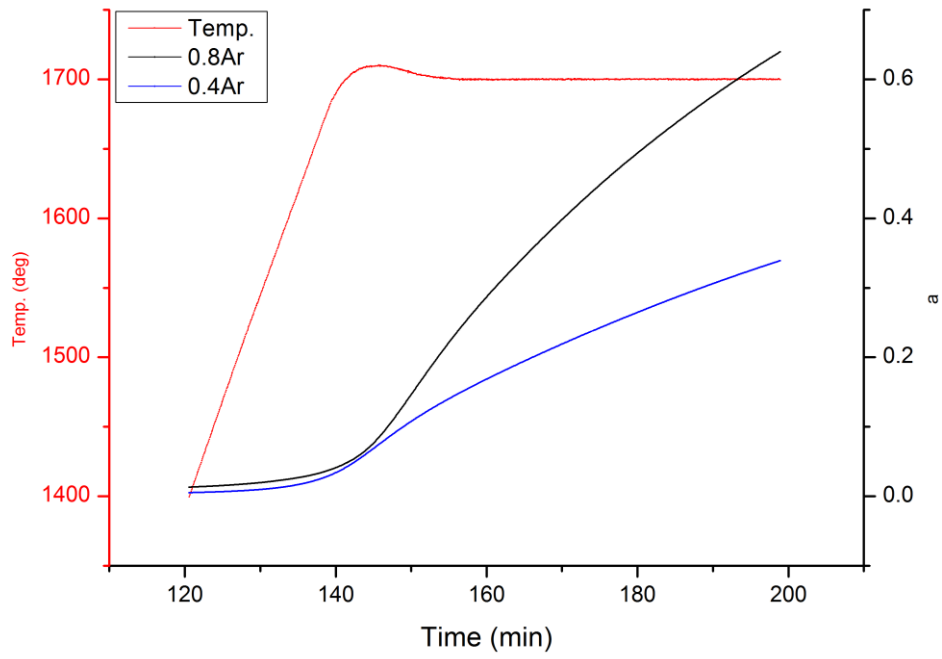
Figure 5-5 (a) conversion rate of $\text{SiO}_2 + \text{SiC}$ reaction with different rate of Ar-CO mixture (25% CO), (b) conversion of $\text{SiO}_2 + \text{SiC}$ reaction in different rate of Ar-CO mixture (25% CO)

5.4 Influence of the flow rate of pure argon in the reaction rate

Figure 5-6 shows the conversion rate and conversion of SiO_2+SiC from run 1 and run 8 versus time. Both conversion and conversion rate of the reaction with 0.8 l/min Ar are almost twice of that with 0.4 l/min Ar. The acceleration of reaction with higher flow rate of Ar is caused by faster CO or SiO gas removal.



(a)



(b)

Figure 5-6 (a) conversion rate of SiO_2+SiC reaction with different rate of Ar, (b) conversion of SiO_2+SiC reaction in different rate of Ar

5.5 Activation energy

The activation energy determined by the iso-conversional method is shown in Figure 5-7. Two isothermal runs were performed at 1700 °C and 1650 °C respectively. The plot between $\ln(d\alpha/dt)$ and $1/T$ gives the activation energy, $E=195\text{kJ/mole}$ ($\alpha = 0.1$), $E=68.3\text{kJ/mole}$ ($\alpha=0.2$) and $E=15.9\text{kJ/mole}$ ($\alpha=0.3$). An explanation of the different value of activation energy is that the activation energy is probably dependent on the conversion of reaction. The reproducible experiments should be done to check the reliability of results.

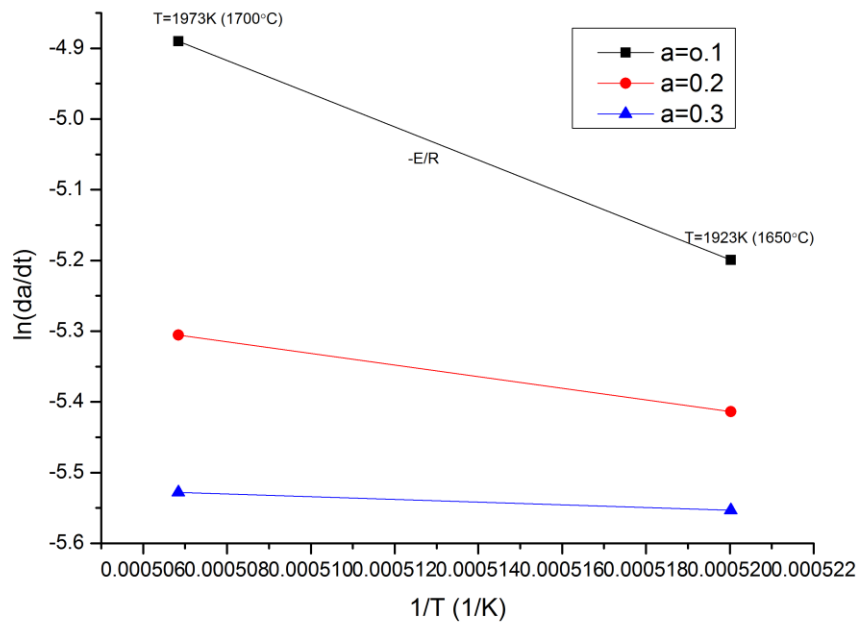
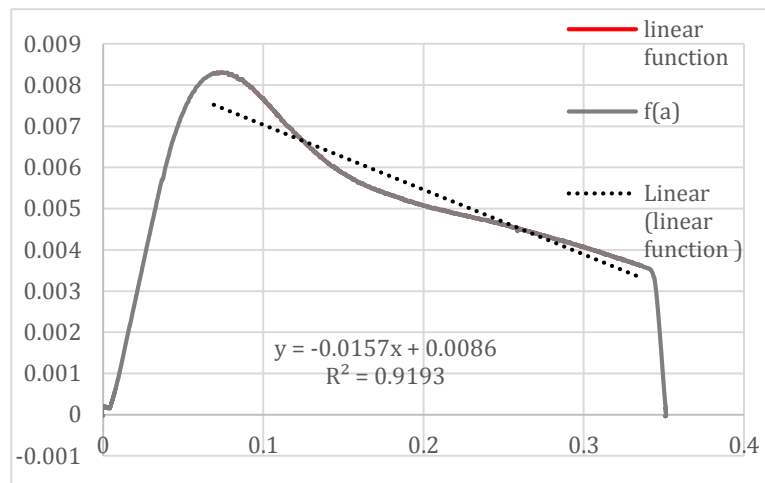


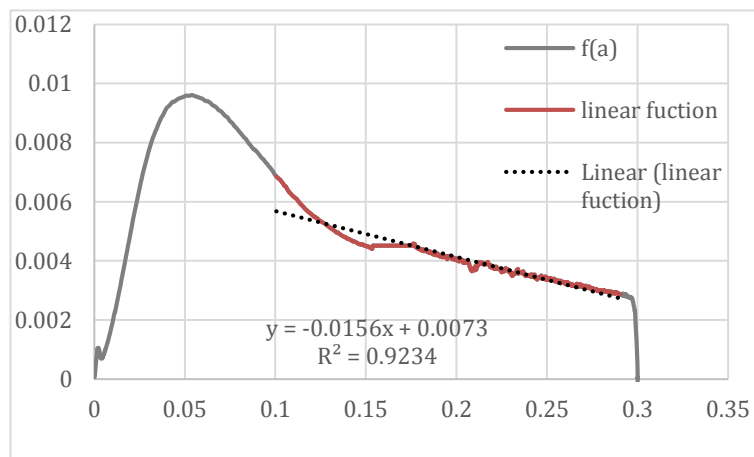
Figure 5-7 Logarithm of the reaction rate plotted against $1/T$ for the SiO_2+SiC reaction. $T=1650\text{ °C}$ and 1700 °C respectively.

5.6 Kinetics modelling

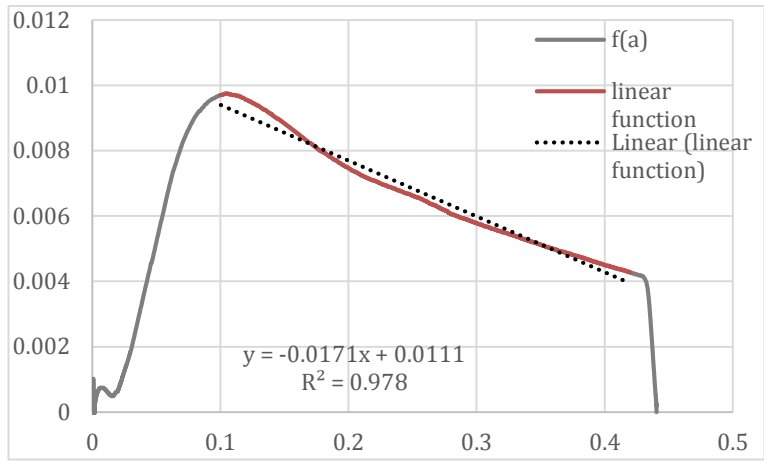
The kinetic model of SiO_2+SiC reaction in solid-solid stage is determined by plotting the auxiliary function $\frac{d\alpha}{dt}/\exp(-\frac{E}{RT})$ versus α . Figure 5-8 shows the reaction model under different gas atmospheres. Assuming that $f(\alpha)$ is supposed to decrease with increasing α , only α value, fitting this case, was selected to plot the reaction model. Linear trend lines are used to determine the kinetics triplets. The proposed reaction models were compared with the reference graphs, as presented in Figure 5-9.



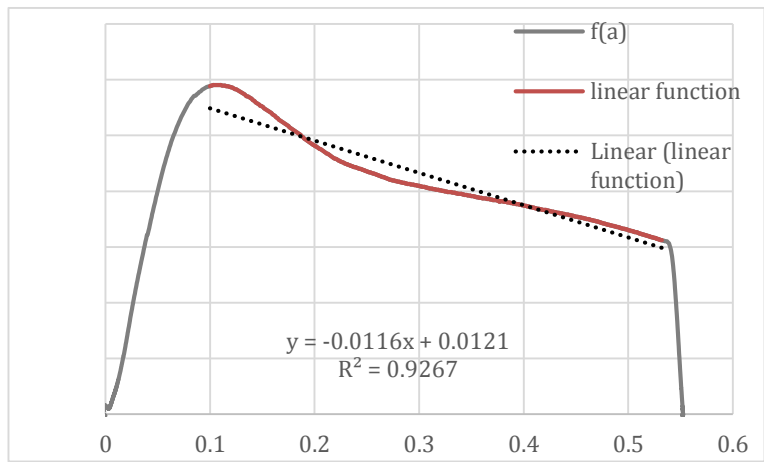
(a)



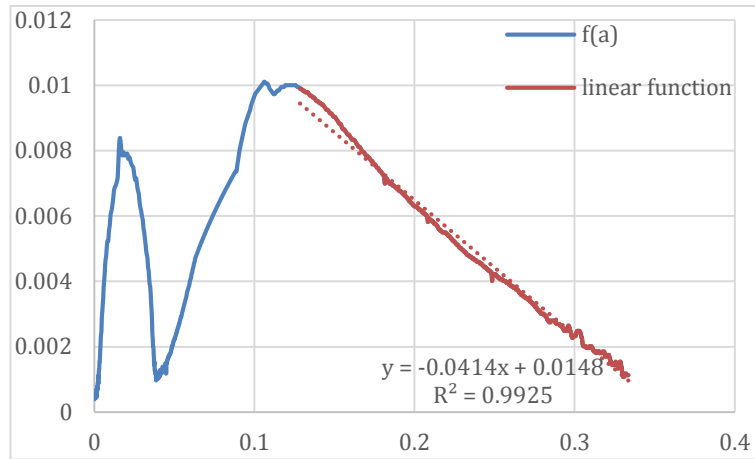
(b)



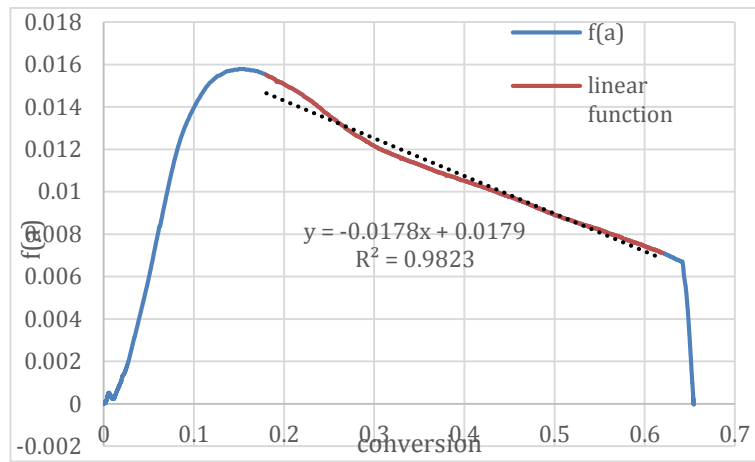
(c)



(d)



(e)

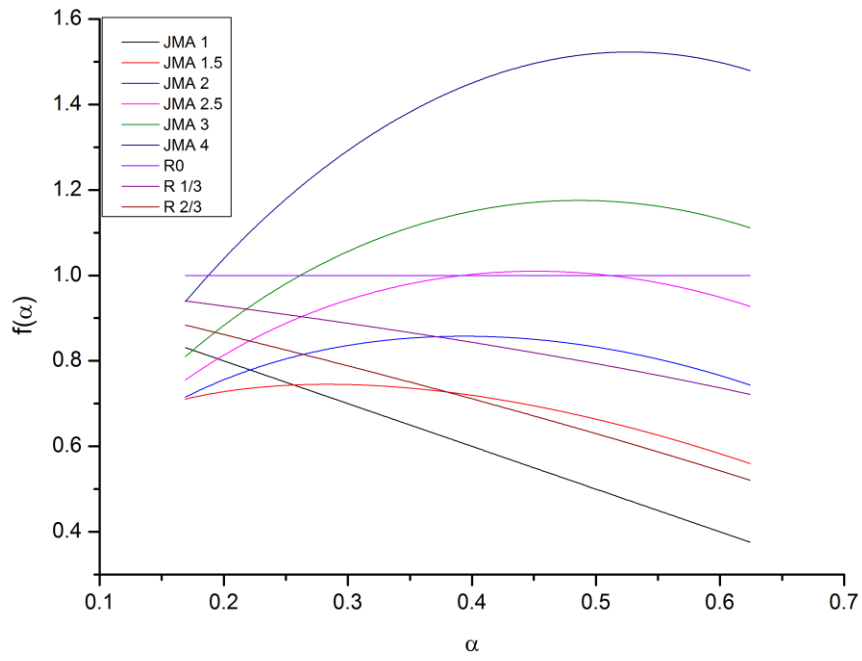


(f)

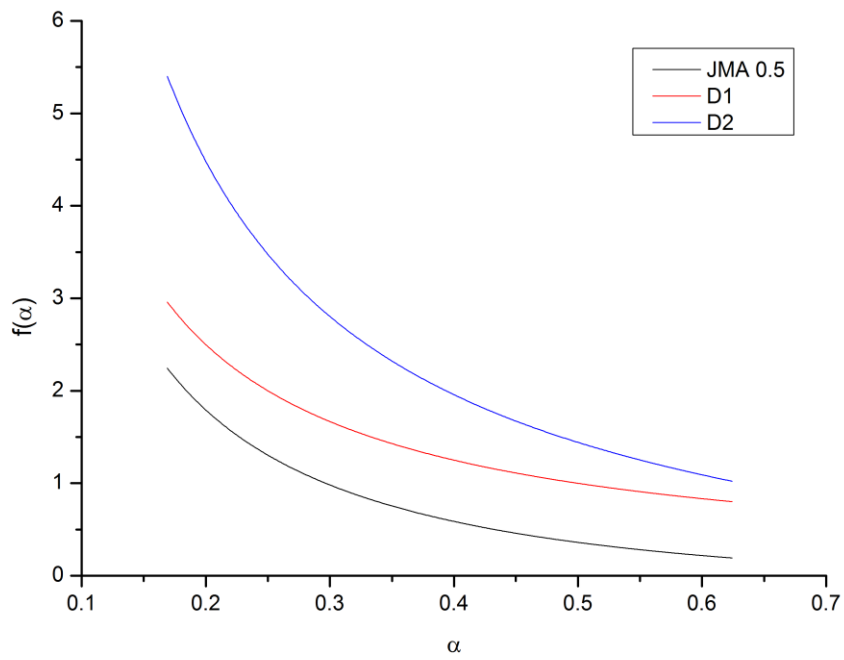
Figure 5-8 Reaction model: $f(\alpha)$ versus α .

(a) Run 1-0.4Ar; (b) Run 2-0.1CO+0.3Ar, (c) Run 4-0.2H₂+0.2Ar, (d) Run 5-0.4H₂,

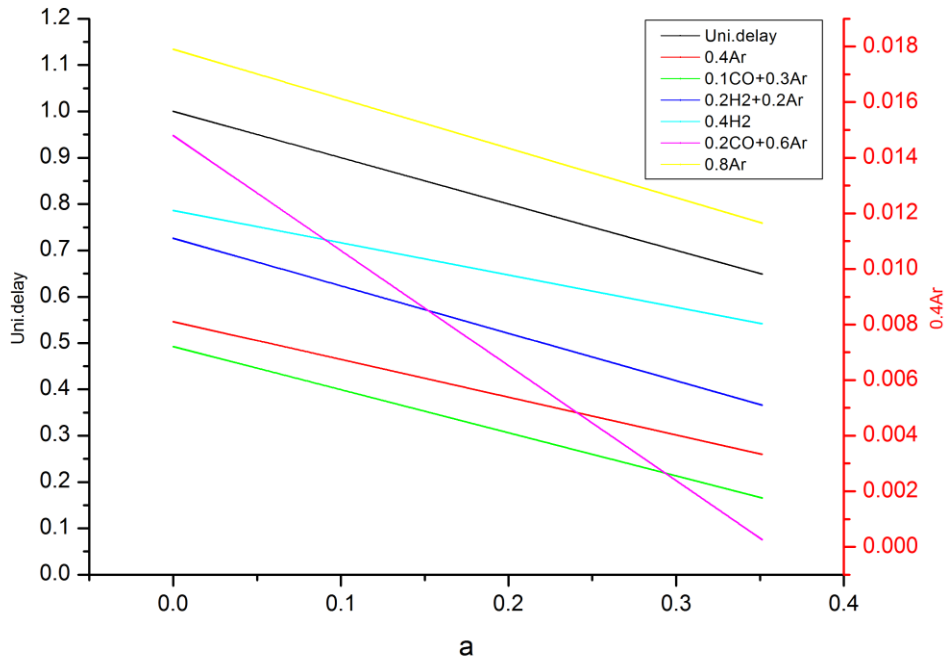
(e) Run 8- 0.2CO+0.6Ar, (f) Run 9- 0.8Ar



(a)



(b)



(c)

Figure 5-9 (a) and (b) shows graphical representation the possible reaction models given in Table 2-1. (c) shows the similarity between the auxiliary function for the SiO_2+SiC reaction and the unimolecular decay model..

A linear relation between and α is shown in Eq.5.3.

$$\frac{\frac{d\alpha}{dt}}{\exp\left(-\frac{E}{RT}\right)} = A(a - b\alpha)g(X_{gas}) \quad (5.3)$$

By comparing the experimental data with reaction models, it is found that the unimolecular decay model (F1) in Table 2-1, describes the reaction rate best in most cases.

$$\frac{\frac{d\alpha}{dt}}{\exp\left(-\frac{E}{RT}\right)} = c(1 - \alpha) + d \quad (5.4)$$

$$d = f(X_{\text{CO}}X_{\text{H}_2}r_{\text{flow}}) \quad (5.5)$$

Where $c=b*A$, d is gas dependent factor, X_{CO} is the CO concentration in Ar-CO gas mixture, X_{H_2} is the H₂ concentration in Ar-H₂ concentration and r_{flow} is the flow rate of process gas. Kinetics triplets of the reaction under different gas species were summarized in Table 5-2.

Table 5-2 Kinetics data under different gas species

Gas species	c	d	E (kJ/mole)	R ²
0.4Ar	0.0157	-0.0071		0.9193
0.1CO+0.3Ar	0.0156	-0.0083		0.9253
0.2H ₂ +0.2Ar	0.0171	-0.0060		0.978
0.4H ₂	0.0116	0.0005	348	0.9267
0.2CO+0.6Ar	0.0414	-0.0266		0.9925
0.8Ar	0.0178	0.0001		0.9823

It can be found that the reaction model of 0.2CO+0.6Ar is an outlier. Except for 0.2CO+0.6Ar, the c values of the other gas species are quite similar. The average c equals 0.0155. d values are recalculated based on the average c value and listed in Table 5-3

Table 5-3 Kinetics data under different gas species (recalculated)

Gas species	c	d'	E (kJ/mole)
0.4Ar		-0.0069	
0.1CO+0.3Ar		-0.0082	
0.2H ₂ +0.2Ar	0.0155	-0.0044	348
0.4H ₂		-0.0034	
0.8Ar		0.0024	

The relation between d (gas factor) and CO concentration, H₂ concentration, flow rate of gas flow is listed below

In Ar-CO gas mixture, the relation between da/dt and CO concentration is

$$\frac{da}{dt} = \exp\left(-\frac{348000}{RT}\right) \times [0.0155(1 - \alpha) - 0.0069 - 0.0052X_{CO}] \quad (5.6)$$

In Ar-H₂ gas mixture, the relation between d factor and H₂ concentration is

$$\frac{da}{dt} = \exp\left(-\frac{348000}{RT}\right) \times [0.0155(1 - \alpha) - 0.0069 + 0.0050X_{H_2}] \quad (5.7)$$

In pure argon, the relation between d factor and the flow rate of process gas is

$$\frac{da}{dt} = \exp\left(-\frac{348000}{RT}\right) \times [0.0155(1 - \alpha) - 0.0162 + 0.0233r_{flow}] \quad (5.8)$$

Where the value of X_{CO} is from 0 to 1.

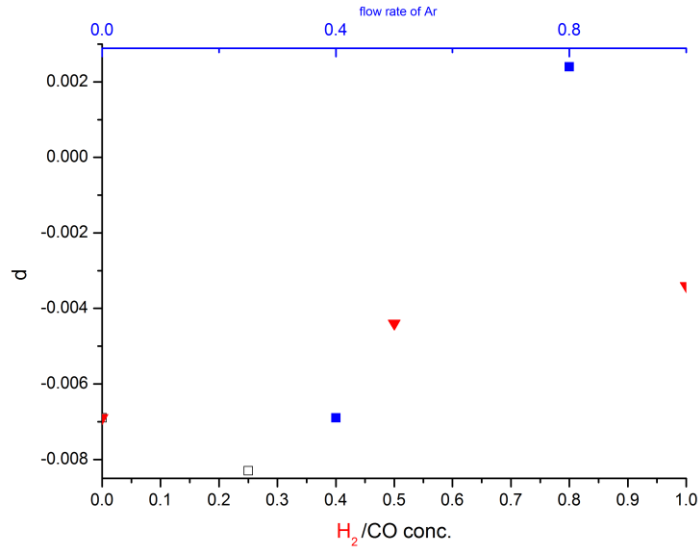


Figure 5-10 d as a function of H₂ concentration, CO concentration and flow rate of gas flow.

Figure 5-11 to Figure 5-15 compares the measured conversions with the estimated conversions under different gas species. An indication of the goodness of the model is the degree of explanation, R². The kinetic models can be summarized as below

0.4Ar

The reaction rate is expressed by

$$\frac{da}{dt} = \exp\left(-\frac{348000}{RT}\right) \times [0.0155(1 - \alpha) - 0.0162 + 0.0233 * 0.4] \quad (5.9)$$

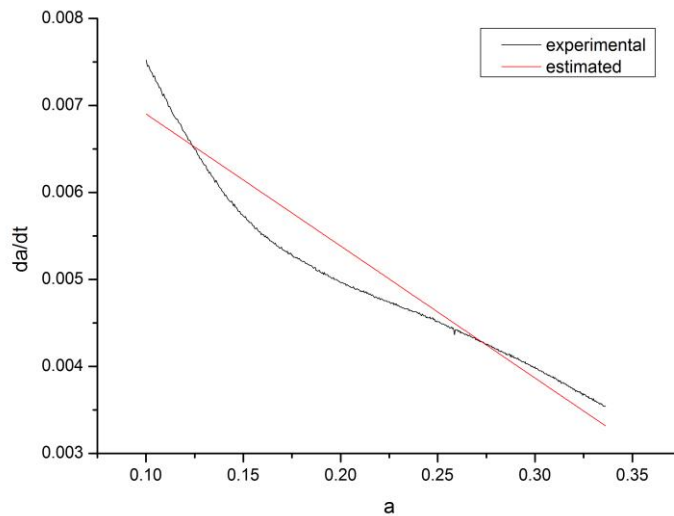


Figure 5-11 Comparison of the measured reaction rate with the estimated values (0.4Ar)

0.1CO+0.3Ar

$$\frac{da}{dt} = \exp\left(-\frac{348000}{RT}\right) \times [0.0155(1 - \alpha) - 0.0069 - 0.0052 * 25\%] \quad (5.10)$$

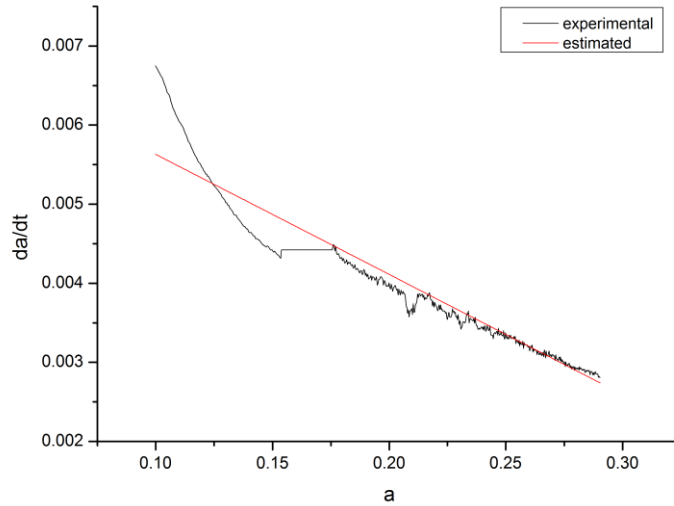


Figure 5-12 Comparison of the measured reaction rate with the estimated values
(0.1CO+0.3Ar)

0.2H₂+0.2Ar

$$\frac{da}{dt} = \exp\left(-\frac{348000}{RT}\right) \times [0.0155(1 - \alpha) - 0.0069 + 0.0050 * 50\%] \quad (5.11)$$

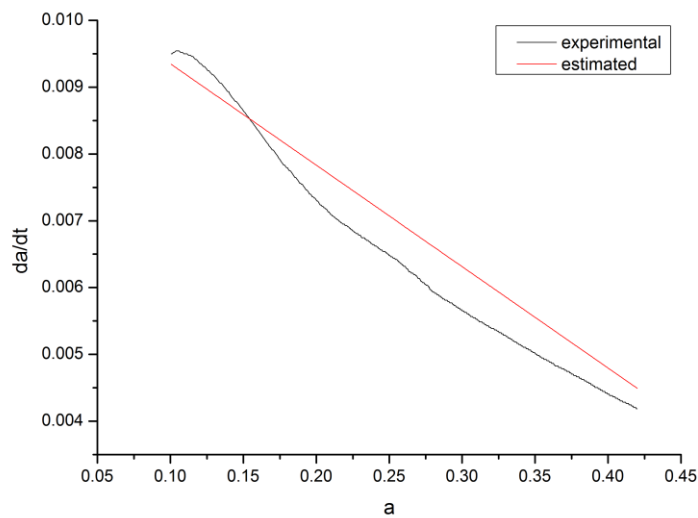


Figure 5-13 Comparison of the measured reaction rate with the estimated values
(0.2H₂+0.2Ar)

0.4H₂

$$\frac{da}{dt} = \exp\left(-\frac{348000}{RT}\right) \times [0.0155(1 - \alpha) - 0.0034] \quad (5.12)$$

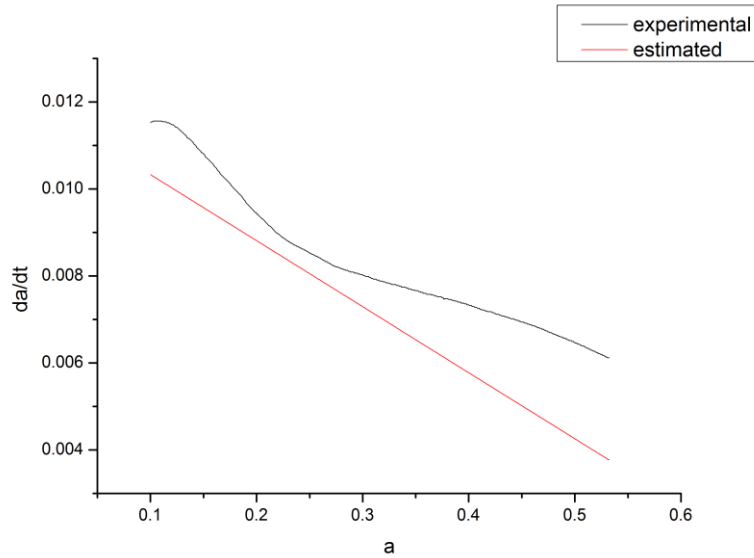


Figure 5-14 Comparison of the measured reaction rate with the estimated values (0.4H₂)

0.8Ar

$$\frac{da}{dt} = \exp\left(-\frac{348000}{RT}\right) \times [0.0155(1 - \alpha) - 0.0162 + 0.0233 * 0.8] \quad (5.13)$$

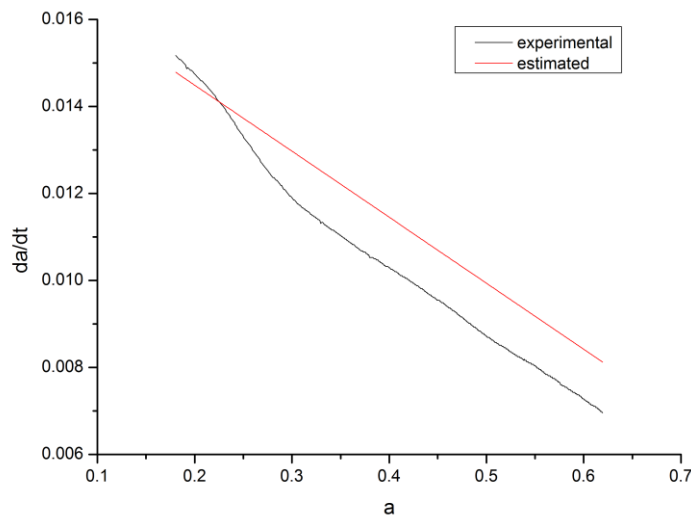


Figure 5-15 Comparison of the measured reaction rate with the estimated values (0.8Ar)

5.7 Evaluation of experimental setup

5.7.1. Condensation chamber

To be able to prevent the SiO gas from blocking the gas tube, a condensation chamber with SiC particles (4-5mm) inside was used. The idea of using SiC particles with large size is to make the SiO gas condense on carbides particles. The XRD analysis shows that silicon formed by chemical reactions in the system is little, indicating that only little amount of SiO gas reacted with silicon carbides.

5.7.2. Flow rate of CO gas

Except for process gas, inert gas was purged into the furnace chamber to remove evolved product gas. Several trials were run with the flow rate of inert gas 0.8 l/min and total flow rate of process gas 0.8 l/min. When both CO and Ar were purged in 0.4l/min as process gas, the CO concentration of the off-gas was not stable, as is shown in Figure 5-16. When the flow rate of CO gas decreased to 0.2 l/min, more stable line was acquired. It seems that CO gas with higher flow rate built pressure inside the gas analyzer, resulting the unstable signal of CO gas module. That is to say, the stability of gas analyzer signal was limited by the flow rate of CO gas. The stable curve of CO concentration was obtained when CO flow rate is decreased to 0.1 l/min. The maximum of CO concentration of the gas analyzer is 20 vol%, which decreased the possible CO concentration range. An alternative solution is to use a gas analyzer without the limitation of CO gas flow rate.

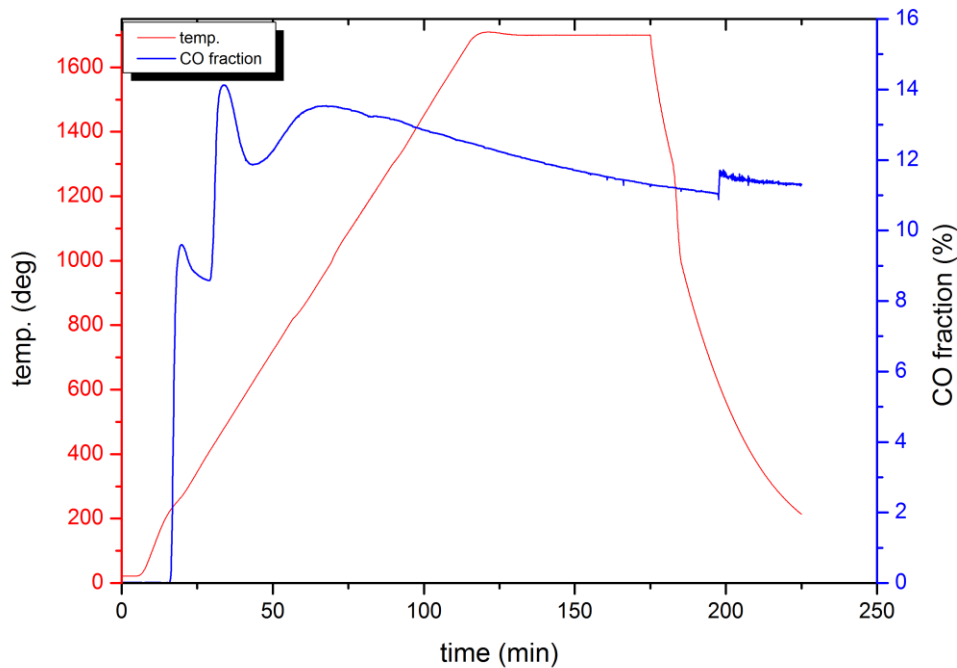


Figure 5-16 CO concentration of off-gas with the process gas 0.4 l/min CO and 0.4 l/min Ar.

5.7.3. Source of error

Several sources of error influence the registered CO concentration in the off gas. This section summarizes the sources and evaluates their influence on reliability of the results

Disturbance from high flow rate of CO gas will build pressure in CO gas module, resulting in unstable signal of CO concentration in the off-gas.

Possible parallel reactions. Several additional reactions were observed during the experiments.

- Silicon metal was found in the reacted pellets closed to SiC particles, indicating that SiO gas reacted with silicon carbides to form silicon and CO gas. CO concentration measured by the gas analyzer was affected by silicon forming reaction. However, the influence of this reaction is rather little as only few silicon was formed in the reacted pellets as shown in the XRD results.

- Condensation of SiO gas on SiC particles occurred in the condensation chamber. Silica and silicon were formed. Silica became softened at high temperature and made SiC particles stick to each other. Gas flow became more difficult to evolve.

Sintering of pellets

After pelletizing process, pellets were sintered at 1200 °C to improve the strength, which introduced a small amount of cristobalite into initial pellets. The reaction between quartz and silicon carbide was accelerated by the cristobalite transformation.

Chapter 6. Conclusion

In general, the different gas species have a profound effect on the reaction rate. The SiO_2+SiC reaction at $1700\text{ }^\circ\text{C}$ (solid-solid stage) can be well described by the unimolecular model (F1). The activation energy is assumed to be a constant value (348kJ/mole).

6.1 Influence of H_2 in the reaction rate

The reaction rate increased with increasing hydrogen content in Ar- H_2 gas mixtures. The higher reaction rate in hydrogen containing gas was attributed to the faster diffusion of SiO gas or CO gas in hydrogen. The reaction rate can be described by F1 model, given in Eq.5.7.

$$\frac{da}{dt} = \exp\left(-\frac{348000}{RT}\right) \times [0.0155(1 - \alpha) - 0.0069 + 0.0050X_{\text{H}_2}] \quad (5.7)$$

6.2 Influence of CO in the reaction rate

The reaction rate decreased with increasing CO gas content in Ar-CO gas mixtures. The reason of the lower reaction rate in CO gas was that CO gas, as one of the products, inhibited the reaction. The reaction rate can be described by Eq.5.6.

$$\frac{da}{dt} = \exp\left(-\frac{348000}{RT}\right) \times [0.0155(1 - \alpha) - 0.0069 - 0.0052X_{\text{CO}}] \quad (5.6)$$

6.3 Influence of the flow rate of CO-Ar gas mixture in the reaction rate

It is found that with the presence of CO gas in the added gas mixture, the reaction is limited by the CO concentration, instead of the flow rate of added gas.

6.4 Influence of the flow rate of pure argon in the reaction rate

Both conversion and conversion rate of the reaction with higher gas flow rate are higher. The acceleration of reaction with higher flow rate of Ar is caused by faster SiO gas or CO gas removal. The reaction rate can be described by Eq5.8

$$\frac{da}{dt} = \exp\left(-\frac{348000}{RT}\right) \times [0.0155(1 - \alpha) - 0.0162 + 0.0233r_{\text{flow}}] \quad (5.8)$$

Chapter 7. Future work

Improvement of material and methods

Sintering process should be conducted at lower temperatures to avoid the cristobalite transformation. A CO gas analyzer with no limitation of CO gas flow should be installed. The temperature measured by the C-type thermocouple should be integrated into computer data logger. Carbon analysis of initial and reacted pellets should be performed to give more accurate final conversion of SiO_2+SiC reaction.

It is suggested that the rate of SiO_2+SiC reaction with $0.2\text{CO}+0.6\text{Ar}$ should be investigated again. Reproducible experiments are also suggest to be done in the future.

Proposal to check the reaction between quartz and CO gas

To be able to check the small peak in CO concentration curves obtained in the runs with CO gas as part of process gas, quartz pellets will be heated up following the same temperature profile with Ar-CO gas mixtures purged into the graphite crucible.

References

1. Schei, A., J.K. Tuset, and H. Tveit, *Production of high silicon alloys*. 1998: Tapir Trondheim, Norway.
2. Abánades, A., et al., *Experimental analysis of direct thermal methane cracking*. International journal of hydrogen energy, 2011. **36**(20): p. 12877-12886.
3. Poch, W. and A. Dietzel, *The formation of silicon carbide from silicon dioxide and carbon*. Ber. Dtsch. Keram. Ges, 1962. **39**: p. 413-426.
4. Ortega, A., *The kinetics of solid-state reactions toward consensus, Part 2: Fitting kinetics data in dynamic conventional thermal analysis*. International journal of chemical kinetics, 2002. **34**(3): p. 193-208.
5. Vyazovkin, S. and C.A. Wight, *Model-free and model-fitting approaches to kinetic analysis of isothermal and nonisothermal data*. Thermochemica acta, 1999. **340**: p. 53-68.
6. Sewry, J.D. and M.E. Brown, *"Model-free" kinetic analysis?* Thermochemica acta, 2002. **390**(1): p. 217-225.
7. Málek, J., *The kinetic analysis of non-isothermal data*. Thermochemica acta, 1992. **200**: p. 257-269.
8. Budrugaec, P., D. Homentcovschi, and E. Segal, *Critical analysis of the isoconversional methods for evaluating the activation energy. II. The activation energy obtained from isothermal data corresponding to two successive reactions*. Journal of thermal analysis and calorimetry, 2000. **63**(2): p. 465-469.
9. Budrugaec, P., D. Homentcovschi, and E. Segal, *Critical analysis of the isoconversional methods for evaluating the activation energy. I. Theoretical background*. Journal of thermal analysis and calorimetry, 2000. **63**(2): p. 457-463.
10. Budrugaec, P., D. Homentcovschi, and E. Segal, *Critical considerations on the isoconversional methods. III. On the evaluation of the activation energy from non-isothermal data*. Journal of thermal analysis and calorimetry,

2001. **66**(2): p. 557-565.
11. Šimon, P., *Isoconversional methods*. Journal of Thermal Analysis and Calorimetry, 2004. **76**(1): p. 123-132.
 12. Orfao, J. and F. Martins, *Kinetic analysis of thermogravimetric data obtained under linear temperature programming—a method based on calculations of the temperature integral by interpolation*. Thermochimica Acta, 2002. **390**(1): p. 195-211.
 13. Friedman, H.L. *Kinetics of thermal degradation of char-forming plastics from thermogravimetry. Application to a phenolic plastic*. in *Journal of Polymer Science Part C: Polymer Symposia*. 1964. Wiley Online Library.
 14. Dickinson, C. and G. Heal, *Solid–liquid diffusion controlled rate equations*. Thermochimica Acta, 1999. **340**: p. 89-103.
 15. Ortega, A., *The kinetics of solid-state reactions toward consensus—Part I: Uncertainties, failures, and successes of conventional methods*. International Journal of Chemical Kinetics, 2001. **33**(6): p. 343-353.
 16. Altorfer, R., *Estimation of kinetic parameters from conversion curves, determined at constant heating rate*. Thermochimica Acta, 1978. **24**(1): p. 17-37.
 17. Ortega, A., *Influence of mass-transfer effect on isoconversional calculations*. Thermochimica Acta, 2008. **475**(1): p. 65-71.
 18. Criado, J., et al., *Influence of mass-transfer phenomena on the shape of EGA traces of solid-state reactions*. Journal of Thermal Analysis and Calorimetry, 1990. **36**(7): p. 2531-2537.
 19. Hertl, W. and W. Pultz, *SiO₂+ SiC reaction at elevated temperatures. Part 2.—Effect of added gases*. Transactions of the Faraday Society, 1966. **62**: p. 3440-3445.
 20. Pultz, W. and W. Hertl, *SiO₂+ SiC reaction at elevated temperatures. Part 1.—Kinetics and mechanism*. Transactions of the Faraday Society, 1966. **62**: p. 2499-2504.
 21. Wiik, K., *Kinetics of reactions between silica and carbon*. 1990: Institutt for uorganisk kjemi, Norges tekniske høgskole, Universitetet i Trondheim.
 22. Adisty, D., *Kinetics Study of Silicon Production from Different Polymorphs of Quartz*. 2012.

23. Filsinger, D.H. and D.B. Bourrie, *Silica to silicon: key carbothermic reactions and kinetics*. Journal of the American Ceramic Society, 1990. **73**(6): p. 1726-1732.
24. Khrushchev, M., *Kinetics and mechanism of reaction between silicon carbide and silica*. Inorganic Materials, 2000. **36**(5): p. 462-464.
25. Andersen, V., *Reaction mechanism and kinetics of the high temperature reactions in the silicon process*. 2010, Master Thesis. 2010, Norwegian University of Science and Technology: Trondheim.
26. Adisty, D., *Kinetic Study of SiO₂+ SiC Reaction in Silicon Production*. 2013.
27. Bao, S., et al., *Production of SiO gas in Si process*. 2014.
28. Ni, F., *Kinetics study of the SiO₂+SiC reaction under different gas species* 2014.
29. Li, X., et al., *Carbothermal Reduction of Quartz in Different Gas Atmospheres*. Metallurgical and Materials Transactions B: p. 1-10.
30. Ostrovski, O., et al., *Carbothermal Solid State Reduction of Stable Metal Oxides*. steel research international, 2010. **81**(10): p. 841-846.
31. Ozturk, B. and R.J. Fruehan, *The rate of formation of SiO by the reaction of CO or H₂ with silica and silicate slags*. Metallurgical Transactions B, 1985. **16**(4): p. 801-806.
32. CEPURITIS, R., GARBOCZI, E. J., FERRARIS, C. F., JACOBSEN, S. & SØRENSEN, B. E., *In review. Particle size distribution and specific surface determination of crushed concrete aggregate fines. Submitted to CCC (Cement and Concrete Composites)*.
33. Dal Martello, E., et al., *Study of pellets and lumps as raw materials in silicon production from quartz and silicon carbide*. Metallurgical and Materials Transactions B, 2011. **42**(5): p. 939-950.

Appendix

Resina furnace Operating procedure

Starting up the furnace

- Step 1:** Open up compressed air valve on the left of the furnace (Figure 1).
- Step 2:** Move to the right side of the furnace, you will find the water valves (Figure 2). First, open the water outlet valve (Figure 2A) and then the water inlet valve (Figure 2B). It is important to carry it in this order to prevent excessive water pressure in the tubes. You can check the water level on an indicator located at the bottom of the furnace (Figure 3). The water level (green) should be above the orange indicator.
- Step 3:** Open up the gas cylinder valve (always open the valve for inert gas and your choice of other process gas) and set pressure to one bar (Figure 4). Plug the argon sensor to the ABB gas analyzer (Figure 5). This will allow monitoring of the gas flow.
- Step 4:** Turn on the main power switch for the furnace located on the side (Figure 6). Directly after powering on, gas-purging cycle will begin. Green indicator on the front panel of the furnace will blink (Figure 7). The cycle usually takes 20minutes.

Preparing your sample and experiment

- Step 5:** After the cycle is complete, open the chamber (Figure 8). There is eight screws in total on the front plate and one additional screw at the bottom, which will allow you to raise and lower the chamber using the appropriate lever (Figure 9A). Place your crucible on the sample holder, raise it and close the chamber again. Do not tighten up the screws very much or else it will be very difficult to unscrew them after the experiment is completed
- Step 6:** Write the program corresponding to your experiment on the pc and save it. Launch it and it will be loaded into the furnace.

Running the experiment

Step 7: Press on the run cycle button on the front panel of the furnace. The vacuum pump will start automatically to evacuate the chamber. The pressure should reach 80mtorr in 20mins. If this is not achieved the gas purging starts again automatically. Once it is over, you can press the button run cycle again. If everything is fine, the program will run and heating will start in the furnace automatically.

Noting: Before vacuum, the vacuum valve, filter valve and gas in valve are supposed to be closed. While vacuuming, open the vacuum valve to make the graphite crucible vacuum. After vacuuming, close vacuum valve and open gas in valve and filter valve. (Figure 10)

Shutting down the furnace

Step 8: Once everything is finished, you have to repeat step to open op the chamber and pick up your sample. Be careful while handling your sample since it might still be warm. Once you are done close the chamber again, turn off the furnace and close the gas bottle.

Step 9: Finally close the compressed air valve and the water inlet than outlet valve.

In case of emergency

Press the red button on the front panel of the furnace (Figure 9B). It will automatically shut down the furnace and start gas-purging sequence.

Gas analyzer (ABB AO2020) operation

1. The gas analyzer is connected with a T-valve. (Figure 11). To calibrate the gas analyzer, the calibration gas goes directly to the gas analyzer by switching the valve to gas analyzer. To run the experiments, the process gas goes into the furnace by switching the valve to furnace.
2. Open protection gas N₂ purged into the gas analyzer and open the pumping machine.

3. The maximum of CO gas flow rate is 0.3l/min to make sure the data of CO concentration is stable
4. The pressure meter is used to stabilize the gas flowing into the gas analyzer. (Figure 12)

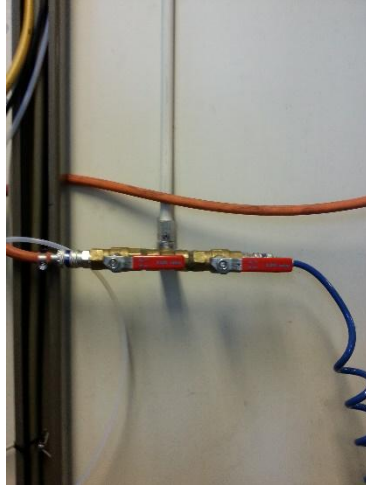





<p>Figure 1: Compressed Air Valves</p>	<p>Figure 2: Water Valves</p>	<p>Figure 3: Water Level Indicator</p>
 <p>A photograph showing a horizontal metal pipe with a red and blue valve assembly mounted on a wall. A blue hose is connected to the right side of the valve.</p>	 <p>A photograph of a complex brass valve assembly with multiple connections. Two green circles highlight specific valves. Blue letters 'A' and 'B' are visible in the background.</p>	 <p>A close-up photograph of a water level indicator, showing a vertical scale and a float mechanism within a tank.</p>
<p>Figure 4: Gas Valves</p>	<p>Figure 5: Mass Flow Controller</p>	<p>Figure 6: Furnace Power Switch</p>
 <p>A photograph of a green gas cylinder with several pressure gauges and valves attached to its top.</p>	 <p>A photograph of three Alicat mass flow controllers on a table, with various cables connected to them.</p>	 <p>A photograph of a white electrical panel with a black power switch. A warning label is visible below the switch.</p>
<p>Figure 7: Furnace Front Panel</p>	<p>Figure 8: Furnace Chamber</p>	<p>Figure 9: Chamber Position Lever</p>



Figure 10 vacuum



Figure 11 T-valve

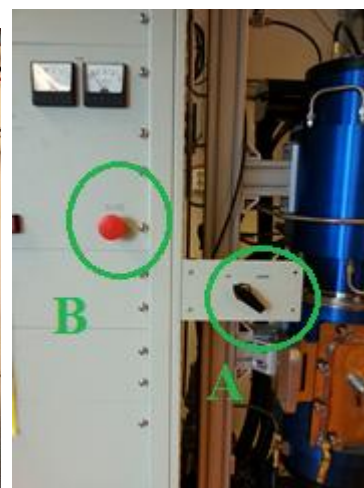


Figure 12 pressure meter

